2011

Advanced Linear Identification Techniques For Signal Processing And Digital Video Broadcasting

Xiaoyu Feng
Louisiana State University and Agricultural and Mechanical College, xfeng4@tigers.lsu.edu

ADVANCED LINEAR IDENTIFICATION TECHNIQUES FOR SIGNAL PROCESSING AND DIGITAL VIDEO BROADCASTING

A Dissertation

Submitted to the Graduate Faculty of the
Louisiana State University and
Agricultural and Mechanical College
in partial fulfillment of the
requirements for the degree of
Doctor of Philosophy

in

The Department of
Electrical and Computer Engineering

by
Xiaoyu Feng
B.S. Beijing University of Aeronautics and Astronautics
M.S.E.E. Louisiana State University
December, 2011

To my parents

ACKNOWLEDGMENTS

First, I am very grateful to my major professor, Dr. Hsiao-Chun Wu, for his continuous support throughout my Ph. D. study. Dr. Wu was always accessible for any question or advice. His academic knowledge and scientific soundness are highly appreciated and very useful for my dissertation research. Without his unwavering encouragement and invaluable guidance, I could not complete this Ph. D. research.

I would also like to thank Dr. Xue-Bin Liang, Dr. Lu Peng , Dr. Guoli Ding, and Dr Konstantin Busch for their kindness to serve on my thesis committee and for their precious suggestions and profound insights for my dissertation work.

In addition, I owe my sincere gratitude to Dr. Kun Yan, Dr. Lu Lu, Mr. Yonas Debessu, and Ms. Hongting Zhang, who are my former and current labmates. They gave me the strong support and warm friendship to help me get through this tough but worthy academic journey.

At last but not least, I will give the full credit for the completion of this dissertation to my dear parents. It is their selflessness and generous love to make me courageous enough to face all challenges, difficulties, and toughness during these years.

TABLE OF CONTENTS

LIST OF FIGURES

ABSTRACT

Linear identification technique is to linearly embed a piece of unique information into digital media data for the purpose of satisfying specific demands such as identification, annotation, and copyright, etc. We need to consider the quantity and the quality of identification data to be embedded as well as the corresponding interference to the original subject signal. However, there exist no generalized computationally-efficient optimization techniques for linear identification up to now. Therefore, in this dissertation work, we try to theoretically investigate the advanced linear identification techniques and combat the tradeoff problems between the quality of the embedded identification data and the quality of the subject signal. Two particular signal processing and telecommunication applications, namely *transmitter identification* and *digital watermarking*, will be exploited in this work. We propose a novel optimization paradigm for both *digital terrestrial television* (DTV) systems and *multiple digital watermarking* systems to maximize the overall *signal-to-interference-plus-noise ratio* (SINR) over both identification and subject signals. The new theories and practice related to *pseudo random sequences*, *extended arithmetic-geometric mean inequality*, and *constrained overall system performance* are also presented in this dissertation.

1. MOTIVATION, APPLICATIONS, AND CURRENT STATE OF KNOWLEDGE

This chapter will motivate the entire dissertation work. The motivation and potential applications will be stated. Then the state-of-the-art of the focused research problems will be introduced.

1.1 Motivation

Signal and transmitter identification technique represents a class of processes used to embed identity data into various forms of subject signals and detect them for particular demands. Two common purposes of signal and transmitter identification in digital media are to identify the received signal and provide the proof of the copyright. The identification data should stay hidden in a subject signal, even if that signal is subjected to manipulations such as filtering, resampling, cropping, or lossy data compression. Meanwhile, the features of the embedded data should be clearly detected after appropriate signal processing. The embedded data in a subject signal should satisfy the following requirements:

- The subject signal should be moderately degraded in the worst scenario and the embedded data should be at least perceptible.
- The embedded data should be directly encoded into the media, rather than into a file header or wrapper.

- The perceptibility of the embedded data should be immune to channel or processing distortions, such as channel noise, filtering, resampling, cropping, encoding, lossy compressing, printing, and scanning, digital-to-analog (D/A) conversion, and analog-to-digital (A/D) conversion, etc.

Therefore, tradeoffs often exist between the perceptibility of the embedded data and the quality of the subject signal in signal and transmitter identification techniques. By constraining the interference from the identification data to the subject signal, one can address a high identification information rate or a high subject signal quality even degraded by the embedded data, but not both. These two objectives always have to be in tradeoff. Meanwhile, the requirements for the identification information rate and the subject signal quality vary among different applications. Since linear identification techniques have been widely employed in wireless communications and digital signal processing area, we would like to exploit this important technique in this dissertation work. To the best of our knowledge, there hardly exists any theoretical framework to govern the relationship between the two aforementioned objectives, so does any efficient systematic algorithm to maneuver their tradeoff. We would like to dedicate this new research work to establish a remarkable milestone in the linear identification problem. To evaluate the effectiveness of our proposed approach, we present two applications, namely digital watermarking and transmitter identification, in this dissertation. The former application is quite popular in signal processing while the latter application is very useful in wireless communications. The further discussion on these two applications can be found in the subsequent section.

1.2 Potential Applications

Transmitter identification in *digital terrestrial television* (DTV) systems and *digital watermarking* problems will be investigated in this dissertation as two underlying applications. Digital communication is employed to transfer the digitalized data (a bit stream) from a geographical location to another over various physical transmission media. The examples of such media include copper wires, optical fibers, and wireless air interfaces [1, 2]. Besides the point-to-point transmission, multiple-access channels are also employed in digital communications, where there are potentially multiple transmitters and receivers often sharing a commonly-used medium. Therefore, the need for transmitter identification in multi-access systems becomes crucial nowadays. Transmitter identification (TxID, or *transmitter fingerprinting*) technique is used to detect, diagnose, and classify the operating status of any radio transmitter of interest [3]. In the DTV broadcasting, the transmitter ID (identification) information is added into the DTV transport data stream and it can be retrieved by demodulating the DTV signal. However, successful reception is not always guaranteed due to many reasons in the real scenario. The transmitter ID acquired this way only provides the identification of the transmitter associated with the strongest signal path. Therefore, the identification of a weak source signal is impossible [1, 4]. A new transmitter identification technique with the capability of identifying multiple transmitters in the ambient interference and noise is highly desired. Thus, a transmitter identification scheme has been proposed using the embedded *pseudo random sequences* recently [3]. A family of pseudo random sequences, Kasami sequences, have been used as the TxID signals in practice [4].

Moreover, the growth of digital imaging technology has drawn an urgent demand for the

techniques that can be employed for protecting the copyrights of images and videos [5–7]. Many approaches are available for copyrighting digital media. Conventional methods include *encryption*, *authentication*, and *time stamping*. Nowadays, the digital watermarking techniques are employed prevalently to prevent or deter unauthorized copying of digital media. Digital watermarking is the process of embedding identification information into a subject signal. The recipient can dewatermark the signal to verify its authenticity or its owner's identity. In digital watermarking, a subject signal may be audio, picture, or video and the subject signal may need to carry several watermarks at the same time.

1.3 Current State of Knowledge

1.3.1 Transmitter Identification

The modern digital terrestrial television and digital video broadcasting systems becomes crucial nowadays, since they have been deployed world-wide recently [8, 9]. In recent decades, various techniques have been proposed for transmitter identification in the DTV broadcasting field. For example, identification techniques such as *video watermarking* have been investigated [10]. The *Advanced Television Systems Committee* (ATSC) standards have been developed for digital television transmission over terrestrial, cable, and satellite networks in North America [11, 12]. The initial ATSC standard was generated in the early 1990s by the *Grand Alliance* [13].

On the other hand, Japanese information theorist Tadao Kasami built a new family of binary sequences called *Kasami sequences* in 1966 [14]. Kasami sequences are excellent candidates for the TxID sequences as they facilitate a large family of nearly-orthogonal

codes [14, 15]. Kasami sequences have period $N = 2^n - 1$, where n is a positive even integer. There are two classes of Kasami sequences: the *small set* and the *large set*. The large set contains all the sequences belonging to the small set. Although the small set of Kasami sequences can provide the better identification performance than the Kasami sequences from the large set due to their correlational properties, the total number of the pseudo-random sequences from the small Kasami set is limited. A transmitter identification system for a distributed DTV transmission network using embedded Kasami sequences has been investigated recently [3, 16]. The simulation results for evaluating the TxID system performance in a single-frequency network can be found in [4].

In [3], two essential properties of pseudo random sequences for transmitter identification are stated: (i) they are nearly orthogonal to each other; (ii) the pseudo random sequence is embedded into the DTV signal in a low power level so that the reception of the DTV signal will not be negatively affected. Thus, transmitter identification is processed simply by calculating the cross-correlation function between the received DTV signal and the originally embedded pseudo random sequence. In addition, the size of the pseudo random sequence set also needs to be considered since each sequence can be used only once to identify a particular TV channel in the world-wide area [3]. Therefore, a sufficient number of pseudo random sequences must be available in practice. Gold sequences (see [2, 17]) and Kasami sequences (see [14, 18]) are two excellent candidate sets for the TxID sequences as they are two large families of nearly-orthogonal codes. However, among all the existing pseudo-random sequences constructed from m-sequences (*maximum-length shift-register sequences*), only the small Kasami set is optimal in the sense of matching Welch's lower bound for the correlation functions [19]. Although the small set of Kasami sequences can provide

the better identification performance than the Kasami sequences from the large set due to their correlational properties, the total number of the pseudo random sequences from the small Kasami set is rather limited (similar restriction can be found for the Gold sequences). Therefore, Kasami sequences from the large set are employed as the most desirable pseudo random sequences for the transmitter identification of DTV signals. Since the transmitter identification technique is quite new in the digital video broadcasting research area, there still remain some interesting and important questions to be answered. In this dissertation, we would like to dedicate the fundamental theoretical exploration on the pseudo random sequence based TxID problems. We will try to answer the geometric capacity studies for TxID. The appropriate (minimum) pseudo random sequence length subject to a mandated received signal-to-interference ratio given a transmitter deployment topology will be studied in this thesis. In duality, the expected received signal-to-interference ratio given a transmitter deployment topology and the fixed TxID sequence length will be investigated here as well. Furthermore, the *buried ratio* or *injection level* of the embedded pseudo random sequences in DTV-TxID systems would affect the identification correctness and the DTV reception quality. Since both the correctness of transmitter identification and the reception quality of subject DTV signals need to be well addressed in practice, how to choose the proper buried ratio (injection level) must be in serious concern. Therefore, we thoroughly investigate this *injection-level optimization problem* for transmitter identification. Besides, some crucial questions emerge relevant to this topic. In this dissertation, we will establish the relationship between the signal-to-interference-plus-noise ratio for the TxID signal detection and the signal-to-interference-plus-noise ratio for the subject TV signal reception. We also attempt to figure out the appropriate TxID-sequence buried-ratio (injection-level)

to attain the optimal broadcasting performance given a transmitter deployment topology. In duality, the expected system performance given a transmitter deployment topology and the fixed TxID-sequence buried-ratio (injection-level) will be studied as well. Finally, we will propose the appropriate overall system performance measure to address both subject DTV signal reception and TxID signal detection and investigate the optimal solution to maximize this overall system performance measure.

1.3.2 Digital Watermarking

The prosperity of digital imaging technology leads to the broad demand for protecting the owners' copyrights [5–7]. A popular way to ensure the copyright authentication is to employ the "data concealing" techniques. Data concealing is the technology to embed a piece of information into the subject media data for some particular purposes. In this emerging field, *digital watermarking* and *steganograhpy* are the two prevalent techniques nowadays [20–22]. The digital watermark was firstly introduced in 1994 [23]. It is a signal that is embedded into a digital image or a video session to identify the ownership or provide any additional information regarding the content [24–26]. Many digital watermarking schemes for copyright protection have emerged in the recent decades [27–29]. There exist two common modalities for image watermarking, namely *spatial-domain watermarking* and *spatial-frequency-domain watermarking*. Since the former technique would lead to fair-quality watermarked signals, we adopt the latter approach as it is the mainstream watermarking technique in digital imaging applications. To facilitate a possible optimal spatial-frequency-domain watermarking technique, we focus on the *linear watermarking methodology* here because it is computationally efficient and very practical for the modern real-time signal processing applications [30].

Henceforth, we will provide the fundamental theoretical exploration on linear watermarking and make the first-ever attempt to deal with the corresponding optimization problem with respect to the crucial watermarking parameter, namely *scale-factor* [27, 31]. We will also attempt to design a new overall system performance measure for multiple-watermarking schemes. Furthermore, as a significant coefficient, the scale-factor in watermark injection has not been rigorously studied until now. The linear watermarking techniques and a novel optimal watermarking scheme will be presented in this dissertation. A new analysis for the signal-to-interference-plus-noise-ratios (SINRs) with respect to the subject signal and the watermark signal(s) will be carried out when multiple embedded watermarks are considered. We will also propose the objective quality measure for the digital watermarking applications, which essentially consists of both signal-to-interference-plus-noise-ratio for the subject signal and similarity coefficients for the watermarks. Furthermore, in order to optimize the aforementioned objective measure, we design a novel efficient optimization scheme, which can lead to the maximum overall SINR for both subject image signal and injected watermarks.

1.4 Dissertation Outline

The rest of this dissertation is organized as follows. The basic mathematical model of linear identification will be introduced in Chapter 2. The new linear identification studies for transmitter identification and digital watermarking are presented in Chapters 3 and 4, respectively. Finally, concluding remarks will be drawn in Chapter 5.

2. INTRODUCTION OF LINEAR IDENTIFICATION INJECTION

In a modern linear identification system, the specific *identification information* can be embedded into the subject signal in both the time- and frequency-domain. We denote $\mathbb{H}$ by the subject signal and $\mathbb{I}$ by the embedded identification information. Since the injection operation is linear, the digital signal with the embedded identification information can be expressed as

$$\mathbb{D} = \mathbb{H} + \mathbb{I}. \tag{2.1}$$

Meanwhile, we consider the injection level $\mathbb{L}$ as the weighting coefficient in the linear injection process since both the identification correctness and the subject signal quality should be addressed. We can rewrite Eq. (2.1) as

$$\mathbb{D} = \mathbb{H} + \mathbb{L} \cdot \mathbb{I}. \tag{2.2}$$

Moreover, multiple identification signals may often be embedded into the subject signal. Consequently, one can attain

$$\mathbb{D} = \mathbb{H} + \sum_{i=1}^{N} \mathbb{L}_i \cdot \mathbb{I}_i. \tag{2.3}$$

Note that $\mathbb{L}_i$ indicates the weighting coefficient for the i^{th} embedded information $\mathbb{I}_i$ and there are N identification signals in this linear injection. Therefore, we can investigate different applications based on the same linear injection model stated in this chapter. The weighting

coefficients $\mathbb{L}_i$, $i = 1, 2, \ldots, N$ are treated as the buried ratios (or injection levels) and the scale-factors for DTV TxID and digital watermarking applications, respectively.

3. TRANSMITTER IDENTIFICATION

The transmitter identification of the DTV systems is quite important nowadays. The pseudo random sequences are designed and embedded into the DTV signals prior to transmission [3]. Thus, their important mathematical properties can help us to study transmitter identification. As previously mentioned, Kasami sequences from the large set are the most desirable candidate family for the TxID of DTV signals.

This chapter is organized as follows. The optimization problem for transmitter identification will be formulated in Section 3.1. The mathematical properties of Kasami sequences and geometric studies for multi-transmitter identification using Kasami sequences will be introduced in Section 3.2. The new injection-level optimization studies for digital television transmitter identification systems and our proposed algorithms will be manifested in Section 3.3. The simulation results will be presented in Section 3.4. Conclusion will be drawn in Section 3.5

3.1 Problem Statement

Due to the rapid DTV development and the increasing number of DTV channels, the need for the television channel identification becomes an urgent issue. In the DTV applications, the transmitter identification refers to as the (static or mobile) station identification. The TxID information is added into the DTV transport data stream and it can be obtained by

demodulating the DTV signal. However, the successful reception of this TxID information is not always guaranteed due to many reasons in the real scenario. Hence, pseudo-random sequences were proposed to be embedded into the DTV signals prior to transmission. Alternatively, the transmitter identification can be realized by invoking the cross-correlation functions between the received signal and the possible candidates of the pseudo-random sequences [32]. The transmitter identification system is specified in the ATSC A/110 standard to allow the identification of the individual DTV transmitters and has been recognized as an essential feature in the ATSC Synchronization Standard for Distributed Transmission [3, 12]. The details for the data frame of the transmitted DTV signals and the injected pseudo-random sequences are presented in [3].

3.2 Geometric Capacity Studies for DTV Transmitter Identification Using Kasami Sequences

Digital terrestrial television broadcasters operate transmitters and receivers according to the geographic locations of their coverage areas. The distribution topologies of transmitters and receivers will affect the TxID sequences performance inevitably. We will propose new studies on the geometric capacity for DTV transmitter identification in different topological scenarios.

3.2.1 Introduction of Current Digital Terrestrial Television Systems

Transmitter identification plays an important role in the ATSC Synchronization Standard for Distributed Transmission. Figure 3.1 shows how every data frame is constructed for the DTV signal transmission [11]. According to Figure 3.1 and [11], a DTV data frame consists of two data fields, each containing 313 data segments. The first segment of each data field

is a unique synchronizing signal (Data Field Sync) and includes the training sequence to be used by the equalizer at the receiver. Each of the remaining 312 data segments carries the data from one 188-byte transport packet plus its associated FEC overhead. The actual data contained in each data segment comes from several transport packets because of data interleaving. Each data segment consists of 832 symbols. The first four symbols are transmitted in binary form to facilitate the segment synchronization data. This Data Segment Sync signal (the four symbols) also represents the sync byte of the 188-byte MPEG-compatible transport packet. The remaining 828 symbols of each data segment carry the remaining 187 bytes of a transport packet and its associated FEC overhead.

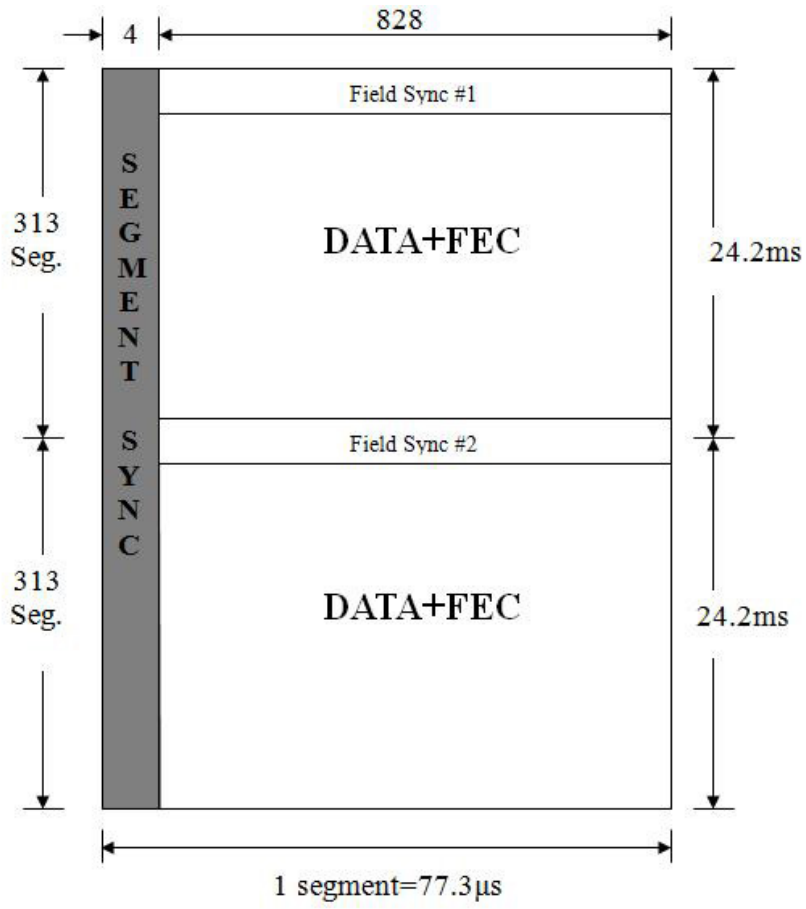

Figure 3.1: Data frame for the DTV signal transmission (FEC: forward error correction, sync: fields to be used for synchronization).

The illustration of the DTV signal with injected pseudo random sequences is shown in Figure 3.2.

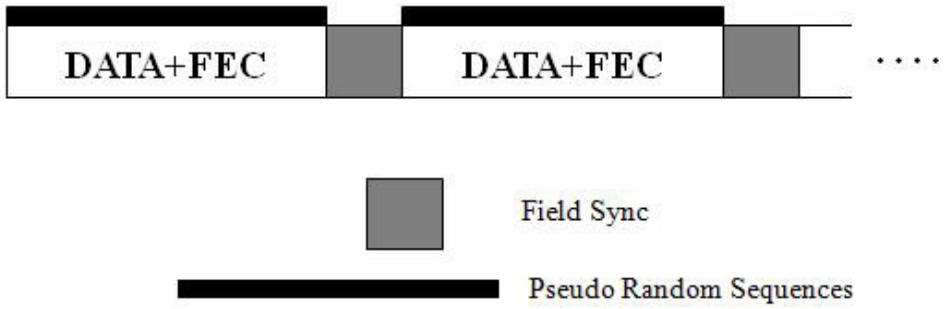

Figure 3.2: One field of the transmitted ATSC signal embedded with pseudo random sequences.

3.2.2 Mathematical Properties of Kasami Sequences

Kasami sequences are adopted as the TxID sequences in the modern DTV systems. Hence, we would like to introduce how to generate Kasami sequences and their essential mathematical properties for TxID in the following sections.

Algebraic Methods for Binary Sequence Construction

Binary sequences are important for spread-spectrum systems, code-division multiple-access (CDMA) systems and broadband satellite communications [33, 34]. Among all binary sequence families, those who have low non-zero-lag autocorrelation values, low cross-correlation values, large family size [35] and large linear span [36] are preferred in practice. These correlation properties are exploited to minimize the interference among the emitted signals so as to facilitate the signal detection even at the low signal-to-noise ratios [37–40].

Many binary sequences are built upon the elementary family, namely the maximal-length binary sequences (m-sequences). The m-sequences can be simply represented based on the trace function $tr_m^n(x) = \sum_{i=0}^{n-1} x^{2^{mi}}$, where $x \in GF(2^n)$ and $GF(2^n)$ denotes the finite field with (2^n) elements . Since the m-sequences have ideal autocorrelation properties, it is natural to study the cross-correlation function between an m-sequence and its decimations. Many families of low-correlation sequences have been constructed using m-sequences and their decimations [41, 42]. For example, the Gold sequence family [43, 44] was constructed from a pair of m-sequences given by

$$\{tr_1^n(x)\} \text{ and } \left\{tr_1^n(x^{2^k+1})\right\}. \tag{3.1}$$

For an odd n and an arbitrary integer k with gcd(n, k)=1. The small set of Kasami sequences can be constructed from

$$\{tr_1^n(x)\} \text{ and } \left\{tr_1^n(x^{2^{n/2}+1})\right\} \text{ for even } n. \tag{3.2}$$

The large set of Kasami sequences can be further extended here [34]. We assume that n is even and take k to satisfy gcd(k, n)=2 for odd $n/2$ or gcd(k, n)=1 for even $n/2$ where gcd denotes to greatest common divisor. The three m-sequences

$$\{tr_1^n(x)\}, \left\{tr_1^n(x^{2^k+1})\right\} \text{ and } \left\{tr_1^{n/2}(x^{2^{n/2}+1})\right\}. \tag{3.3}$$

can be used to obtain the large set of Kasami sequences [34]. The Gold sequence and Kasami sequences both can be constructed by the maximum-length sequences [45]. Often, maximal linear feedback shift registers are used for generating the maximum-length sequences. The resulting sequences are periodic and can be reproduced by the shift registers (i.e., a length-m register produces an m-sequence of length $2^m - 1$). The autocorrelation function of

a maximum-length sequence is very similar to a train of Kronecker delta functions. An example of maximum-length sequence generated by a shift register of length 4 is shown in Figure 3.3.

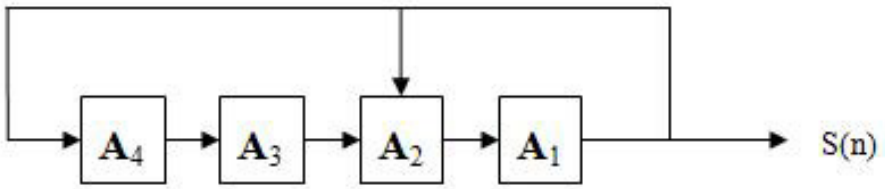

Figure 3.3: A maximum-length sequence generator of length 4.

The sequence generation illustrated by Figure 3.3 can be expressed as follows:

$$A_k[n+1] = \begin{cases} A_3[n] + A_1[n], k = 2 \\ A_{k+1}[n], \text{otherwise} \end{cases} \tag{3.4}$$

where n is the time index, k is the register position, and $+$ represents a modulo-2 addition.

Correlation Properties of m-sequences, Gold Sequences and Kasami Sequences

The arbitrary pair of m-sequences s_i and s_j lead to a three-valued cross-correlation over a code period $N = 2^n - 1$, which is given by

$$\rho_{ij}(\tau) = \begin{cases} -1, \\ -t(n), \\ t(n) - 2, \end{cases} \tag{3.5}$$

where $t(n) = 2^{(n+2)/2} + 1$ will serve as the backbone for the correlation properties of Gold sequences and Kasami sequences since the latter families are built upon the m-sequences. A Gold sequence is produced by the binary addition of two maximum-length sequences which have the same sequence length $N = 2^n - 1$. Gold sequences take advantage of the

fact that, the favorable correlation property of the resulted sequences is guaranteed because only the τ_1- and τ_2- step time-shifting operations and the modulo-2 addition are involved with two distinct m-sequences. Consider every unique combination of (τ_1, τ_2), which can engender a unique Gold sequence. Thus, a large number of distinct Gold sequences can be generated for the communications applications. However, the Gold sequences possess worse autocorrelation properties than the maximal-length sequences but better cross-correlation properties on the other hand. Similar to Eq. (3.5), an arbitrary pair of Gold sequences s_i and s_j lead to a three-valued cross-correlation over a code period $N = 2^n - 1$ [46]:

$$\rho_{ij}(\tau) = \begin{cases} -1, \\ -t(n), \\ t(n) - 2, \end{cases} \tag{3.6}$$

. where

$$t(n) = \begin{cases} 2^{(n+1)/2} + 1, \text{if } n \text{ is odd.} \\ 2^{(n+2)/2} + 1, \text{if } n \text{ is even.} \end{cases}$$

Besides, Kasami sequences have the similar correlation properties to the Gold sequences since they also arise from the maximum-length sequences. However, the Kasami sequences have an even better cross-correlation property than the Gold sequences. As mentioned in Section 3.2.1, there are two different sets of Kasami sequences, namely the large set and the small set. For an arbitrary pair of sequences s_i and s_j drawn from the small set of Kasami sequences, the autocorrelation and the cross-correlation over a code period $N = 2^n - 1$, both

can be characterized as the following three-valued function:

$$\rho_{ij}(\tau) = \begin{cases} -1, \\ -s(n), \\ s(n) - 2, \end{cases} \tag{3.7}$$

. where $s(n) = 2^{n/2} + 1$. Since $|s(n)| < |t(n)|$ according to Eqs. (3.6) and (3.7), Kasami sequences have better autocorrelation and cross-correlation properties than Gold sequences. In fact, Kasami sequences have excellent cross-correlation properties because they approach the Welch lower bound [1]. Hence, Kasami sequences are significantly effective for the transmission identification. Here, the Welch lower bound in [47] addresses that the cross-correlation value between any pair of binary sequences in a set consisting of M distinct sequences with the period N is bounded as

$$\phi_{max} \geq N\sqrt{\frac{M-1}{MN-1}}, \tag{3.8}$$

where ϕ_{max} specifies the maximum magnitude of any cross-correlation value among this set. The large set of Kasami sequences have a much larger population than that of the small set of Kasami sequences and hence the former can serve for a large capacity of users. The autocorrelation and the cross-correlation for the large set of Kasami sequences over a code period $N = 2^n - 1$ can be characterized as the following five-valued function:

$$\rho_{ij}(\tau) = \begin{cases} -t(n), \\ -s(n), \\ -1, \\ s(n) - 2, \\ t(n) - 2, \end{cases} \tag{3.9}$$

. where

$$t(n) = 1 + 2^{(n+2)/2}$$

and

$$s(n) = \frac{t(n) + 1}{2}$$

For example, a 16-bit Kasami sequence drawn from the large set can have the cross-correlation values as -513, -257, -1, 255, and 511 according to Eq. (3.9). For the auto-correlation values of an n-bit Kasami sequence, we can still employ to obtain the non-zero-lag values except that we have a constant value of $2^n - 1$ for the zero-lag autocorrelation. Note that the actual length for an "n-bit Kasami sequence" should be $2^n - 1$ due to the name convention by most literature. The family populations differ from the way of generating Kasami sequences. To generate the small set of Kasami sequences, we begin with a maximal-length sequence s of length $N = 2^n - 1$ where n is an even integer. A new shorter sequence s' (with length $2^{n/2} + 1$) can be formed by sampling every $2^{n/2} + 1$ elements of the original sequence s. The resulted sequence s' is periodic with a period of $2^{n/2} - 1$ thereby. Then we can generate the small set of Kasami sequences by taking the modulo-2 sum of s with all $(2^{n/2} - 1)$ cyclic shifts of s' including itself. The collection of all cyclic shifts of s' will form a new sequence of length $2^n - 1$.To obtain the Kasami sequences of the large set, we also take a maximal-length sequence s of length $N = 2^n - 1$ where n is an even integer. Similarly, two new shorter sequences s' and s" can be formed by sampling every $2^{n/2} + 1$ and every $2^{(n+2)/2} + 1$ elements, respectively. By taking the modulo-2 sum of s with all cyclic shifts of s' and s", we can generate the large set of Kasami sequences. The family size of the large-set Kasami

sequences is $2^{3n/2}$ if n is a multiple of 4 and $2^{3n/2} + 2^{n/2}$ if (n mod 4)=2.

Statistical Studies of the TxID Using Kasami Sequences

Following the discussion in Section 3.2.2, we would like to study and illustrate the correlation properties for the transmitter identification when the Kasami sequences are adopted for DTV systems. In this disseratation, we focus on the large set of Kasami sequences since it will be used in practice. All Kasami sequences are periodic. Hence, we need to study the periodic correlation functions. In general, the periodic correlation function $R_{i,j}(\tau)$ of the two binary sequences $s_i(t)$ and $s_j(t)$ of period $2^n - 1$ is defined as

$$R_{ij}(\tau) = \sum_{t=0}^{2^n-1} (-1)^{s_i(t)-s_j(t+\tau)}. \tag{3.10}$$

Kasami sequences from the large set as addressed in Section 3.2.2 are employed for the DTV transmitter identification. It can be verified that the cross-correlation values $R_{i,j}(\tau)$, $\forall \tau, i, j$, can only be either -513, -257, -1, 255 or 511 when $n = 16$.

3.2.3 Geometric Studies for Multi-Transmitter Identification Using Kasami Sequences

In the previous sections, we introduce the emerging need of the DTV transmitter identification and the adoption of the Kasami sequences mandated by the modern ATSC DTV standards. The correlational and statistical properties are also discussed therein. However, there hardly exists any geometric study on the capacity of the multiple transmitter identification using the Kasami sequences to the best of our knowledge. Hence we would like to address this important issue in this dissertation. Note that for simplification, here we only consider the *handshaking stage* when the continuous and periodic TxID sequences are sent

from the transmitters to the receiver.

Introduction of the Geometric Model for DTV TxID

Based on the mathematical properties and the relevant discussion stated in Section 3.2.2, new geometric studies of the multiple-transmitter-identification using Kasami sequences will be carried out in this section. Assume that several DTV signals are sent to one user (or station) simultaneously. The interference and noise need to be considered for the multi-transmitter identification thereby. For example, a television station dispatches several broadcasting vehicles for live news reports. Different DTV signals returned from different vehicles should be identified by the television station. In this dissertation, we assume that the omnidirectional antenna is used at the television station to sense the broadcasting vehicles for the worst scenario. Thus, the geometric model for this scenario is illustrated in Figure 3.4. The total

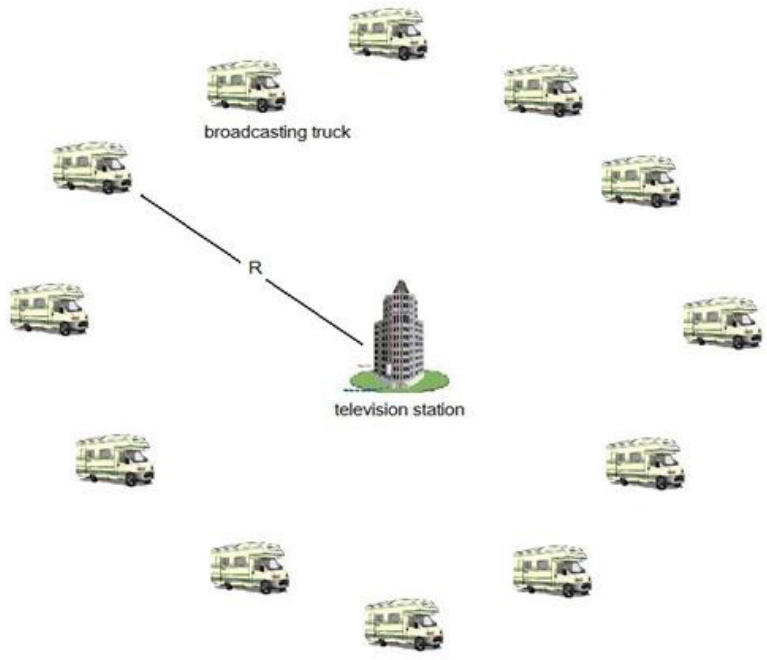

Figure 3.4: An example of geometric model for multiple-transmitter.

number of the transmitters is assumed to be L. Consider the subject transmitter (indexed by k_1) delivers its transmitter ID sequence $s_{k_1}(t)$ to the station. It will be interfered by the signal $s_{k_l}(t)$ sent by another transmitter (indexed by k_l and $l \neq 1$). For simplicity, we further assume that all transmissions occur in the open area such that no multiple paths exist. And consider the near-far problem, we employ d_{k_l} to indicate the distance from the transmitter to the station, where l is from 1 to L. Thus, for each broadcasting truck, the signal-to-interference ratio (SIR) can be defined as

$$SIR = \frac{\frac{1}{d_{k_1}^2}\frac{1}{d_{k_1}^2}R_{k_1k_1}(0)}{\sum_{l=2}^{L}\frac{1}{d_{k_1}^2}\frac{1}{d_{k_l}^2}R_{k_1k_l}(\tau_{1,l})} \tag{3.11}$$

where both $R_{k_1k_1}(0)$ and $R_{k_1k_l}(\tau_{1,l})$ are defined by Eq. (3.10) and $\tau_{l,l'}$ specifies the arrival time difference at the receiver between the l^{th} and the l'^{th} transmitted ID signals. The numerator in Eq. (3.11) refers to the autocorrelation of the subject broadcasting truck while the denominator refers to the summed cross correlation between the subject TxID sequence and the others.

Bounding Analysis of the Signal-to-Interference Ratio for Multiple-Transmitter ID Sequences

According to Eq. (3.11), we have the following bound for the SIR when the multiple TxID sequences are simultaneously sent, such that

$$\begin{aligned} SIR &= \frac{\frac{1}{d_{k_1}^2}\frac{1}{d_{k_1}^2}R_{k_1k_1}(0)}{\sum_{l=2}^{L}\frac{1}{d_{k_1}^2}\frac{1}{d_{k_l}^2}R_{k_1k_l}(\tau_{1,l})} \\ &\geq \frac{\frac{1}{d_{k_1}^2}\frac{1}{d_{k_1}^2}R_{k_1k_1}(0)}{\frac{1}{d_{k_1}^2}\frac{1}{d_{k_2}^2} \mid R_{k_1k_2}(\tau_{1,2}) \mid + \frac{1}{d_{k_1}^2}\frac{1}{d_{k_3}^2} \mid R_{k_1k_3}(\tau_{1,3}) \mid \ldots\ldots + \frac{1}{d_{k_1}^2}\frac{1}{d_{k_L}^2} \mid R_{k_1k_L}(\tau_{1,L}) \mid} \end{aligned} \tag{3.12}$$

For the worst scenario (lowest SIR bound given by Eq. (3.12)), we set $|R_{k_1k_l}(\tau_l)|$ as its maximum value $\mid -t(n) \mid = 1+2(n+2)/2, \forall l$, according the Eq. (3.9) and set $R_{k_1k_1}(0) = 2^n - 1$.

Thus,the inequality in Eq. (3.12) can be simplified as

$$SIR \geq \frac{\frac{1}{d_{k_1}^2}\frac{1}{d_{k_1}^2}(2^n - 1)}{\sum_{l=2}^{L}\frac{1}{d_{k_1}^2}\frac{1}{d_{k_l}^2}(1 + 2^{\frac{n+2}{2}})} \tag{3.13}$$

Note that Eq (3.13) can be utilized to measure the geometric capacity for sending multiple TxID sequences simultaneously in the same region.

An Example for 10 Transmitters within a Circular Area

In this subsection, we would like to present a simple example to illustrate the geometric studies of the TxID capacity. Assume that there are 10 broadcasting trucks (L=10) sent by the same TV station in the same circular area and the distance between each broadcasting truck and the TV station is equal to r (the radius of this circle), this simple model is shown in Figure 3.5. Small circles denote the transmitters' locations. According the geomet-

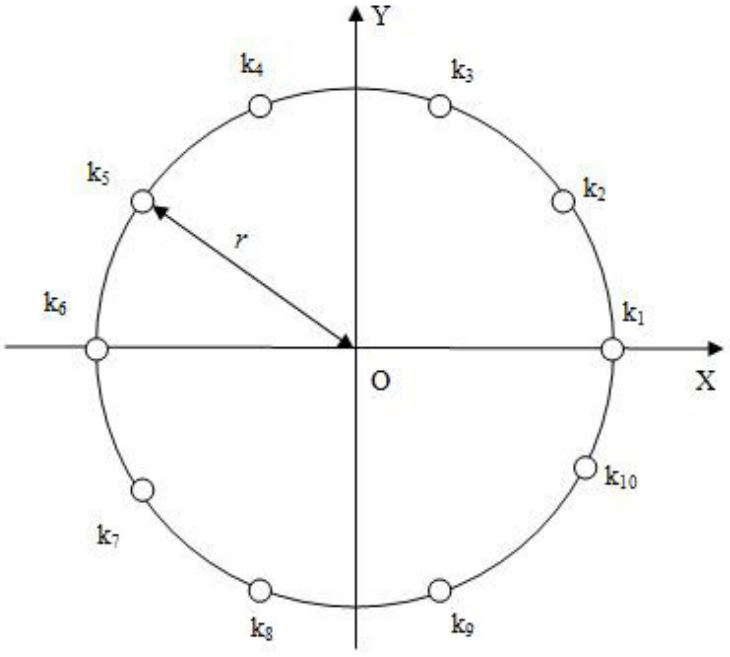

Figure 3.5: An example of 10 transmitters gathering within a circular area of radius r. Small circles denote the transmitters' locations.

ric layout of the multiple transmitters as depicted in Figure 3.5, Figure 3.6 illustrates the corresponding relationship between the SIR and the Kasami sequence length according to Eq. (3.13). Figure 3.7 demonstrates the same figure as Figure 3.6 while the SIR is measured in dB instead. Note that the SIR measures are considered at the receiver for the primary TxID purpose.

A minimum allowable SIR threshold is usually predetermined to guarantee the fidelity of

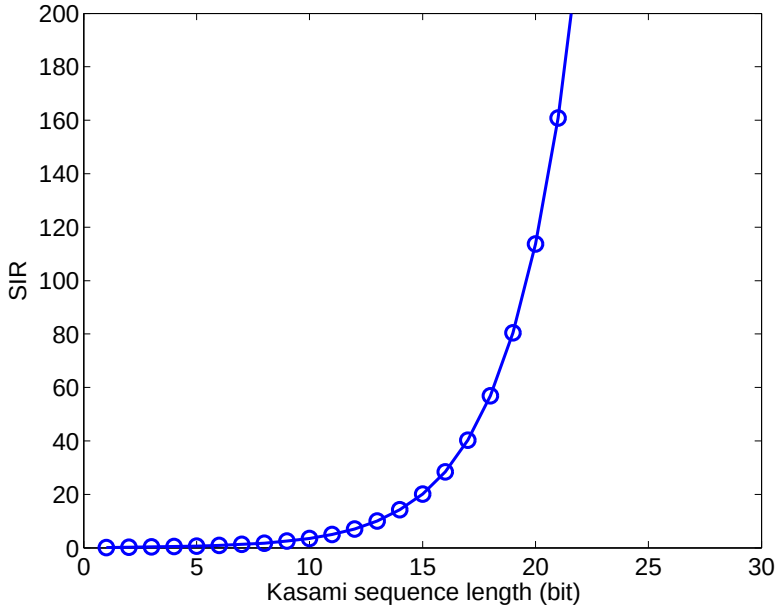

Figure 3.6: The relationship between the SIR and the Kasami sequence length for the multiple TX layout in Figure 3.5.

the received TxID sequences at the receiver. For instance, we take 10 dB as such an SIR threshold in practice. Therefore, for a satisfactory reception of DTV TxID signal, the SIR has to be larger than or equal to 10 dB for the reception of any transmitter ID sequence. Consequently, according to Figure 3.7, the Kasami sequence length has to be larger than 10 bits. The received SIR is 33.47dB when the Kasami sequence length is 16 bits, which greatly exceeds the minimum required SIR.

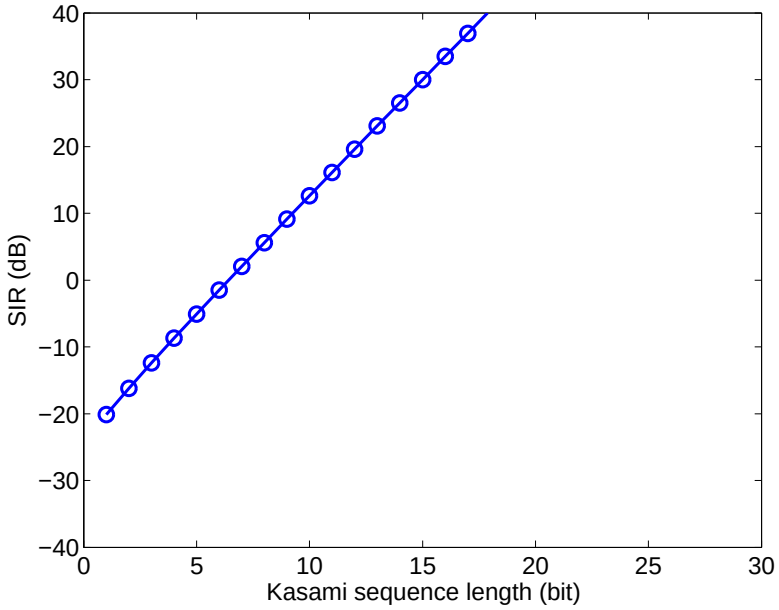

Figure 3.7: The relationship between the SIR (in dB) and the Kasami sequence length for the multiple TX layout in Figure 3.5.

Signal-to-Interference Ratio Analysis for Multiple TxID Transmission with Mobility

Assume that one of the transmitter, say k_l, in Figure 3.5 moves a distance D away from or toward the origin, where a negative D means that k_l moves into the circle of radius r and a positive D means that k_l moves out of this circle. Based on this mobility, we would like to study the impact on the received SIR of the multiple TxID transmission. Figure 3.8 illustrates this scenario.

Consider that the radius r is significantly larger than the height difference between any transmitter and the receiver; one ray model is therefore appropriate for our discussion. In the one ray model, we assume that is no obstruction between the receiver and any transmitter so that each ID signal propagates along a straight line to reach the station. Then the channel model is called line-of-sight (LOS), and the corresponding received signal is called the LOS signal or ray. In this type of LOS channels, the relationship between the transmitted signal

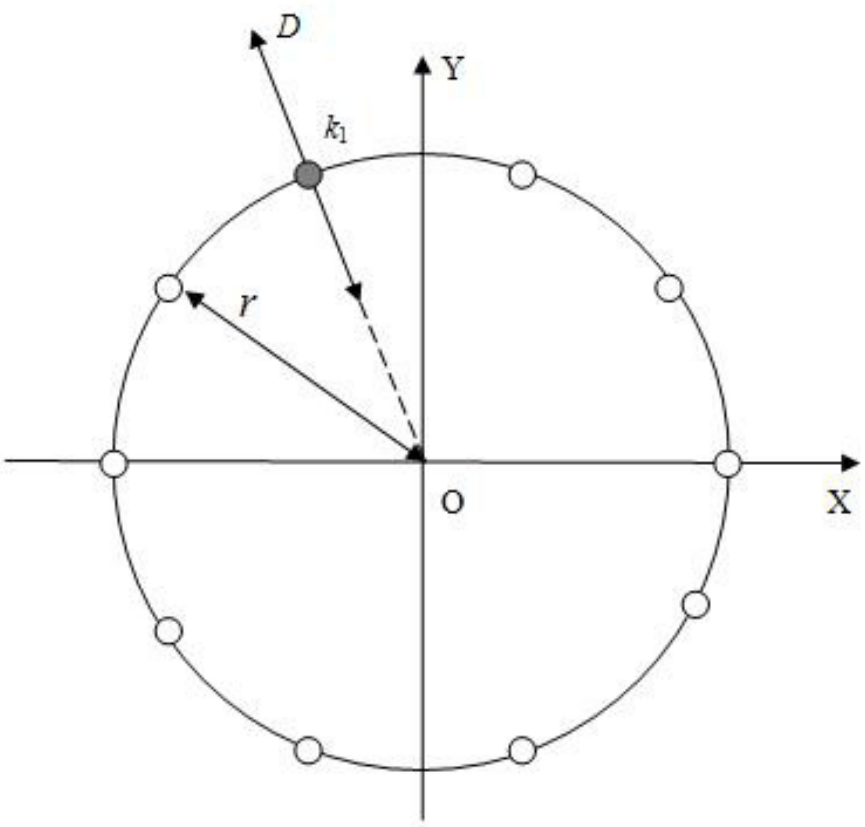

Figure 3.8: An example of the circularly employed transmitters with some mobility.

power P_t and the received signal power P_r with respect to the distance C between them is characterized as

$$\frac{P_r}{P_t} = \left[\frac{\sqrt{G_l}\lambda}{4\pi C}\right]^2 \tag{3.14}$$

where $\sqrt{G_l}$ is the product of the transmitting- and receiving-antenna field-radiation patterns along the LOS direction and λ is the signal wavelength [46]. From Eq. (3.14), we can derive the new expression of SIR when the mobility of a transmitter is addressed. Without loss of generality, we consider that the transmitter k_1 moves and tries to evaluate the SIR for the l^{th} received ID signal associated with the transmitter k_l, which is denoted by SIR_l ,

$l = 1, 2, \ldots, L$. For the transmitter k_1, we have

$$\begin{aligned} SIR_1 &\geq \frac{\frac{1}{(r+D)^2(r+D)^2} R_{k_1k_1}(0)}{\sum_{l=2}^{L} \frac{1}{(r+D)^2 r^2} R_{k_1k_1}(\tau_{1,l})} \\ &= \frac{\frac{1}{(r+D)^2} R_{k_1k_1}(0)}{\sum_{l=2}^{L} \frac{1}{r^2} R_{k_1k_1}(\tau_{1,l})} \\ &= \frac{r^2}{(r+D)^2} \frac{R_{k_1k_1}(0)}{\sum_{l=2}^{L} R_{k_1k_1}(\tau_{1,l})} \end{aligned} \tag{3.15}$$

For any other transmitter $k_l (l \neq 1)$, we have

$$\begin{aligned} SIR_l &\geq \frac{\frac{1}{r^2 r^2} R_{k_lk_l}(0)}{\frac{1}{(r+D)^2 r^2} R_{k_lk_1}(\tau_{l,1}) + \sum_{l'=2, l' \neq l}^{L} \frac{1}{r^2 r^2} R_{k_lk_{l'}}(\tau_{l,l'})} \\ &= \frac{\frac{1}{r^2} R_{k_lk_l}(0)}{\frac{1}{(r+D)^2} R_{k_lk_1}(\tau_{l,1}) + \sum_{l'=2, l' \neq l}^{L} \frac{1}{r^2} R_{k_lk_{l'}}(\tau_{l,l'})} \\ &= \frac{(r+d)^2 R_{k_lk_l}(0)}{r^2 R_{k_lk_1}(\tau_{l,1}) + \sum_{l'=2, l' \neq l}^{L} (r+d)^2 R_{k_lk_{l'}}(\tau_{l,l'})} \end{aligned} \tag{3.16}$$

where $R_{k_lk_{l'}}(\tau_{l'})$ refers to the cross-correlation between the transmitter k_l and a transmitter other than k_1. Consider the worst SIR scenario and choose the Kasami ID sequence of n bits according to Eqs. (3.12) and (3.13). SIR_l , $l = 1, 2, \ldots, L$, can be expressed as

$$SIR_l \geq \begin{cases} \frac{r^2}{(r+D)^2(L-1)} \frac{2^n - 1}{1 + 2^{\frac{n+2}{2}}}, l = 1 \\ \frac{(r+D)^2}{[r^2 + (L-2)(r+D)^2]} \frac{2^n - 1}{1 + 2^{\frac{n+2}{2}}}, l \neq 1 \end{cases} \tag{3.17}$$

where L is the total number of the transmitters and n is the bit-length of the Kasami ID sequences. Let's take an example here to illustrate Eq. (3.17). If $SIR_l \geq 10dB, \forall l$ are required, when $L = 10$ and $n = 16$, the range of D is given by

$$-0.5432r \leq D \leq 0.1914r. \tag{3.18}$$

Therefore, the allowable moving area for the transmitter k_1 to achieve $SIR_l \geq 10dB, \forall l$ is shown in Figure 3.9.

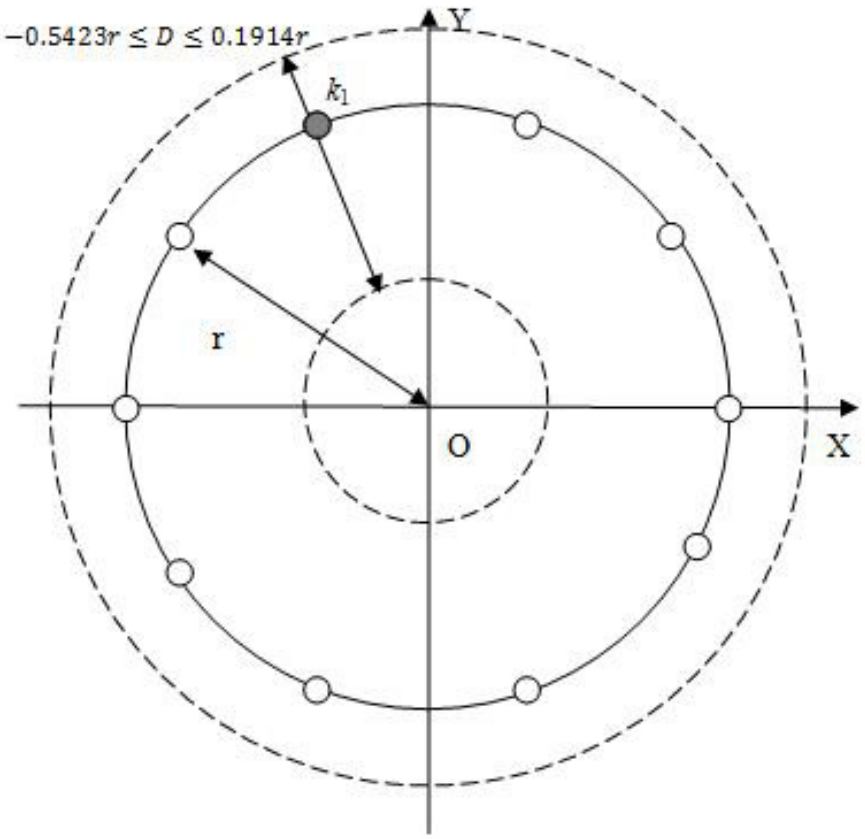

Figure 3.9: The allowable moving area for transmitter to achieve the required SIR.

Signal-to-Interference Ratio Analysis for Multiple TxID Transmission Subject to Different Topologies

In order to investigate the sensitivity of the transmitter identification in different topologies, we present the analysis here for four different geometric TX layouts, namely (i) circular distribution, (ii) doubly concentric and circular distribution, (iii) square array and (iv) hexagonal tessellation. They are discussed in the following subsections.

Transmission by Circularly Distributed Transmitters

Similar to Section 3.2.2, the circularly distributed transmitters ($L = 16$) transmitters as depicted in Figure 3.10 and 16-bit Kasami sequences from the large set are considered in

this example (Scenario I). In this section, d is always defined as the distance from the station to the nearest transmitter. Hence, d is the radius in Figure 3.10. From Figure 3.10,

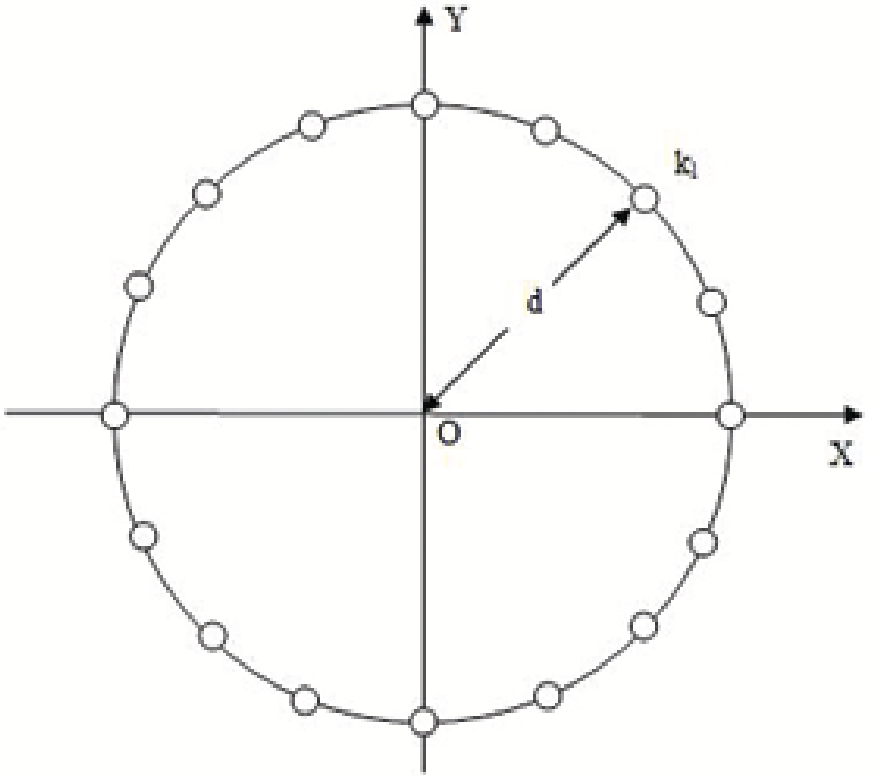

Figure 3.10: The transmitters are circularly distributed (Scenario I).

we can find that the received SIRs for all transmitters are the same. In Scenario I, for any transmitter, we have

$$\begin{aligned} SIR &\geq \frac{\frac{1}{d_{k_1}^2}\frac{1}{d_{k_l}^2}R_{k_1k_l}(0)}{15\cdot\frac{1}{d_{k_1}^2}\frac{1}{d_{k_l}^2}R_{k_1k_l}(\tau_{1,l})} \\ &= \frac{R_{k_1k_1}(0)}{15\cdot R_{k_1k_l}(\tau_{1,l})} \end{aligned} \tag{3.19}$$

where all d_{k_1}=d_{k_l}=d and $R_{k_1k_l}(\tau_{1,l})$ indicates the cross-correlation values between the different Kasami ID sequences which arrive at the receiver. For the worst situation, we set $R_{k_1k_l}(\tau_{1,l})$ as its maximum absolute value $|-t(n)| = 1+2^{(n+2)/2}$ and $R_{k_1k_1}(0)$ equals to 2^n-1 for

$n = 16$. Thus, we have the lower bound of any received SIR as

$$SIR \geq 8.5167. \tag{3.20}$$

Transmission by Doubly and Concentrically Circularly Distributed Transmitters

A more complex topology can be shown in Figure 3.11 (Scenario II).

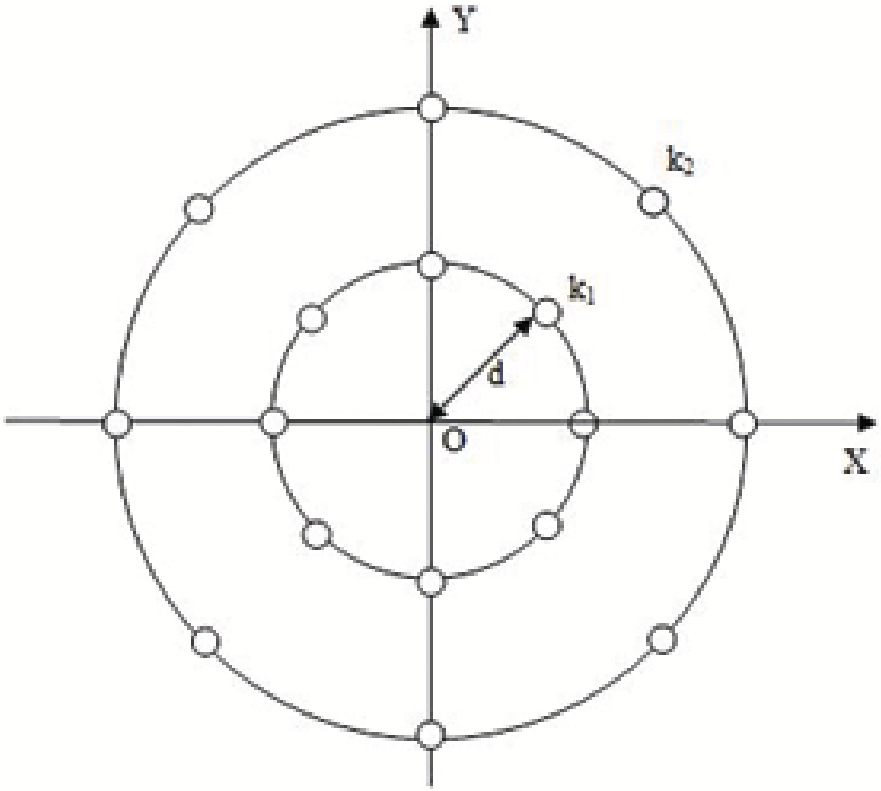

Figure 3.11: The transmitters are doubly- and concentrically-circularly distributed (Scenario II).

From Figure 3.11, we only need to consider two different sets of transmitters. Within each individual set, the received SIRs for all transmitters perform the isotropic property. Two arbitrary transmitters (k_1, k_2), each from an individual set, can be considered for the SIR analysis and they are illustrated in Figure 3.11. Note that d_{k_1}=d_{k_l}=d and d_{k_2}=$d_{k_{l'}}$=$2d$.

Consequently, for the any transmitter k_1 along the inner circle as depicted in Figure 3.11, we get

$$\begin{aligned} SIR_1 &\geq \frac{\frac{1}{d_{k_1}^2}\frac{1}{d_{k_1}^2}R_{k_1k_1}(0)}{7\cdot\frac{1}{d_{k_1}^2}\frac{1}{d_{k_l}^2}R_{k_1k_l}(\tau_{1,l})+8\cdot\frac{1}{d_{k_1}^2}\frac{1}{d_{k_{l'}}^2}R_{k_1k_{l'}}(\tau_{1,l'})} \\ &\geq \frac{R_{k_1k_1}(0)}{9\cdot R_{k_1k_l}^{max}}. \end{aligned} \tag{3.21}$$

where

$$R_{k_1k_l}^{max} = \max_{l,l',\tau_l}\left\{\mid R_{k_1k_l}(\tau_{1,l}) \mid, \mid R_{k_1k_{l'}}(\tau_{1,l'}) \mid\right\} \forall l, l'.$$

For the any transmitter k_2 along the outer circle as depicted in Figure 3.11, we get

$$\begin{aligned} SIR_2 &\geq \frac{\frac{1}{d_{k_2}^2}\frac{1}{d_{k_2}^2}R_{k_2k_2}(0)}{8\cdot\frac{1}{d_{k_2}^2}\frac{1}{d_{k_l}^2}R_{k_2k_l}(\tau_{2,l})+7\cdot\frac{1}{d_{k_2}^2}\frac{1}{d_{k_{l'}}^2}R_{k_2k_{l'}}(\tau_{2,l'})} \\ &\geq \frac{\frac{1}{16}R_{k_2k_2}(0)}{(2+\frac{7}{16})R_{k_2k_l}^{max}}. \end{aligned} \tag{3.22}$$

where

$$R_{k_2k_l}^{max} = \max_{l,l',\tau_l}\left\{\mid R_{k_2k_l}(\tau_{2,l}) \mid, \mid R_{k_2k_{l'}}(\tau_{2,l'}) \mid\right\} \forall l, l'. \tag{3.23}$$

For the worst situation, we set $R_{k_1k_l}^{max} = R_{k_2k_l}^{max} = \mid -t(n) \mid = 1 + 2^{(n+2)/2}$, and $R_{k_1k_1}(0) = R_{k_2k_2}(0) = 2^n - 1$ for $n = 16$. The SIR values for the transmitters k_1 and k_2 on the inner and outer circles, which are denoted by SIR_1 and SIR_2 respectively, are bounded as

$$SIR_1 \geq 14.1945, \tag{3.24}$$

$$SIR_2 \geq 3.2757, \tag{3.25}$$

Transmission by an Array of Transmitters

Now we consider another example where the transmitters are distributed in an array as depicted in Figure 3.12. Similar to the discussion in Section 3.2.2, we can categorize the transmitters into three isotropic groups. Within each group, we can arbitrarily pick up a transmitter to evaluate the received SIR for representing all other peer transmitters. For instance, three represented transmitters (k_1, k_2, k_3), each from an individual group, are illustrated in Figure 3.12. Note that d_{k_1}=d_{k_l}=d,d_{k_2}=$d_{k_{l'}}$=$\sqrt{5}d$ and d_{k_3}=$d_{k_{l''}}$=$3d$.

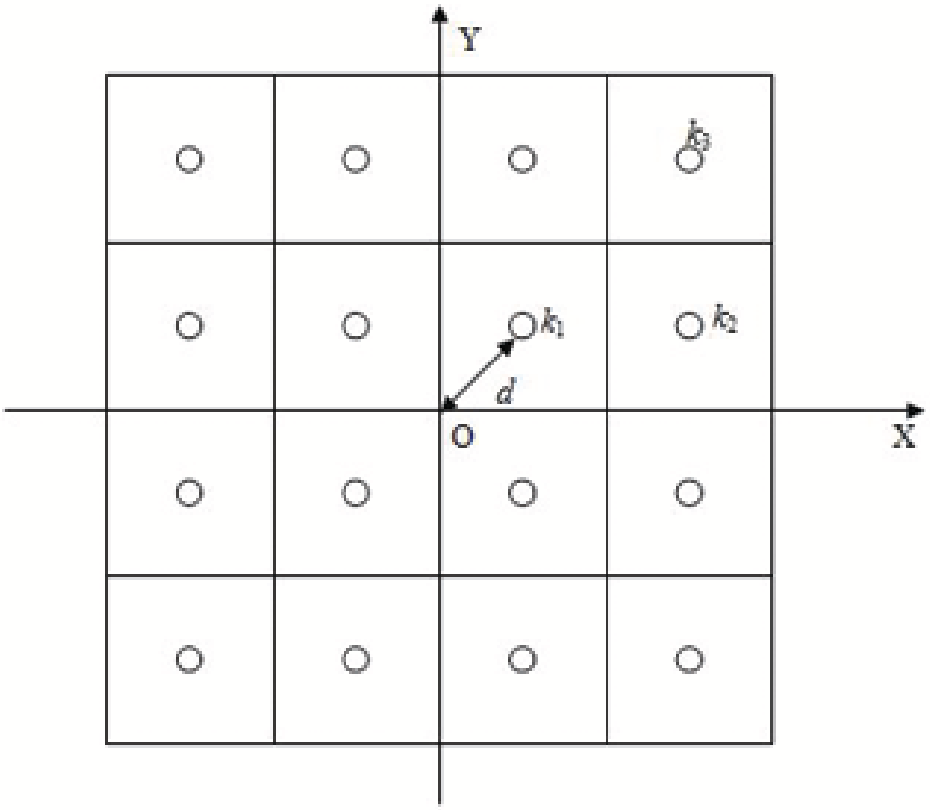

Figure 3.12: The transmitters are distributed in an array (Scenario III).

For any transmitter k_1 from Group 1, we get

$$\begin{aligned} SIR_1 &\geq \frac{\frac{1}{d_{k_1}^2}\frac{1}{d_{k_1}^2}R_{k_1k_1}(0)}{3\cdot\frac{1}{d_{k_1}^2}\frac{1}{d_{k_l}^2}R_{k_1k_l}(\tau_{1,l})+8\cdot\frac{1}{d_{k_1}^2}\frac{1}{d_{k_{l'}}^2}R_{k_1k_{l'}}(\tau_{1,l'})+4\cdot\frac{1}{d_{k_1}^2}\frac{1}{d_{k_{l''}}^2}R_{k_1k_{l''}}(\tau_{1,l''})} \\ &\geq \frac{R_{k_1k_1}(0)}{(3+\frac{8}{15}+\frac{4}{9})R_{k_1k_l}^{max}}. \end{aligned} \tag{3.26}$$

where

$$R_{k_1k_l}^{max}=\max\{\mid R_{k_1k_l}(\tau_{1,l})\mid,\mid R_{k_1k_l'}(\tau_{1,l'})\mid,\mid R_{k_1k_{l''}}(\tau_{1,l''})\mid\}\forall l,l',l''.$$

For any transmitter k_2 from Group 2, we can bound its SIR as

$$\begin{aligned} SIR_2 &\geq \frac{\frac{1}{d_{k_2}^2}\frac{1}{d_{k_2}^2}R_{k_2k_2}(0)}{4\cdot\frac{1}{d_{k_2}^2}\frac{1}{d_{k_l}^2}R_{k_2k_l}(\tau_{2,l})+7\cdot\frac{1}{d_{k_2}^2}\frac{1}{d_{k_{l'}}^2}R_{k_2k_{l'}}(\tau_{2,l'})+4\cdot\frac{1}{d_{k_2}^2}\frac{1}{d_{k_{l''}}^2}R_{k_2k_{l''}}(\tau_{2,l''})} \\ &\geq \frac{\frac{1}{25}R_{k_2k_2}(0)}{(\frac{4}{5}+\frac{7}{25}+\frac{4}{25})R_{k_2k_l}^{max}}. \end{aligned} \tag{3.27}$$

where

$$R_{k_2k_l}^{max}=\max\{\mid R_{k_2k_l}(\tau_{2,l})\mid,\mid R_{k_2k_{l'}}(\tau_{2,l'})\mid,\mid R_{k_2k_{l''}}(\tau_{2,l''})\mid\},\forall l,l',l''.$$

Finally, for any transmitter k_3 from Group 3, we can bound the corresponding SIR as

$$\begin{aligned} SIR_3 &\geq \frac{\frac{1}{d_{k_3}^2}\frac{1}{d_{k_3}^2}R_{k_3k_3}(0)}{4\cdot\frac{1}{d_{k_3}^2}\frac{1}{d_{k_l}^2}R_{k_3k_l}(\tau_{3,l})+8\cdot\frac{1}{d_{k_3}^2}\frac{1}{d_{k_{l'}}^2}R_{k_3k_{l'}}(\tau_{3,l'})+3\cdot\frac{1}{d_{k_3}^2}\frac{1}{d_{k_{l''}}^2}R_{k_3k_{l''}}(\tau_{3,l''})} \\ &\geq \frac{\frac{1}{81}R_{k_3k_3}(0)}{(\frac{4}{9}+\frac{8}{25}+\frac{3}{81})R_{k_3k_l}^{max}}. \end{aligned} \tag{3.28}$$

where

$$R_{k_3k_l}^{max}=\max\{\mid R_{k_3k_l}(\tau_{3,l})\mid,\mid R_{k_3k_{l'}}(\tau_{3,l'})\mid,\mid R_{k_3k_{l''}}(\tau_{3,l''})\mid\},\forall l,l',l''.$$

For the worst situation, we set

$$R_{k_1k_l}^{max}=R_{k_2k_l}^{max}=R_{k_3k_l}^{max}=\mid -t(n)\mid=1+2^{(n+2)/2},$$

and $R_{k_1k_1}(0) = R_{k_2k_2}(0) = R_{k_3k_3}(0) = 2^n - 1$ for $n = 16$. According to Eqs. (3.26), (3.27), and (3.28), we can have the numerical bounds for the SIRs of the transmitters belonging to each individual group as

$$SIR_1 \geq 25.3250, \tag{3.29}$$

$$SIR_2 \geq 4.3717, \tag{3.30}$$

$$SIR_3 \geq 2.3923. \tag{3.31}$$

Transmission by a Hexagonal Tessellation of Transmitters

The scenario has this kind of topological distribution and the Figure 3.13 is shown as below.

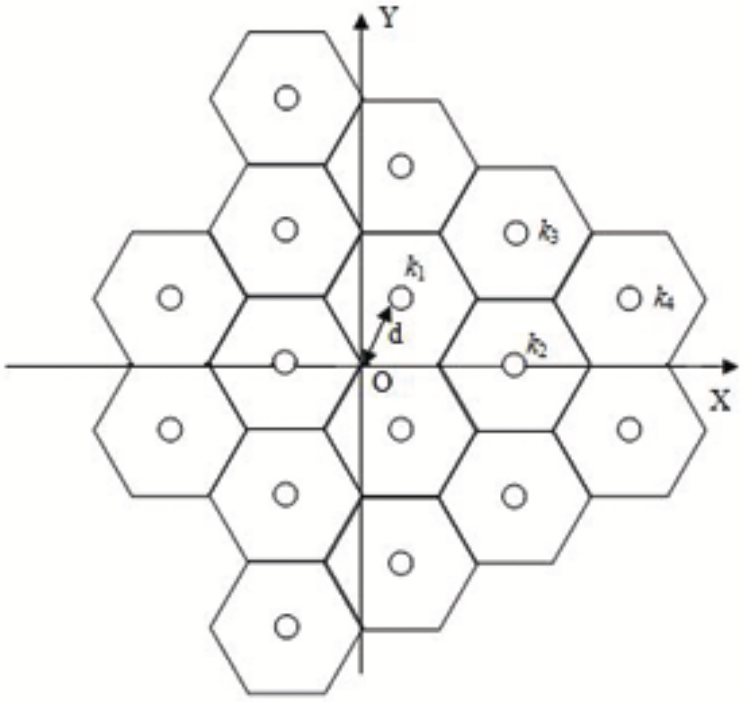

Figure 3.13: The transmitters are distributed in a hexagonal tessellation (Scenario IV).

Finally, we consider a topology depicted in Figure 3.13. From Figure 3.13, four isotropic groups of transmitters can be categorized similarly. We denote the transmitter indices (k_1, k_2, k_3, k_4), each drawn from an individual group, are illustrated in Figure 3.13. Note that d_{k_1}=d_{k_l}=d,d_{k_2}=$d_{k_{l'}}$=$2d$,d_{k_3}=$d_{k_{l''}}$=$\sqrt{7}d$ and d_{k_4}=$d_{k_{l'''}}$=$\frac{5}{\sqrt{2}}d$. For any transmitter k_1 from Group 1, we get

$$\begin{aligned} & SIR_1 \\ \geq & \frac{\frac{1}{d_{k_1}^2}\frac{1}{d_{k_1}^2}R_{k_1k_1}(0)}{2\cdot\frac{1}{d_{k_1}^2}\frac{1}{d_{k_l}^2}R_{k_1k_l}(\tau_{1,l})+3\cdot\frac{1}{d_{k_1}^2}\frac{1}{d_{k_{l'}}^2}R_{k_2k_{l'}}(\tau_{1,l'})+6\cdot\frac{1}{d_{k_1}^2}\frac{1}{d_{k_{l''}}^2}R_{k_1k_{l''}}(\tau_{1,l''})+4\cdot\frac{1}{d_{k_1}^2}\frac{1}{d_{k_{l'''}}^2}R_{k_1k_{l'''}}(\tau_{1,l'''})} \\ \geq & \frac{R_{k_1k_1}(0)}{(2+\frac{3}{4}+\frac{6}{7}+\frac{8}{25})R_{k_1k_l}^{max}} \end{aligned} \tag{3.32}$$

where

$$R_{k_1k_l}^{max}=\max\{|\ R_{k_1k_l}(\tau_{1,l})\ |,|\ R_{k_1k_{l'}}(\tau_{1,l'})\ |,|\ R_{k_1k_{l''}}(\tau_{1,l''})\ |,|\ R_{k_1k_{l'''}}(\tau_{1,l'''})\ |\},\forall l,l',l'',l'''.$$

For any transmitter k_2 from Group 2, we get

$$\begin{aligned} & SIR_2 \\ \geq & \frac{\frac{1}{d_{k_2}^2}\frac{1}{d_{k_2}^2}R_{k_2k_2}(0)}{3\cdot\frac{1}{d_{k_2}^2}\frac{1}{d_{k_l}^2}R_{k_2k_l}(\tau_{2,l})+2\cdot\frac{1}{d_{k_2}^2}\frac{1}{d_{k_{l'}}^2}R_{k_2k_{l'}}(\tau_{2,l'})+6\cdot\frac{1}{d_{k_2}^2}\frac{1}{d_{k_{l''}}^2}R_{k_2k_{l''}}(\tau_{2,l''})+4\cdot\frac{1}{d_{k_2}^2}\frac{1}{d_{k_{l'''}}^2}R_{k_2k_{l'''}}(\tau_{2,l'''})} \\ \geq & \frac{\frac{1}{16}R_{k_2k_2}(0)}{(\frac{3}{4}+\frac{1}{8}+\frac{3}{14}+\frac{2}{25})R_{k_2k_l}^{max}} \end{aligned} \tag{3.33}$$

where

$$R_{k_2k_l}^{max}=\max\{|\ R_{k_2k_l}(\tau_{2,l})\ |,|\ R_{k_2k_{l'}}(\tau_{2,l'})\ |,|\ R_{k_2k_{l''}}(\tau_{2,l''})\ |,|\ R_{k_2k_{l'''}}(\tau_{2,l'''})\ |\},\forall l,l',l'',l'''.$$

For any transmitter k_3 from Group 3, we get

$$\begin{aligned} & SIR_3 \\ \geq & \frac{\frac{1}{d_{k_3}^2}\frac{1}{d_{k_3}^2}R_{k_3k_3}(0)}{3\cdot\frac{1}{d_{k_3}^2}\frac{1}{d_{k_l}^2}R_{k_3k_l}(\tau_{3,l})+3\cdot\frac{1}{d_{k_3}^2}\frac{1}{d_{k_{l'}}^2}R_{k_3k_{l'}}(\tau_{3,l'})+5\cdot\frac{1}{d_{k_3}^2}\frac{1}{d_{k_{l''}}^2}R_{k_3k_{l''}}(\tau_{3,l''})+4\cdot\frac{1}{d_{k_3}^2}\frac{1}{d_{k_{l'''}}^2}R_{k_3k_{l'''}}(\tau_{3,l'''})} \\ \geq & \frac{\frac{1}{49}R_{k_3k_3}(0)}{(\frac{3}{7}+\frac{3}{28}+\frac{5}{49}+\frac{8}{175})R_{k_3k_l}^{max}} \end{aligned} \tag{3.34}$$

where

$$R_{k_3k_l}^{max}=\max\{\mid R_{k_3k_l}(\tau_{3,l})\mid,\mid R_{k_3k_{l'}}(\tau_{3,l'})\mid,\mid R_{k_3k_{l''}}(\tau_{3,l''})\mid,\mid R_{k_3k_{l'''}}(\tau_{3,l'''})\mid\},\forall l,l',l'',l'''.$$

For any transmitter k_4, we can bound its SIR as

$$\begin{aligned} & SIR_4 \\ \geq & \frac{\frac{1}{d_{k_4}^2}\frac{1}{d_{k_4}^2}R_{k_4k_4}(0)}{3\cdot\frac{1}{d_{k_4}^2}\frac{1}{d_{k_l}^2}R_{k_4k_l}(\tau_{4,l})+3\cdot\frac{1}{d_{k_4}^2}\frac{1}{d_{k_{l'}}^2}R_{k_4k_{l'}}(\tau_{4,l'})+6\cdot\frac{1}{d_{k_4}^2}\frac{1}{d_{k_{l''}}^2}R_{k_4k_{l''}}(\tau_{4,l''})+3\cdot\frac{1}{d_{k_4}^2}\frac{1}{d_{k_{l'''}}^2}R_{k_4k_{l'''}}(\tau_{4,l'''})} \\ \geq & \frac{\frac{4}{625}R_{k_4k_4}(0)}{(\frac{6}{25}+\frac{3}{50}+\frac{12}{175}+\frac{12}{625})R_{k_4k_l}^{max}} \end{aligned} \tag{3.35}$$

where

$$R_{k_4k_l}^{max}=\max\{\mid R_{k_4k_l}(\tau_{4,l})\mid,\mid R_{k_4k_{l'}}(\tau_{4,l'})\mid,\mid R_{k_4k_{l''}}(\tau_{4,l''})\mid,\mid R_{k_4k_{l'''}}(\tau_{4,l'''})\mid\},\forall l,l',l'',l'''.$$

For the worst situation, we set

$$R_{k_1k_l}^{max}=R_{k_2k_l}^{max}=R_{k_3k_l}^{max}=R_{k_4k_l}^{max}=\mid -t(n)\mid=1+2^{(n+2)/2},$$

and

$$R_{k_1k_1}(0)=R_{k_2k_2}(0)=R_{k_3k_3}(0)=R_{k_4k_4}(0)=2^n-1$$

for $n = 16$. According to Eqs. (3.32), (3.33), (3.34), and (3.35), we can bound the received SIRs for each group as

$$SIR_1 \geq 32.5301, \tag{3.36}$$

$$SIR_2 \geq 6.8284, \tag{3.37}$$

$$SIR_3 \geq 3.8146, \tag{3.38}$$

$$SIR_4 \geq 2.1085. \tag{3.39}$$

Assume that the radius for the coverage area by every broadcasting truck is d. We depict the relationships between the covered area and the lowest received SIR (absolute value or dB value) in Figures 3.14, 3.15.

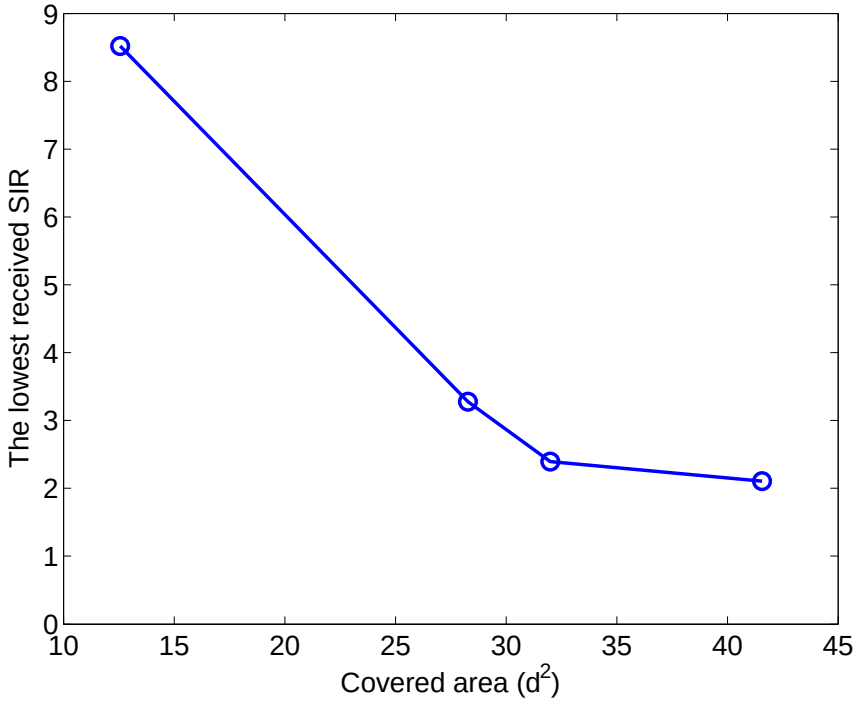

Figure 3.14: The relationship between the covered area and the lowest received SIR among four different layouts ($n = 16$).

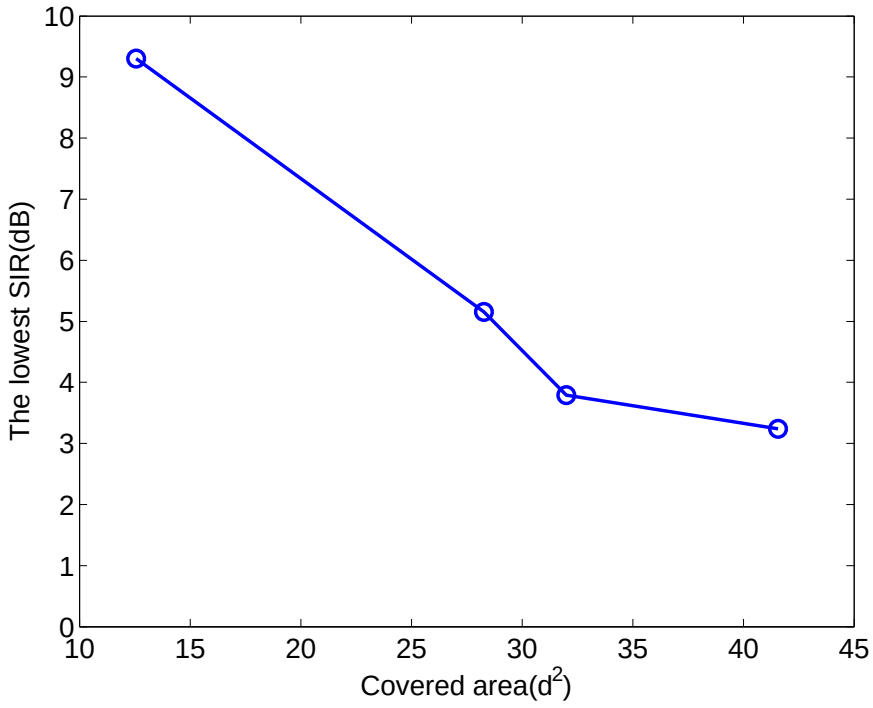

Figure 3.15: The relationship between the covered area and the lowest received SIR (in dB) among four different layouts ($n = 16$).

Comparative Studies for Different Kasami Sequence Lengths

Now we vary the Kasami sequence length ($n = 14, 18$) to follow Section 3.2.2 for the SIR analysis again. Different scenarios described in Section 3.2.2 are also considered here. We depict the relationships between the covered area and the lowest received SIR among the four aforementioned layouts (absolute value or dB value) for three different Kasami sequence lengths. According to Figures 3.16, we can find that the larger the Kasami sequence length, the larger the received SIR. However, the receiver processing time and complexity both are proportional to the ID sequence length and there should be some tradeoff to seek.

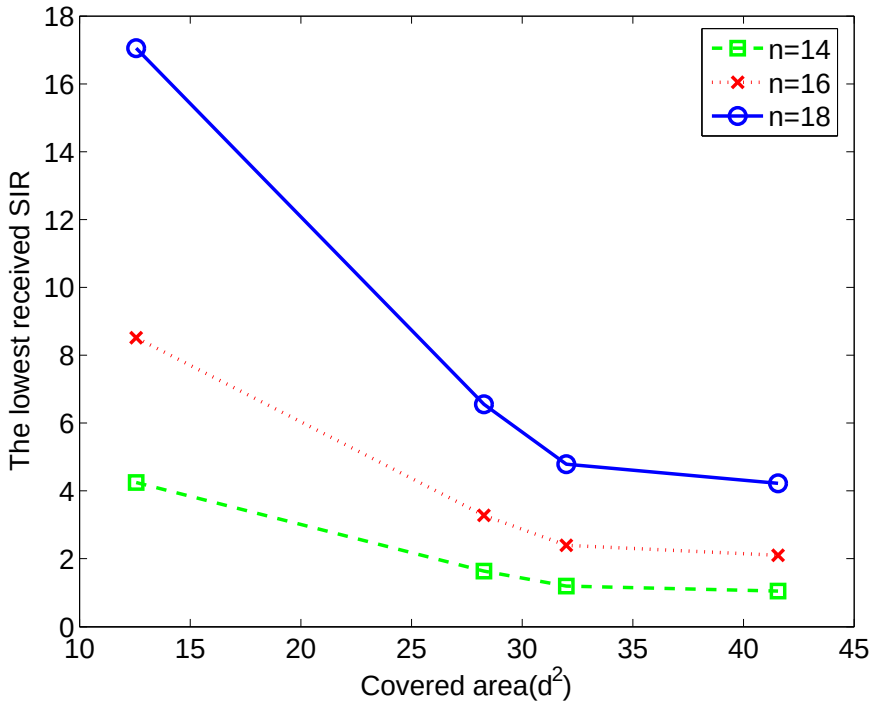

Figure 3.16: The relationship between the covered area and the lowest received SIR among all four layouts for three different Kasami sequence lengths.

3.3 On the Injection-Level Optimization for Digital Television Transmitter Identification Systems

In both analog and digital television broadcasting, *multiple-frequency networks* (MFNs) that assign different channels to each transmitter and receiver have been used to cover service areas [48, 49]. However, the use of MFNs is very inefficient in the aspect of spectrum occupancy since it is unable to share channels among a number of transmitters and receivers unless the distance between two coverage areas is far enough. Therefore, *single-frequency networks* (SFNs) that operate multiple transmitters and receivers on the same frequency are desirable for the efficient use of spectrum [4]. Especially, in the recent transition period from analog to digital broadcasting, the need of SFNs is unavoidable due to the lack of frequencies for additional transmitters and repeaters. SFNs provide not only high signal-to-noise ratios

(SNRs), but also the mobile DTV services [50]. SFNs are considered in terrestrial ATSC DTV services because they can improve the performance of DTV receivers which are able to remove strong multipath signals with long time delay [51]. In this dissertation, we will discuss the transmitter identification systems for DTV broadcasting under the SFNs. The transmitter identification sequences embedded into DTV signal are defined in the ATSC RP A/111 standard. Kasami sequences of the large set with period $n = 16$ are employed in DTV systems [52].

3.3.1 Principles of Transmitter Identification in DTV Systems

According to the ATSC standard, the output of the Kasami sequence generator shall be sent to the equivalent of a BPSK modulator for transmission with the 8-VSB subject signal. As depicted in Figure 3.17, the injection-level controller is employed to set the proper buried ratio (BR) for TxID.

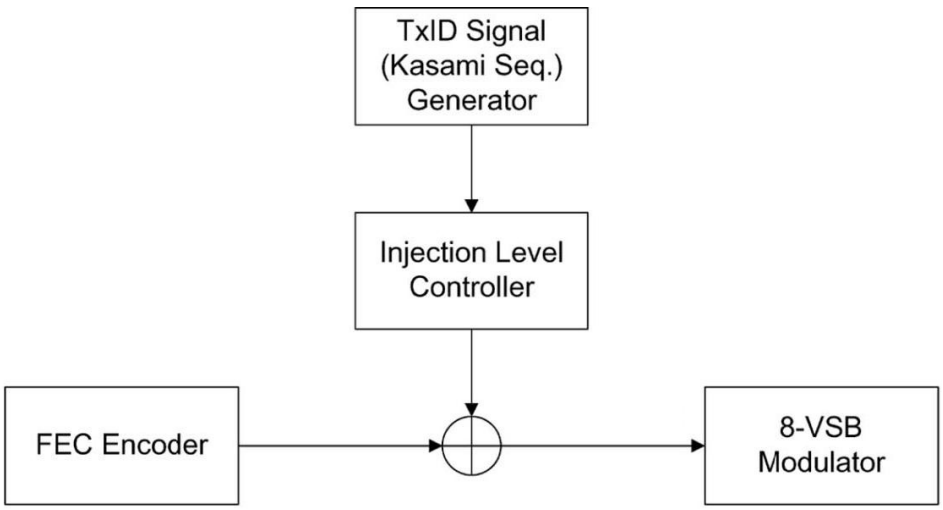

Figure 3.17: The illustration of the Kasami sequence insertion in a transmitter.

We denote $a_i(k)$ by the subject DTV signal and $s_i(k)$ by the embedded Kasami sequence corresponding to i-th transmitter, respectively, where λ_i indicates the ID sequence injection level. Consequently, the DTV signal with the embedded ID sequences $t_i(k)$ can be expressed as

$$t_i(k) = a_i(k) + \lambda_i s_i(k). \tag{3.40}$$

According to the signal model given by Eq. (3.40), the *average power ratio* of the injected Kasami sequences to the 8-VSB signals, referred to as BR φ, is defined as

$$\varphi \stackrel{\text{def}}{=} 10 \cdot \log_{10} \left(\frac{\lambda_i^2 \cdot \mathbb{E}\left\{ {s_i}^2(k) \right\}}{\mathbb{E}\left\{ {a_i}^2(k) \right\}} \right), \tag{3.41}$$

where $\mathbb{E}\{\ \}$ denotes the statistical expectation. Since the average powers $\mathbb{E}\{{a_i}^2(k)\}$, $\mathbb{E}\{{s_i}^2(k)\}$ of the 8-VSB signals and the BPSK modulated Kasami sequences are 21 and 1, respectively, the injection level λ_i according to Eq. (3.41) is

$$\lambda_i = \sqrt{\frac{21}{10^{-\varphi/10}}}. \tag{3.42}$$

3.3.2 New Studies for Kasami-Sequence Buried-Ratios

Based on the mathematical properties and the transmitter identification principle stated in Section 3.2.2 and Section 3.3.1, new geometric studies of the multiple-transmitter-identification using Kasami sequences involving buried ratio will be carried out in this section. Our proposed analysis here can be easily used for multiple-transmitter identification in any SFN. Assume that the total number of transmitters operating in the same area is L and an additive white Gaussian noise (AWGN) channel is present. The signal $r(k)$ obtained by the subject

receiver can be expressed as

$$r(k) = \sum_{i=1}^{L} t_i(k) + w(k), \tag{3.43}$$

where $w(k)$ is AWGN and $t_i(k)$ is defined by Eq. (3.40). For two signals (sequences) f and g, the cross-correlation operation is defined by

$$R_{f,g} = R_{f,g}(k) = f \star g \stackrel{\text{def}}{=} \sum_{m=-\infty}^{\infty} f(m)g(m+k). \tag{3.44}$$

According to Eq. (3.44), we often drop the argument (k) from the sequences for notional convenience. Hence we can easily read $R_{f,g} = R_{f,g}(k)$ and $f \star g = f(k) \star g(k)$.

In order to identify a transmitter, we undertake the correlation between the received signal and the candidate TxID sequence. Here we define the subject TxID sequence as $s_1(k)$. The correlation sequence between the received signal and the subject ID sequence R_{r,s_1} can thus be expressed as

$$\begin{aligned} R_{r,s_1} &= r(k) \star s_1(k) \\ &= \left[\sum_{i=1}^{L} t_i(k) + w(k)\right] \star s_1(k) \\ &= \sum_{i=1}^{L} \Big(a_i(k) + \lambda_i s_i(k)\Big) \star s_1(k) + w(k) \star s_1(k) \\ &= \big[\lambda_1 s_1(k) \star s_1(k)\big] + \sum_{i=2}^{L} \lambda_i s_i(k) \star s_1(k) + \sum_{i=1}^{L} a_i(k) \star s_1(k) + w(k) \star s_1(k) \end{aligned} \tag{3.45}$$

Consequently, we obtain the correlation sequence of two TxID sequences $s_i(k)$ and $s_j(k)$ with period $2^n - 1$ as

$$R_{s_i,s_j}(\tau) = s_i(k) \star s_j(k) = \sum_{k=0}^{2^n-1} (-1)^{s_i(k) \oplus s_j(k+\tau)}, \tag{3.46}$$

where $\bigoplus$ denotes an exclusive-OR operator. According to Eqs. (3.45) and (3.46), we get

$$R_{r,s_1} = \lambda_1 R_{s_1,s_1} + \sum_{i=2}^{L} \lambda_i R_{s_i,s_1} + \sum_{i=1}^{L} a_i(k) \star s_1(k) + w(k) \star s_1(k). \tag{3.47}$$

Note that the first term $\lambda R_{s_1,s_1}$ in Eq. (3.47) is the received subject TxID sequence energy while the other terms are all related to interference or noise. Therefore, the signal-to-interference-plus-noise ratio $SINR_{\text{TXID}}$ for transmitter identification can be defined as

$$\begin{aligned} SINR_{\text{TxID}} &\stackrel{\text{def}}{=} \frac{\lambda_1 \mathbb{E}\{R_{s_1,s_1}\}}{\sum_{i=2}^{L} \lambda_i \mathbb{E}\{R_{s_i,s_1}\} + \sum_{i=1}^{L} \mathbb{E}\{a_i(k) \star s_1(k)\} + \mathbb{E}\{w(k) \star s_1(k)\}} \\ &= \frac{\lambda_1 R_{s_1,s_1}}{\sum_{i=2}^{L} \lambda_i R_{s_i,s_1} + \sum_{i=1}^{L} \mathbb{E}\{a_i(k) \star s_1(k)\} + \mathbb{E}\{w(k) \star s_1(k)\}}. \end{aligned} \tag{3.48}$$

On the other hand, the subject DTV signal quality should be considered as well. We define $SINR^p_{\text{DTV}}$ as the signal-to-interference-plus-noise ratio for the p-th DTV signal transmission, $p = 1, 2, \ldots, L$. It is

$$SINR^p_{\text{DTV}} = \frac{\mathbb{E}\{{a_p}^2(k)\}}{\lambda_p^2 \, \mathbb{E}\{{s_p}^2(k)\} + \mathbb{E}\{w^2(k)\}}. \tag{3.49}$$

According to Eqs. (3.41), (3.42) and (3.49) , we have

$$\begin{aligned} SINR^p_{\text{DTV}} &= \frac{\mathbb{E}\{{a_p}^2(k)\}}{\lambda_p^2 \, \mathbb{E}\{{s_p}^2(k)\} + \mathbb{E}\{w^2(k)\}} \\ &= \left\{ \frac{\lambda_p^2 \, \mathbb{E}\{{s_p}^2(k)\}}{\mathbb{E}\{{a_p}^2(k)\}} + \frac{\mathbb{E}\{w^2(k)\}}{\mathbb{E}\{{a_p}^2(k)\}} \right\}^{-1} \\ &= \left\{ \frac{\lambda_p^2}{21} + \frac{\mathbb{E}\{w^2(k)\}}{\mathbb{E}\{{a_p}^2(k)\}} \right\}^{-1}. \end{aligned} \tag{3.50}$$

Obviously, we can define $\mathbb{E}\{{a_p}^2(k)\}/\,\mathbb{E}\{w^2(k)\}$ as the signal-to-noise ratio SNR_{SYS} in the DTV transmission system and measure it in practice.

Therefore, $SINR^{p}_{\mathrm{DTV}}$ for the p-th transmitter is given by

$$SINR^{p}_{\mathrm{DTV}} = \left\{ \frac{\lambda_p^2}{21} + \frac{1}{SNR_{\mathrm{SYS}}} \right\}^{-1}. \tag{3.51}$$

Consider that the broadcasting distance is significantly larger than the height difference between any transmitter and the receiver; one-ray model is therefore appropriate in our discussion. In the one-ray model, we assume that there is no obstruction between the receiver and any transmitter and hence each signal propagates along a straight line to reach the station. Meanwhile, for the DTV signal propagation, the path-loss exponent channel model is employed for our analysis. In the path-loss exponent model, the relationship between the transmitted signal power P_t and the received signal power P_r with respect to the distance d between them is characterized as

$$\frac{P_r}{P_t} = \kappa \left(\frac{d}{d_0} \right)^{\xi}, \tag{3.52}$$

where κ is a constant factor, d_0 is a reference distance, and ξ is the *path-loss exponent*. Path-loss exponent depends on carrier-frequency, environment, obstructions, etc. Typically, it ranges from 2 to 8. In our DTV broadcasting model, we choose $\xi = 2$ in the following studies.

For notational convenience, we define D_{pq} as

$$D_{pq} \stackrel{\mathrm{def}}{=} \frac{1}{d_{pq}^2}, \tag{3.53}$$

where d_{pq} is the distance between the p-th transmitter and the q-th receiver. According to Eqs. (3.48), (3.53), $SINR_{\mathrm{TxID}}$ from the p-th transmitter to the q-th receiver, can be rewritten

as

$$SINR_{\text{TxID}}^{pq} = \frac{D_{pq}\lambda_p R_{s_p,s_p}}{\sum\limits_{i\neq p}^{L} D_{iq}\lambda_i R_{s_i,s_p} + \sum\limits_{i=1}^{L} D_{iq}\mathbb{E}\{a_i(k) \star s_p(k)\} + \mathbb{E}\{w(k) \star s_p(k)\}}. \tag{3.54}$$

In order to investigate the TxID qualities in different scenarios, we present the definition $SINR_{\text{SYS}}$ here in order to carry out the optimization of the buried ratios in embedded sequences. It is

$$SINR_{\text{SYS}} \stackrel{\text{def}}{=} \prod_{p=1}^{L} \left\{ SINR_{\text{TxID}}^{pq} \times SINR_{\text{DTV}}^{p} \right\}. \tag{3.55}$$

Note that the overall system performance at the receiver to address both *subject TV signal reception quality* and *TxID signal detection quality* in balance can be well evaluated using our proposed measure given by Eq. (3.55). These two aforementioned major signal reception qualities in DTV systems can be related via the well-known convenient *additive separatability* in mathematics, once they are measured in the commonly-used quality unit, decibels. It yields

$$\log_{10}\left(SINR_{\text{SYS}}\right) = \sum_{p=1}^{L} \left\{ \log_{10}\left(SINR_{\text{TxID}}^{pq}\right) + \log_{10}\left(SINR_{\text{DTV}}^{p}\right) \right\}. \tag{3.56}$$

According to Eq. (3.56), the overall system performance $\log\left(SINR_{\text{SYS}}\right)$ (in dB) is the balance (addition) between the subject TV signal reception quality $\log\left(SINR_{\text{DTV}}^{p}\right)$ and the TxID signal detection quality $\log\left(SINR_{\text{TxID}}^{pq}\right)$. Consequently, the optimal buried ratios (or injection levels) for DTV TxID system in different scenarios can be undertaken. We may also define two relevant measures to (3.55) and (3.56), namely the *average system signal-to-interference-plus-noise ratio* $SINR_{\text{SYS,Ave}}$ as

$$SINR_{\text{SYS,Ave}} \stackrel{\text{def}}{=} \left[\prod_{p=1}^{L} \left\{ SINR_{\text{TxID}}^{pq} \times SINR_{\text{DTV}}^{p} \right\} \right]^{1/(2L)}, \tag{3.57}$$

and its logarithm as

$$\log_{10}\left(SINR_{\mathrm{SYS,Ave}}\right)=\frac{1}{2L}\sum_{p=1}^{L}\left\{\log_{10}\left(SINR_{\mathrm{TxID}}^{pq}\right)+\log_{10}\left(SINR_{\mathrm{DTV}}^{p}\right)\right\}. \tag{3.58}$$

3.3.3 TxID Study for Single-Transmitter-Single-Receiver Scenario

For the simplest scenario, we assume one transmitter and one receiver in the coverage area. According to Eqs. (3.51) and (3.54), we have

$$SINR_{\mathrm{DTV}}^{1}=\left\{\frac{\lambda_1^2}{21}+\frac{1}{SNR_{\mathrm{SYS}}}\right\}^{-1}, \tag{3.59}$$

and

$$\begin{aligned} SINR_{\mathrm{TxID}}^{11} &= \frac{D_{11}\lambda_1 R_{s_1,s_1}}{D_{11}\mathbb{E}\{a_1(k)+w(k)\}\star s_1(k)} \\ &= \frac{\lambda_1 R_{s_1,s_1}}{\mathbb{E}\{a_1(k)+w(k)\}\star s_1(k)}. \end{aligned} \tag{3.60}$$

Therefore, $SINR_{\mathrm{SYS}}$ for the single-transmitter-single-receiver system can be written as

$$\begin{aligned} SINR_{\mathrm{SYS}} &= SINR_{\mathrm{TxID}}^{11}\times SINR_{\mathrm{DTV}}^{1} \\ &= \frac{\lambda_1 R_{s_1,s_1}}{\mathbb{E}\{a_1(k)+w(k)\}\star s_1(k)}\cdot\left\{\frac{\lambda_1^2}{21}+\frac{1}{SNR_{\mathrm{SYS}}}\right\}^{-1} \\ &= \frac{R_{s_1,s_1}}{\mathbb{E}\{a_1(k)+w(k)\}\star s_1(k)}\cdot\left\{\frac{\lambda_1}{21}+\frac{1}{\lambda_1 SNR_{\mathrm{SYS}}}\right\}^{-1}. \end{aligned} \tag{3.61}$$

Since $\frac{R_{s_1,s_1}}{\mathbb{E}\{a_1(k)+w(k)\}\star s_1(k)}$ is a constant with respect to λ_1 obviously, we have

$$\max_{\lambda_1}\left(SINR_{\mathrm{SYS}}\right)=\max_{\lambda_1}\left\{\frac{\lambda_1}{21}+\frac{1}{\lambda_1 SNR_{\mathrm{SYS}}}\right\}^{-1}. \tag{3.62}$$

The optimal solution to Eq. (3.62) can be easily obtained as

$$\lambda_1^{\mathrm{opt}}=\sqrt{\frac{21}{SNR_{\mathrm{SYS}}}}. \tag{3.63}$$

For example, if $SNR_{\text{SYS}} = 20$ dB is given for a broadcasting area, the optimal injection level should be $\lambda_1^{\text{opt}} = \sqrt{\frac{21}{10^{20/10}}} = \sqrt{0.21} = 0.458$ accordingly.

The overall system performances in terms of $SINR_{\text{SYS,Ave}}$ versus different chosen injection levels λ_1 are depicted in Figure 3.18. Obviously, the best performance appears at $\lambda_1 = 0.458$.

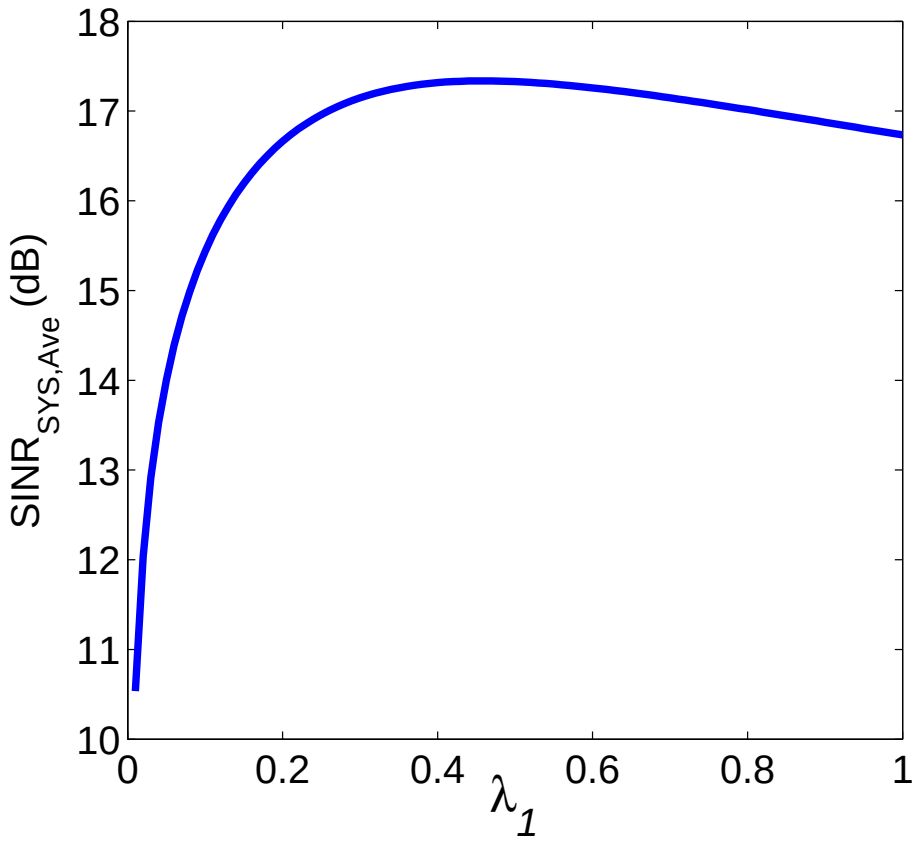

Figure 3.18: The overall system performances in terms of $SINR_{\text{SYS,Ave}}$ versus different chosen injection levels λ_1 (single-transmitter-single-receiver) for $SNR_{\text{SYS}} = 20$ dB.

3.3.4 TxID Study for Multiple-Transmitter-Single-Receiver Scenario

In this subsection, we would like to present a example for the TxID study for multiple-transmitter-single-receiver scenario. Assume that there are $L = 3$ transmitters which send DTV signals to the same receiver and the distance between each transmitter p and the receiver (indexed by 1) is equal to d_{p1}. This is shown in Figure 3.19, where the symbol "$\diamondsuit$" denotes the receiver and the symbol "$\times$" denotes a transmitter. For this particular

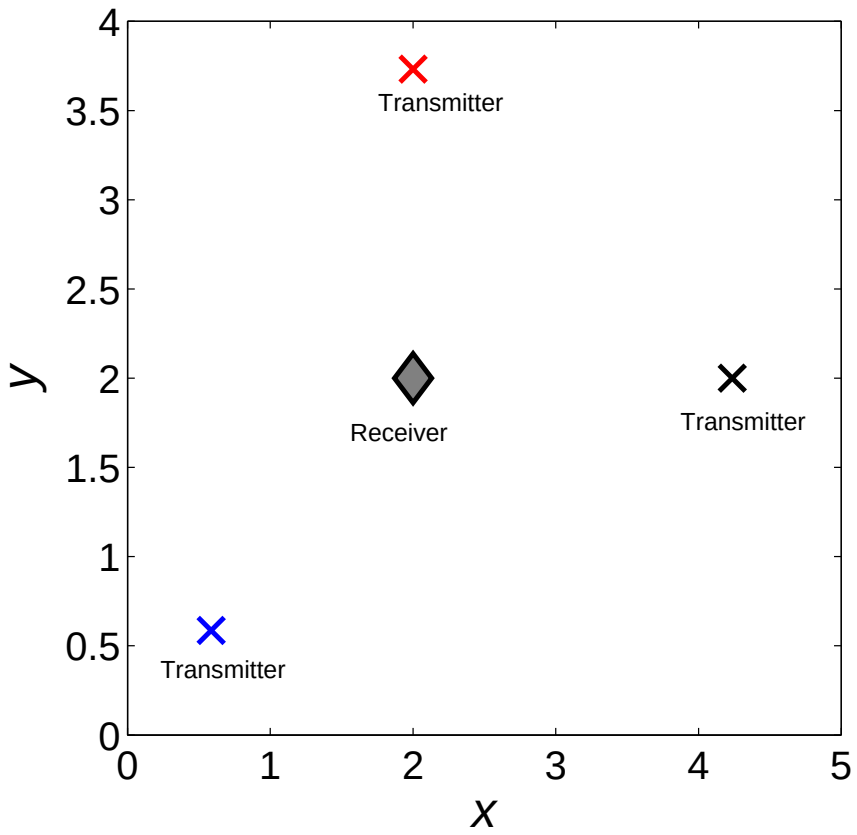

Figure 3.19: The broadcasting topology for a three-transmitters-single-receiver scenario.

broadcasting topology, we calculate the following crucial parameters for the TxID buried ratio optimization.

$$D_{11} = \frac{1}{d_{11}^2} = \frac{1}{3d_0^2}, \tag{3.64}$$

$$D_{21} = \frac{1}{d_{21}^2} = \frac{1}{4d_0^2}, \tag{3.65}$$

$$D_{31} = \frac{1}{d_{31}^2} = \frac{1}{5d_0^2}, \tag{3.66}$$

where d_0 is a reference distance. According to Eqs. (3.51) and (3.54), we get

$$SINR_{\text{DTV}}^1 = \left\{ \frac{\lambda_1^2}{21} + \frac{1}{SNR_{\text{SYS}}} \right\}^{-1}, \tag{3.67}$$

$$SINR_{\text{DTV}}^2 = \left\{ \frac{\lambda_1^2}{21} + \frac{1}{SNR_{\text{SYS}}} \right\}^{-1}, \tag{3.68}$$

$$SINR_{\text{DTV}}^3 = \left\{ \frac{\lambda_1^2}{21} + \frac{1}{SNR_{\text{SYS}}} \right\}^{-1}, \tag{3.69}$$

$$SINR_{\text{TxID}}^{11} = \frac{D_{11}\lambda_1 R_{s_1,s_1}}{D_{21}\lambda_1 R_{s_2,s_1} + D_{31}\lambda_1 R_{s_3,s_1} + \sum_{i=1}^{3} D_{i1}\mathbb{E}\{a_i(k) \star s_1(k)\} + \mathbb{E}\{w(k) \star s_1(k)\}}, \tag{3.70}$$

$$SINR_{\text{TxID}}^{21} = \frac{D_{21}\lambda_1 R_{s_2,s_2}}{D_{11}\lambda_1 R_{s_1,s_2} + D_{31}\lambda_1 R_{s_3,s_2} + \sum_{i=1}^{3} D_{i1}\mathbb{E}\{a_i(k) \star s_2(k)\} + \mathbb{E}\{w(k) \star s_2(k)\}}, \tag{3.71}$$

$$SINR_{\text{TxID}}^{31} = \frac{D_{31}\lambda_1 R_{s_3,s_3}}{D_{11}\lambda_1 R_{s_1,s_3} + D_{21}\lambda_1 R_{s_2,s_3} + \sum_{i=1}^{3} D_{i1}\mathbb{E}\{a_i(k) \star s_3(k)\} + \mathbb{E}\{w(k) \star s_3(k)\}}. \tag{3.72}$$

Here we assume that all transmitters adopt the same injection level for TxID. The 16-bit length Kasami sequence ($n = 16$) is employed for TxID. According to Eq. (3.9), we have

$$R_{s_p,s_q} = \begin{cases} 2^n - 1, & p = q \\ 1 + 2^{(n+2)/2}, & p \neq q \end{cases} \tag{3.73}$$

for the worst case. Since the subject DTV signal sequence $a_i(k)$ can be deemed random, it is modeled as a Gaussian process. Furthermore, we define

$$\mathbb{W}(k) \stackrel{\text{def}}{=} a_i(k) + \frac{1}{L} w(k). \tag{3.74}$$

Thus, $\mathbb{W}(k)$ is a new Gaussian process according to Eq. (3.74). We get

$$\sum_{i=1}^{L} D_{iq}\mathbb{E}\{a_i(k) \star s_p(k)\} + \mathbb{E}\{w(k) \star s_p(k)\} \approx \mathbb{E}\{\mathbb{W}(k)\} \star s_p(k) \sum_{i=1}^{L} D_{iq}. \tag{3.75}$$

Furthermore, we have $\mathbb{E}\{\mathbb{W}(k)\} \star s_p(k) = 1 + 2^{(n+2)/2}$ for the worst case in our study. For notational convenience, we denote

$$\mathbb{A} \stackrel{\text{def}}{=} 2^n - 1, \tag{3.76}$$

and

$$\mathbb{X} \stackrel{\text{def}}{=} 1 + 2^{(n+2)/2}. \tag{3.77}$$

According to Eq. (3.55), we have

$$SINR_{\text{SYS}} = SINR_{\text{TxID}}^{11}\, SINR_{\text{TxID}}^{21}\, SINR_{\text{TxID}}^{31}\, SINR_{\text{DTV}}^{1}\, SINR_{\text{DTV}}^{2}\, SINR_{\text{DTV}}^{3}. \tag{3.78}$$

Substituting Eqs. (3.64)-(3.77) into Eq. (3.78), we can rewrite the objective function for the buried-ratio optimization such that

$$\begin{aligned} SINR_{\text{SYS}} \;=\; & \frac{\frac{1}{3}\lambda_1\mathbb{A}}{\frac{1}{4}\lambda_1\mathbb{X} + \frac{1}{5}\lambda_1\mathbb{X} + (\frac{1}{3}+\frac{1}{4}+\frac{1}{5})\mathbb{X}} \times \frac{\frac{1}{4}\lambda_1\mathbb{A}}{\frac{1}{3}\lambda_1\mathbb{X} + \frac{1}{5}\lambda_1\mathbb{X} + (\frac{1}{3}+\frac{1}{4}+\frac{1}{5})\mathbb{X}} \\ & \times \frac{\frac{1}{5}\lambda_1\mathbb{A}}{\frac{1}{3}\lambda_1\mathbb{X} + \frac{1}{4}\lambda_1\mathbb{X} + (\frac{1}{3}+\frac{1}{4}+\frac{1}{5})\mathbb{X}} \times \left\{\frac{\lambda_1^2}{21} + \frac{1}{SNR_{\text{SYS}}}\right\}^{-3} \end{aligned} \tag{3.79}$$

Here we employ the 16-bit-length Kasami sequences ($n = 16$) for TxID. Assume $SNR_{\text{SYS}} =$ 20 dB for a broadcasting topology; we choose the optimal injection level $\lambda_1^{\text{opt}} = 0.38$ in order to maximize $SINR_{\text{SYS}}$. The overall system performances in terms of $SINR_{\text{SYS,Ave}}$ versus different chosen injection levels λ_1 are depicted in Figure 3.20. Obviously, the best performance appears at $\lambda_1 = 0.38$.

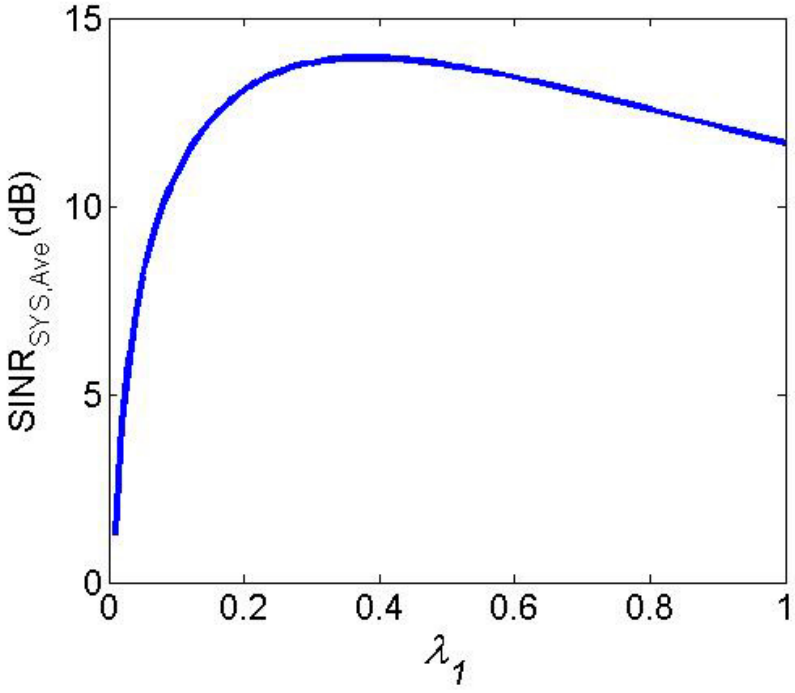

Figure 3.20: The overall system performances in terms of $SINR_{\text{SYS,Ave}}$ versus different chosen injection levels λ_1 (three-transmitters-single-receiver) for $SNR_{\text{SYS}} = 20$ dB.

3.3.5 TxID Study for Multiple-Transmitter-Multiple-Receiver Scenario

Finally, we would like to present the most complicated broadcasting scenario in this subsection, namely multiple-transmitter-multiple-receiver topology. Three transmitters and three receivers are spotted in a broadcasting area. Each transmitter sends DTV signal to its corresponding receiver individually and different transmitters adopt different buried ratios for TxID.

According to the scheme, we have

$$D_{pq} = \frac{1}{d_{pq}^2}, \quad 1 \leq p, q \leq 3. \tag{3.80}$$

This particular broadcasting topology is shown in Figure 3.21.

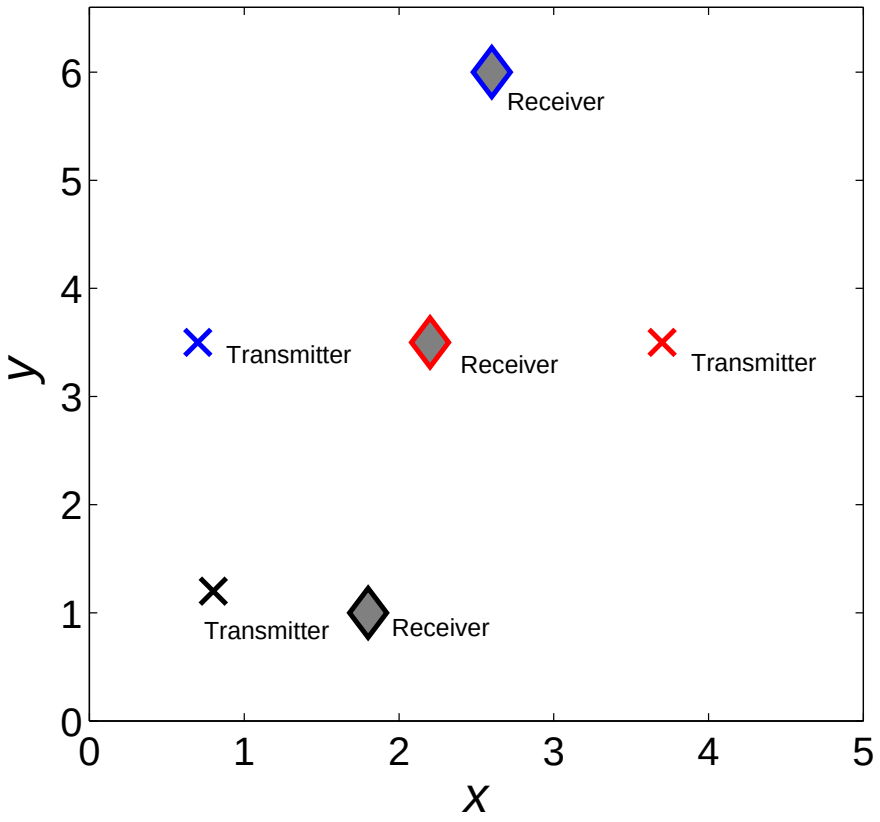

Figure 3.21: The broadcasting topology for a three-transmitters-three-receivers scenario.

Consequently, according to Eqs. (3.51) and (3.54), the individual signal-to-interference-plus-noise ratios are given by

$$SINR^{1}_{\mathrm{DTV}} = \left\{ \frac{\lambda_1^2}{21} + \frac{1}{SNR_{\mathrm{SYS}}} \right\}^{-1}, \tag{3.81}$$

$$SINR^{2}_{\mathrm{DTV}} = \left\{ \frac{\lambda_2^2}{21} + \frac{1}{SNR_{\mathrm{SYS}}} \right\}^{-1}, \tag{3.82}$$

$$SINR^{3}_{\mathrm{DTV}} = \left\{ \frac{\lambda_3^2}{21} + \frac{1}{SNR_{\mathrm{SYS}}} \right\}^{-1}, \tag{3.83}$$

$$SINR^{11}_{\mathrm{TxID}} = \frac{D_{11}\lambda_1 R_{s_1,s_1}}{D_{21}\lambda_2 R_{s_2,s_1} + D_{31}\lambda_3 R_{s_3,s_1} + \sum_{i=1}^{3} D_{i1}\mathbb{E}\{a_i(k) \star s_1(k)\} + \mathbb{E}\{w(k) \star s_1(k)\}}, \tag{3.84}$$

$$SINR_{\text{TxID}}^{22} = \frac{D_{22}\lambda_2 R_{s_2,s_2}}{D_{12}\lambda_1 R_{s_1,s_2} + D_{32}\lambda_3 R_{s_3,s_2} + \sum_{i=1}^{3} D_{i2}\mathbb{E}\{a_i(k) \star s_2(k)\} + \mathbb{E}\{w(k) \star s_2(k)\}}, \quad (3.85)$$

$$SINR_{\text{TxID}}^{33} = \frac{D_{33}\lambda_3 R_{s_3,s_3}}{D_{13}\lambda_1 R_{s_1,s_3} + D_{23}\lambda_2 R_{s_2,s_3} + \sum_{i=1}^{3} D_{i3}\mathbb{E}\{a_i(k) \star s_3(k)\} + \mathbb{E}\{w(k) \star s_3(k)\}}. \quad (3.86)$$

From the geometric layout of Figure 3.21, we obtain $D_{11} = 0.10d_0^{-2}$, $D_{12} = 0.44d_0^{-2}$, $D_{13} = 0.13d_0^{-2}$, $D_{21} = 0.13d_0^{-2}$, $D_{22} = 0.44d_0^{-2}$, $D_{23} = 0.10d_0^{-2}$, $D_{31} = 0.04d_0^{-2}$, $D_{32} = 0.14d_0^{-2}$, and $D_{33} = 0.91d_0^{-2}$.

According to Eq. (3.55), Eqs. (3.75)-(3.77) and Eqs. (3.81)-(3.86), we can get

$$\begin{aligned} SINR_{\text{SYS}} &= SINR_{\text{TxID}}^{11}\, SINR_{\text{TxID}}^{22}\, SINR_{\text{TxID}}^{33}\, SINR_{\text{DTV}}^{1}\, SINR_{\text{DTV}}^{2}\, SINR_{\text{DTV}}^{3} \\ &= \left\{\frac{\mathbb{A}}{\mathbb{X}}\right\}^3 \cdot \frac{0.10\lambda_1}{0.13\lambda_2 + 0.04\lambda_3 + 0.27} \cdot \frac{0.44\lambda_2}{0.44\lambda_1 + 0.14\lambda_3 + 1.02} \\ &\quad \times \frac{0.91\lambda_3}{0.13\lambda_1 + 0.10\lambda_2 + 1.14} \cdot \left\{\frac{\lambda_1^2}{21} + \frac{1}{SNR_{\text{SYS}}}\right\}^{-1} \\ &\quad \times \left\{\frac{\lambda_2^2}{21} + \frac{1}{SNR_{\text{SYS}}}\right\}^{-1} \cdot \left\{\frac{\lambda_3^2}{21} + \frac{1}{SNR_{\text{SYS}}}\right\}^{-1}. \end{aligned} \quad (3.87)$$

In order to attain the best overall system performance $SINR_{\text{SYS}}$, one has to optimize the individual injection levels λ_1, λ_2, and λ_3 in this example. On the other hand, we also need to ensure $SINR_{\text{TxID}}^{pq} \geq 2$, $1 \leq p, q \leq 3$ (see [53]) since the correctness of TxID must be considered simultaneously. Therefore, the constraints for this TxID injection-level optimization problem are given as follows:

$$\left(\frac{\mathbb{A}}{\mathbb{X}}\right) \cdot \frac{0.10\lambda_1}{0.13\lambda_2 + 0.04\lambda_3 + 0.27} \geq 2, \quad (3.88)$$

$$\left(\frac{\mathbb{A}}{\mathbb{X}}\right) \cdot \frac{0.44\lambda_2}{0.44\lambda_1 + 0.14\lambda_3 + 1.02} \geq 2, \quad (3.89)$$

$$\left(\frac{\mathbb{A}}{\mathbb{X}}\right) \cdot \frac{0.91\lambda_3}{0.13\lambda_1 + 0.10\lambda_2 + 1.14} \geq 2. \quad (3.90)$$

Here we employ the 16-bit length Kasami sequences ($n = 16$) for TxID. According to Eqs. (3.76) and (3.77), we can rewrite the constraints given by (3.88)-(3.90) as follows:

$$0.0203\lambda_1^{-1}\lambda_2 + 0.0063\lambda_1^{-1}\lambda_3 + 0.0422\lambda_1^{-1} \leq 1, \tag{3.91}$$

$$0.0156\lambda_1\lambda_2^{-1} + 0.0050\lambda_2^{-1}\lambda_3 + 0.0363\lambda_2^{-1} \leq 1, \tag{3.92}$$

$$0.0022\lambda_1\lambda_3^{-1} + 0.0017\lambda_2\lambda_3^{-1} + 0.0196\lambda_3^{-1} \leq 1. \tag{3.93}$$

Notes that $SINR_{\text{SYS}}$ is positive for all $\mathbf{\Lambda}$, where $\mathbf{\Lambda} = (\lambda_1, \lambda_2, \lambda_3)$. The optimal solution to minimize $\frac{1}{SINR_{\text{SYS}}}$ will also maximize $SINR_{\text{SYS}}$ as well. Therefore, we can transform the optimization problem into a *constrained geometric program*. The objective constrained geometric program (CGP) for this example can be expressed as follows:

$$\begin{aligned}
\text{CGP} \stackrel{\text{def}}{=} \quad & \arg\min_{\mathbf{\Lambda}} \quad g_0(\mathbf{\Lambda}) = \frac{1}{SINR_{\text{SYS}}} \\
& \text{subject to} \begin{cases} g_1(\mathbf{\Lambda}) = 0.0203\lambda_1^{-1}\lambda_2 + 0.0063\lambda_1^{-1}\lambda_3 + 0.0422\lambda_1^{-1} \leq 1, \\ g_2(\mathbf{\Lambda}) = 0.0156\lambda_1\lambda_2^{-1} + 0.0050\lambda_2^{-1}\lambda_3 + 0.0363\lambda_2^{-1} \leq 1, \\ g_3(\mathbf{\Lambda}) = 0.0022\lambda_1\lambda_3^{-1} + 0.0017\lambda_2\lambda_3^{-1} + 0.0196\lambda_3^{-1} \leq 1, \end{cases} \\
& \text{where } \lambda_1 > 0, \lambda_2 > 0, \lambda_3 > 0.
\end{aligned} \tag{3.94}$$

According to the *extended arithmetic-geometric mean inequality*, we can find the feasible solution for the CGP above (see Section 5).

3.4 Simulation

Assume $SNR_{\text{SYS}} = 20$ dB; we get the optimal solutions $\lambda_1^{\text{opt}} = 0.38$, $\lambda_2^{\text{opt}} = 0.38$, and $\lambda_3^{\text{opt}} = 0.42$ to maximize $SINR_{\text{SYS}}$. Figure 3.22 illustrates the TxID performance in terms

of the cross-correlation function R_{r,s_i}, $i = 1, 2, 3$, versus the time lag t for $SNR_{\text{SYS}} = 20$ dB, $\lambda_1^{\text{opt}} = 0.38$, $\lambda_2^{\text{opt}} = 0.38$, and $\lambda_3^{\text{opt}} = 0.42$.

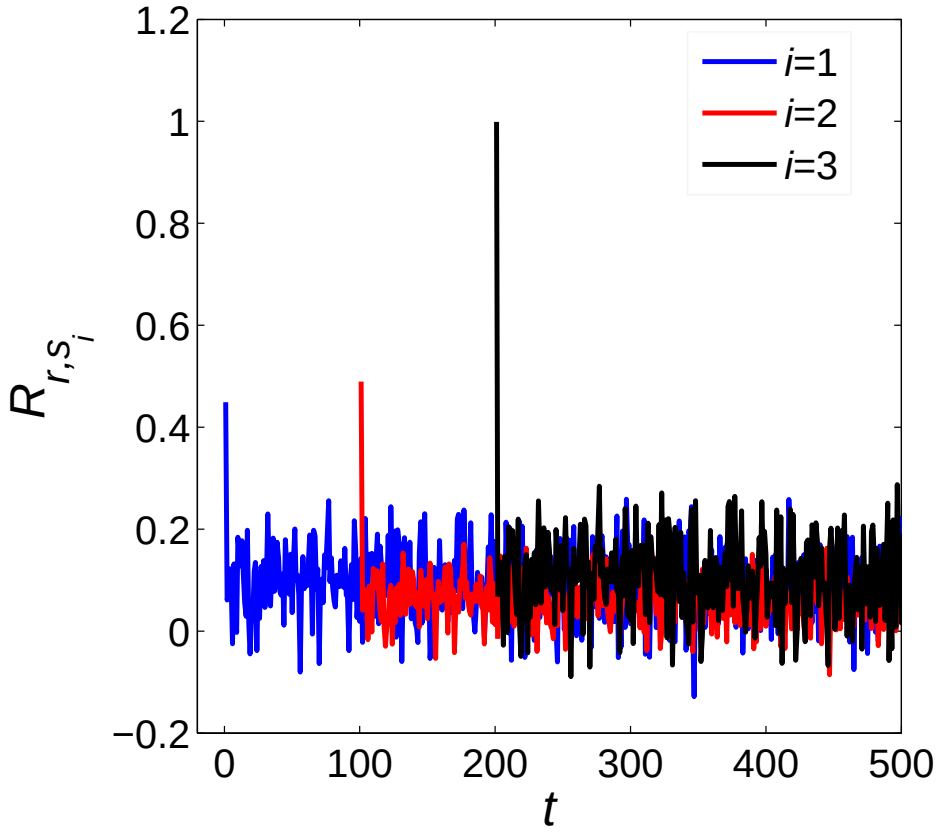

Figure 3.22: The TxID performances in terms of the cross-correlation functions R_{r,s_i}, $i = 1, 2, 3$, versus the time lag t for $SNR_{\text{SYS}} = 20$ dB, $\lambda_1^{\text{opt}} = 0.38$, $\lambda_2^{\text{opt}} = 0.38$, and $\lambda_3^{\text{opt}} = 0.42$ (three-transmitters-three-receivers).

Moreover, the overall system performances in terms of $SINR_{\text{SYS,Ave}}$ versus different chosen injection levels are delineated in Figures 3.23-3.25. In Figure 3.23, we fix $\lambda_2 = 0.38$, $\lambda_3 = 0.42$ and vary λ_1 to calculate $SINR_{\text{SYS,Ave}}$ thereupon. In a similar manner, we fix $\lambda_1 = 0.38$, $\lambda_3 = 0.42$ and vary λ_2 to depict $SINR_{\text{SYS,Ave}}$ in Figure 3.24; we also fix $\lambda_1 = 0.38$, $\lambda_2 = 0.38$ and vary λ_3 to depict $SINR_{\text{SYS,Ave}}$ in Figure 3.25.

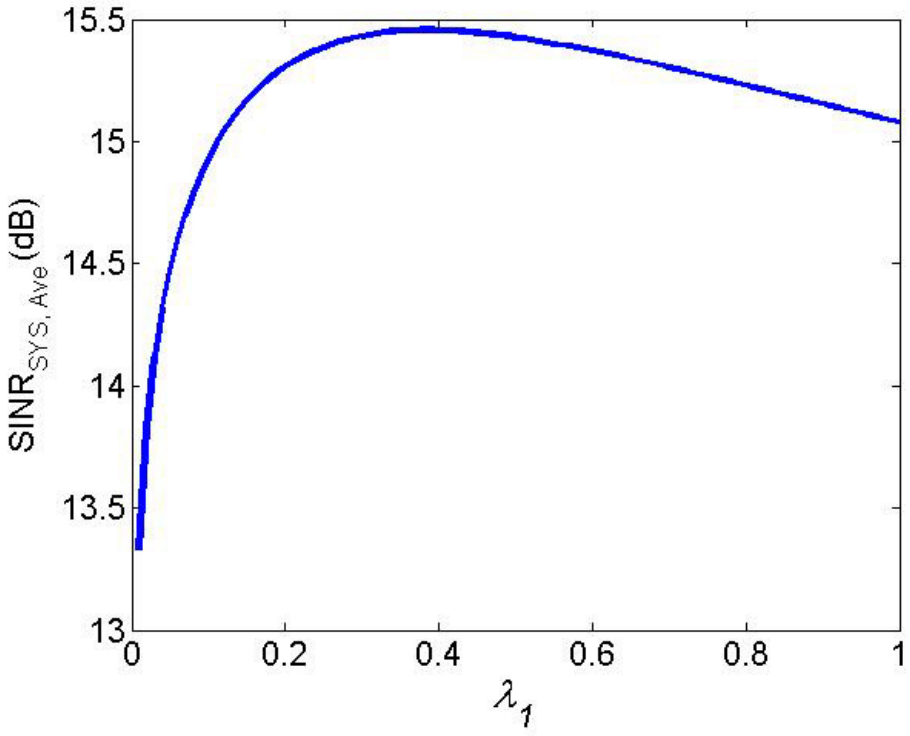

Figure 3.23: The overall system performances in terms of $SINR_{\mathrm{SYS,Ave}}$ versus different chosen injection levels λ_1 (three-transmitters-three-receivers) for $SNR_{\mathrm{SYS}} = 20$ dB, λ_2=0.38, and λ_3=0.42.

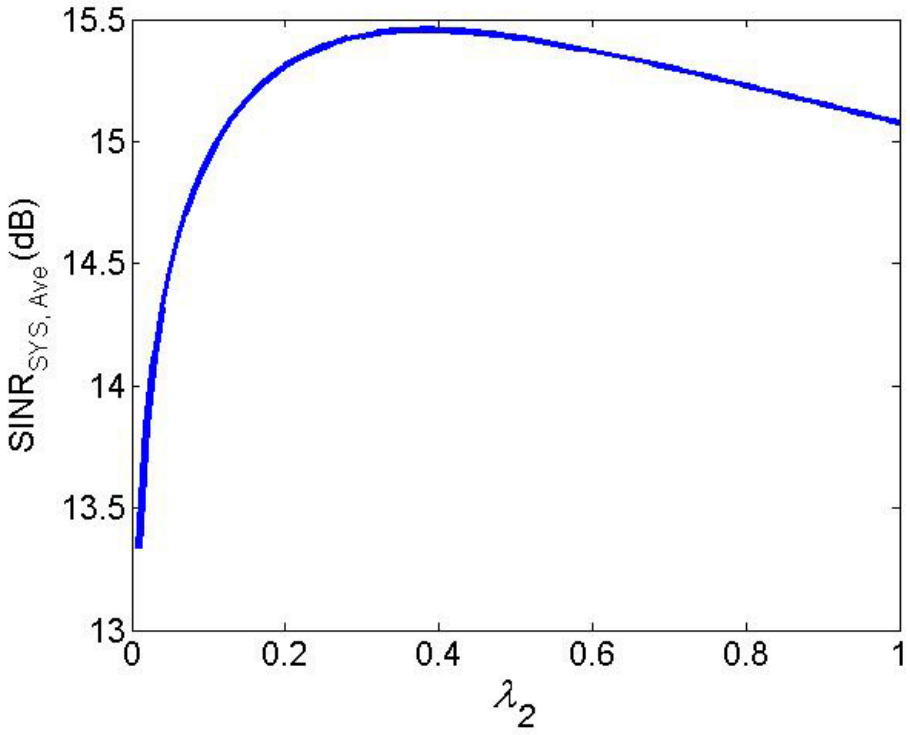

Figure 3.24: The overall system performances in terms of $SINR_{\mathrm{SYS,Ave}}$ versus different chosen injection levels λ_2 (three-transmitters-three-receivers) for $SNR_{\mathrm{SYS}} = 20$ dB, λ_1=0.38, and λ_3=0.42.

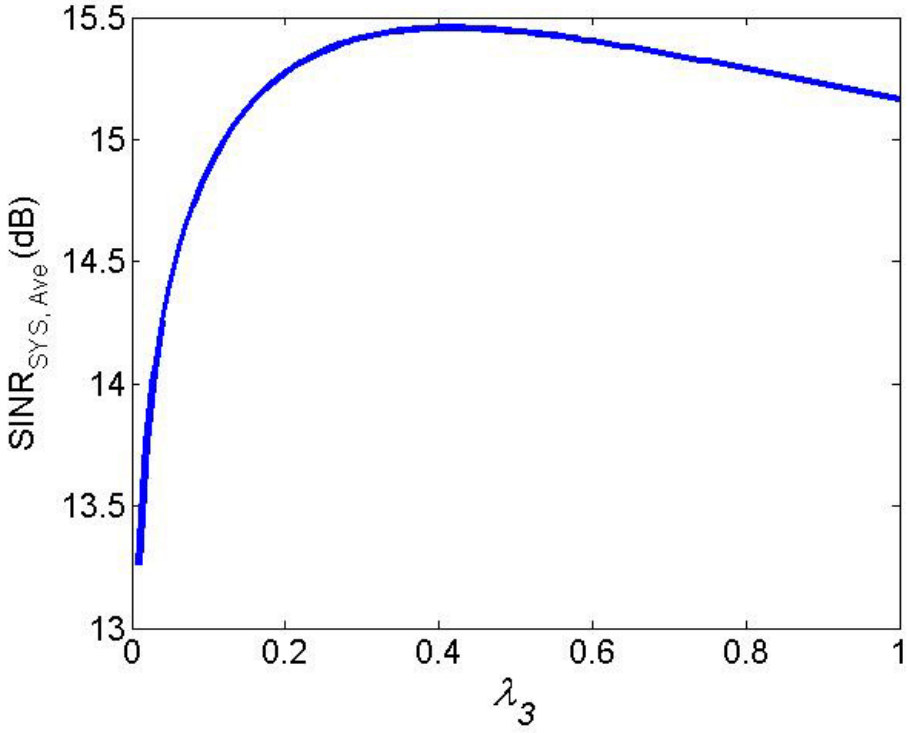

Figure 3.25: The overall system performances in terms of $SINR_{\mathrm{SYS,Ave}}$ versus different chosen injection levels λ_3 (three-transmitters-three-receivers) for $SNR_{\mathrm{SYS}} = 20$ dB, λ_1=0.38, and λ_2=0.38.

Note that when two optimal injection levels are fixed for any two transmitters, the other optimal injection level as shown in Figures 3.23-3.25 appears to coincide with our calculated value according to the optimization procedure in Section 5. As a result, Figures 3.18, 3.20, and 3.23-3.25 justify that our proposed optimization procedure actually attains the global signal-to-interference-plus-noise-ratio optimality by determining the appropriate injection level(s) for the three aforementioned scenarios. In addition, for these examples, we discover that the overall system performances do not vary much (within a $1 \sim 2$ dB margin) when the injection level is arbitrarily chosen to be larger than the optimal value. However, the sensitivity of the system performance is rather high when the injection level varies between 0 and its optimal value. For any number of transmitters and receivers ($L \geq 3$), we can follow the appendix to facilitate the CGP given by (5.4) to carry out $\mathbf{\Lambda}^{\text{opt}}$.

3.5 Conclusion

The multiple-transmitter identification in digital terrestrial television systems has been thoroughly studied in this chapter. According to the ATSC standard, the Kasami sequences are adopted as the embedded ID sequences due to its excellent correlational properties compared to other pseudo-random sequences. We start from the crucial mathematical properties of Kasami sequences and then evaluate the received signal-to-interference-plus-noise ratios for both subject TV signal reception and TxID signal detection. In order to investigate the sensitivity of the transmitter identification to different topologies and Kasami sequences with different lengths, we present the analysis here for four different geometric layouts, namely circular distribution, doubly concentric and circular distribution, square array, and hexag-

onal tessellation. The covered area and the lowest received signal-to-interference ratio are considered as two essential factors for the multiple-transmitter identification. It turns out to be that the larger the Kasami sequence length, the larger the received signal-to-interference ratio. Our new analysis can be used to determine the required Kasami sequence length for a specific broadcasting coverage.

Besides, we also propose a new measure to evaluate the overall DTV system performance to address both vital factors at the receiver thereupon. Based on this new measure, the optimization of buried-ratios or injection-levels can be carried out accordingly. Given the signal-to-noise ratio at the receiver and the locations of the transmitters and the receiver(s), one can optimize the overall system performance by selecting the optimal injection levels (or buried ratios). We also show that the corresponding optimization problem can be transformed into a well-known constrained geometric programming problem. Thus, we can benefit from the existing solution to this transformed optimization problem and determine the optimal injection levels.

4. DIGITAL WATERMARKING

An approach for digital copyright protection is to employ advanced watermarking techniques, where watermarks can reveal the ownership identities. Hence, we will investigate digital watermarking techniques and propose a new optimal watermarking scheme in this chapter. When multiple embedded watermarks are considered, a new analysis for the signal-to-interference-plus-noise-ratios (SINRs) with respect to the subject signal and the watermark signals is carried out. The objective quality measure for the digital watermarking applications should essentially consist of both signal-to-interference-plus-noise-ratio for the subject signal and similarity coefficients for the watermarks. In order to optimize the aforementioned objective measure, we design a novel efficient scale-factor optimization scheme, which can lead to the maximum overall SINR for both subject image signal and injected watermarks. Simulation results are demonstrated to illustrate the effectiveness of our proposed method as well.

This chapter is organized as follows. The optimization problem for multiple watermarking system will be stated in Section 4.1. The fundamental mathematical model of the spatial-frequency-domain watermarking techniques and the definition of overall signal-to-interference-plus-noise ratio for the watermarking/dewatermarking system will be introduced in Section 4.2. The new scale-factor optimization studies and our proposed algorithms will be proposed in Section 4.3. The simulation results are presented in Section 4.4. At last,

concluding remarks will be drawn in Section 4.5.

4.1 Problem Statement

Multiple watermarking is an embranchment of digital watermarking with many desirable characteristics that *singular watermarking* does not have. In order to increase the watermark information, one can embed multiple watermarks into the original subject signal. The subject signal and the watermarks are linearly scrambled (combined) in the transform-domain in linear watermarking. During the watermarking process, the weighting coefficients for the watermarks are called *scale-factors* [54,55]. Obviously, the subject signal and the watermarks negatively affect each other's signal quality this way. Moreover, since the watermark signals are different from each other in content, the scale-factor corresponding to each individual watermark thus needs to be determined separately. In the existing literature, the scale-factors are simply arbitrarily chosen without any sophisticated elaboration [56, 57]. Hence, the existing linear watermarking approach is not optimal. To combat this crucial optimization problem remaining challenging in the signal processing field, we propose a novel multiple scale-factor optimization scheme for digital watermarking in this dissertation, which can seek the *best tradeoff* between the subject signal quality and the watermark fidelities.

4.2 Mathematical Model

In this dissertation, all the watermarks will be embedded in the DCT (discrete cosine transform) domain due to its favorable compaction property. Each of the L watermark signals $W_i(k)$, $i = 1, 2, \ldots, L$ can be either a sequence consisting of a zero-mean, unit-variance Gaus-

sian process or some pre-specified image signal. A two-dimensional (2-D) DCT is performed on the entire image and then the samples of $W_i(k)$, $i = 1, 2, \ldots, L$ are added to the selected DCT bins. Assume that the 2-D DCT of the original image (K_1 pixels by K_2 pixels) is $v(k_1, k_2)$, $0 \leq k_1 \leq K_1 - 1$, $0 \leq k_2 \leq K_2 - 1$. We can stretch $v(k_1, k_2)$ as a vector $V(k)$ such that

$$V(k) = v(k_1, k_2), \tag{4.1}$$

where $k \stackrel{\text{def}}{=} k_1 K_1 + k_2$, for $0 \leq k_1 \leq K_1 - 1$, $0 \leq k_2 \leq K_2 - 1$. Then, we can sort the samples in $V(k)$ according to their magnitudes to generate a re-ordered sequence $V'(k)$ such that

$$V'(k) \stackrel{\text{def}}{=} V(\Pi(k)), \qquad k = 0, 1, \ldots, K_1 K_2 - 1, \tag{4.2}$$

where

$$V(\Pi(k)) \geq V(\Pi(k+1)), \qquad k = 0, 1, \ldots, K_1 K_2 - 2. \tag{4.3}$$

According to Eqs. (4.2), (4.3), we can obtain

$$V(k) = V'(\Pi^{-1}(k)), \qquad k = 0, 1, \ldots, K_1 K_2 - 1, \tag{4.4}$$

where $\Pi^{-1}(k)$ is the *inverse ordering* of $\Pi(k)$ such that $\Pi(\Pi^{-1}(k)) = \Pi^{-1}(\Pi(k)) = k$, $\forall k$. For the *multiple injected watermarks scenario*, we may embed the watermarks in two different ways. They are stated in the following subsections in details.

4.2.1 Type-I Watermarking

The *Type-I* watermarking technique is introduced in this subsection. The *Type-I* watermarked signal $S^I(k)$ is given by

$$S^I(k) = V'(k) + \sum_{i=1}^{L} \lambda_i W_i(k), \quad k = 0, 1, \ldots, K-1, \tag{4.5}$$

where $K \stackrel{\text{def}}{=} K_1 K_2$ and λ_i, $i = 1, 2, \ldots, L$ denote the L scale-factors (see [58] for the details of this linear watermarking technique). In our study, we embed the multiple watermarks in a non-overlapping way, which means each watermark signal sequence is injected into a different subset of $V'(k)$ in the DCT domain so as to cause the minimum interference to the subject image. Consider the realistic situation. We rewrite Eq. (4.5) as

$$S^I(k) = V'(k) + \sum_{i=1}^{L} \lambda_i W_i(k) + E(k), \quad k = 0, 1, \ldots, K-1, \tag{4.6}$$

where $E(k)$ is the additive noise or interference incurred during signal transmission. The *signal-to-noise ratio* (SNR) during signal transmission is thus defined as

$$SNR \stackrel{\text{def}}{=} \frac{\sum_{k=0}^{K-1} |V'(k)|^2}{\sum_{k=0}^{K-1} |E(k)|^2}. \tag{4.7}$$

For the watermarked signal $S^I(k)$, one often uses the following two measures to evaluate the signal qualities, namely the SINR for the subject image ($SINR^I_{\text{image}}$) and the similarity coefficient for the watermarks (SIM_i, $i = 1, 2, \ldots, L$). They are given by

$$SINR^I_{\text{image}} \stackrel{\text{def}}{=} \frac{\sum_{k=0}^{K-1} |V'(k)|^2}{\sum_{k=0}^{K-1} \left| \sum_{i=1}^{L} \lambda_i W_i(k) + E(k) \right|^2}, \tag{4.8}$$

and

$$SIM_i \stackrel{\text{def}}{=} \frac{\sum_{k=0}^{K} \lambda_i W_i(k) \mathcal{W}_i(k)}{\sum_{k=0}^{K} \mathcal{W}_i^2(k)}, \qquad i = 1, 2, \ldots, L, \tag{4.9}$$

where $\mathcal{W}_i(k)$ is the i^{th} extracted watermark. Besides, we can define the *signal-to-error ratio* (SER) $SER_{\text{wm},i}$ for each individual watermark as

$$SER_{\text{wm},i} \stackrel{\text{def}}{=} \frac{\sum_{k \in \mathcal{K}_i} |W_i(k)|^2}{\sum_{k \in \mathcal{K}_i} |W_i(k) - \mathcal{W}_i(k)|^2}, \tag{4.10}$$

where $\mathcal{K}_i$ is the subset of indices k in the presence of the i^{th} watermark. Consequently, the average SER over all watermarks is given by

$$SER_{\text{wm,ave}} \stackrel{\text{def}}{=} \sqrt[L]{\prod_{i=1}^{L} SER_{\text{wm},i}} \tag{4.11}$$

In this dissertation, we define a new objective performance measure as the *overall SINR* such that

$$SINR^I_{\text{overall}} = SINR^I_{\text{image}} \times \prod_{i=1}^{L} SIM_i. \tag{4.12}$$

Meanwhile, $SINR^I_{\text{overall}}$ can also be measured in the commonly-used units, decibels (dB). It yields

$$\begin{aligned} SINR^I_{\text{overall}}(\text{dB}) \quad &\stackrel{\text{def}}{=} 10 \log_{10}\left(SINR^I_{\text{overall}}\right) \\ &= 10 \log_{10}\left(SINR^I_{\text{image}}\right) \\ &\quad + 10 \sum_{i=1}^{L} \log_{10}\left(SIM_i\right). \end{aligned} \tag{4.13}$$

We can also write

$$SINR^I_{\text{image}}(\text{dB}) = 10 \log_{10}\left(SINR^I_{\text{image}}\right), \tag{4.14}$$

$$SER_{\text{wm},i}(\text{dB}) = 10\ \log_{10}\left(SER_{\text{wm},i}\right), \tag{4.15}$$

and

$$SER_{\text{wm,ave}}(\text{dB}) = 10\ \log_{10}\left(SER_{\text{wm,ave}}\right). \tag{4.16}$$

Since $SINR^I_{\text{overall}} > 0$, the alternative objective measure can be defined as

$$G^I(\mathbf{\Lambda}) \stackrel{\text{def}}{=} \frac{1}{SINR^I_{\text{overall}}}, \tag{4.17}$$

where $\mathbf{\Lambda} \stackrel{\text{def}}{=} \{\lambda_1, \lambda_2, \cdots, \lambda_L\}$. Note that $G^I(\mathbf{\Lambda})$ is a multinomial function of $\lambda_1, \lambda_2, \ldots, \lambda_L$ and the total number of terms is n. Thus, the objective function $G^I(\mathbf{\Lambda})$ can be expressed as

$$G^I(\mathbf{\Lambda}) = \sum_{i=1}^{n} c_i \prod_{j=1}^{L} \lambda_j^{\beta_{ij}}, \tag{4.18}$$

where c_i is the coefficient for each term in Eq. (4.18). We propose to employ the extended arithmetic-geometric mean inequality to solve this optimization problem:

$$\underset{\{\lambda_i\}_{i=1,\ldots,L}}{\arg\min}\ G^I(\mathbf{\Lambda}) = \underset{\{\lambda_i\}_{i=1,\ldots,L}}{\arg\max}\ SINR^I_{\text{overall}}. \tag{4.19}$$

In order to quantify the ultimate signal quality, we define the *a posteriori signal quality*, namely $SQ^I_{\text{apos}}(\text{dB})$, as follows:

$$SQ^I_{\text{apos}}(\text{dB}) \stackrel{\text{def}}{=} \frac{SINR^I_{\text{image}}(\text{dB}) + \sum_{i=1}^{L} SER_{\text{wm},i}(\text{dB})}{L+1}. \tag{4.20}$$

4.2.2 Type-II Watermarking

However, the watermark injection scheme based on Eq. (4.5) might not be appropriate when $V'(k)$ has a large dynamic range. It is easily found that *Type-I* watermarking scheme would reach a dilemma. If $|V'(k)| \gg |\lambda_i W_i(k)|$, the quality of an extracted watermark may often

be unacceptable. On the other hand, if $|V'(k)| \ll |\lambda_i W_i(k)|$, the watermarked image would be significantly distorted from the original image.

Therefore, an advanced watermarking scheme, namely the *Type-II* watermarking technique, was also proposed in [58] to combat the aforementioned problem. The *Type-II* watermarked signal is given by

$$S^{II}(k) = V'(k)\left[1 + \sum_{i=1}^{L} \lambda_i W_i(k)\right]. \tag{4.21}$$

Consider noise and/or interference during signal transmission. We have

$$S^{II}(k) = V'(k)\left[1 + \sum_{i=1}^{L} \lambda_i W_i(k)\right] + E(k). \tag{4.22}$$

Thus, the SINR $SINR^{II}_{\text{image}}$ for the subject image is defined as

$$SINR^{II}_{\text{image}} \stackrel{\text{def}}{=} \frac{\sum\limits_{k=0}^{K-1} |V'(k)|^2}{\sum\limits_{k=0}^{K-1} \left|\sum_{i=1}^{L} \lambda_i W_i(k) V'(k) + E(k)\right|^2}. \tag{4.23}$$

Meanwhile, the i^{th} extracted watermark $\mathcal{W}_i(k)$ can be expressed as

$$\mathcal{W}_i(k) = \lambda_i W_i(k) + \frac{E(k)}{V'(k)}. \tag{4.24}$$

Obviously, the same definitions for SIM_i, $SER_{\text{wm},i}$, and $SER_{\text{wm,ave}}$ given by Eqs. (4.9), (4.10), and (4.11) are still valid here for the *Type-II* watermarking technique. Consequently, one can define the new objective performance measure for *Type-II* watermarking as

$$SINR^{II}_{\text{overall}} = SINR^{II}_{\text{image}} \times \prod_{i=1}^{L} SIM_i. \tag{4.25}$$

Similarly, we may have

$$\begin{aligned} SINR^{II}_{\text{overall}}(\text{dB}) &\stackrel{\text{def}}{=} 10\ \log_{10}\left(SINR^{II}_{\text{overall}}\right) \\ &= 10\ \log_{10}\left(SINR^{II}_{\text{image}}\right) \\ &\quad + 10\sum_{i=1}^{L}\log_{10}\left(SIM_i\right), \end{aligned} \tag{4.26}$$

$$SINR^{II}_{\text{image}}(\text{dB}) = 10\ \log_{10}\left(SINR^{II}_{\text{image}}\right), \tag{4.27}$$

and

$$SQ^{II}_{\text{apos}}(\text{dB}) \stackrel{\text{def}}{=} \frac{SINR^{II}_{\text{image}}(\text{dB}) + \sum_{i=1}^{L} SER_{\text{wm},i}(\text{dB})}{L+1}. \tag{4.28}$$

The alternative objective measure can be defined as

$$G^{II}(\mathbf{\Lambda}) \stackrel{\text{def}}{=} \frac{1}{SINR^{II}_{\text{overall}}}, \tag{4.29}$$

where $\mathbf{\Lambda} \stackrel{\text{def}}{=} \{\lambda_1, \lambda_2, \cdots, \lambda_L\}$. Note that $G^{II}(\mathbf{\Lambda})$ is a multinomial function of $\lambda_1, \lambda_2, \ldots, \lambda_L$ and the total number of terms is n as well. The corresponding optimization problem can be facilitated as

$$\underset{\{\lambda_i\}_{i=1,\ldots,L}}{\arg\min}\ G^{II}(\mathbf{\Lambda}) = \underset{\{\lambda_i\}_{i=1,\ldots,L}}{\arg\max}\ SINR^{II}_{\text{overall}}. \tag{4.30}$$

4.3 Scale-Factor Optimization for Multiple Watermarks

According to the problem statement for the linear watermarking techniques introduced in Section 4.2, we propose the new efficient optimization methods to determine the optimal scale-factors $\lambda_1, \lambda_2, \ldots, \lambda_L$ in the following subsections.

4.3.1 Scale-Factor Optimization for Type-I Watermarking

In this subsection, we will formulate the scale-factor optimization problem mathematically for *Type-I* watermarking. Assume that L different watermarks are embedded in the original image DCT domain with no overlapping. According to Eqs. (4.8), (4.9) and (4.12), the overall SINR can be expressed as

$$\begin{aligned} SINR^{I}_{\text{overall}} &= \left[\frac{\sum_{k=0}^{K-1} |V'(k)|^2}{\sum_{k=0}^{K-1} \left| \sum_{i=1}^{L} \lambda_i W_i(k) + E(k) \right|^2} \right] \\ &\quad \times \prod_{i=1}^{L} \frac{\sum_{k=0}^{K-1} \lambda_i W_i(k) \mathcal{W}_i(k)}{\sum_{k=0}^{K-1} \mathcal{W}_i^2(k)}. \end{aligned} \tag{4.31}$$

Since $\mathcal{W}_i(k) = \lambda_i W_i(k) + E(k)$ according to Eq. (4.6), we can rewrite Eq. (4.31) as

$$\begin{aligned} & SINR^{I}_{\text{overall}} \\ &= \left[\frac{\sum_{k=0}^{K-1} |V'(k)|^2}{\sum_{k=0}^{K-1} |\lambda_1 W_1(k) + \cdots + \lambda_L W_L(k) + E(k)|^2} \right] \\ &\times \prod_{i=1}^{L} \frac{\sum_{k=0}^{K-1} \lambda_i^2 W_i^2(k) + \sum_{k=0}^{K-1} \lambda_i W_i(k) E(k)}{\sum_{k=0}^{K-1} \lambda_i^2 W_i^2(k) + \sum_{k=0}^{K-1} 2\lambda_i W_i(k) E(k) + \sum_{k=0}^{K-1} E^2(k)}. \end{aligned} \tag{4.32}$$

Since $E(k)$ is additive white Gaussian noise, it yields

$$\sum_{k=0}^{K} W_i(k) E(k) \approx 0. \tag{4.33}$$

Thus,

$$
\begin{aligned}
&SINR^{I}_{\text{overall}} \\
&= \left[\frac{\sum_{k=0}^{K-1} |V'(k)|^2}{\sum_{k=0}^{K-1} |\lambda_1 W_1(k) + \cdots + \lambda_L W_L(k)|^2 + \sum_{k=0}^{K-1} E^2(k)} \right] \\
&\quad \times \prod_{i=1}^{L} \frac{\sum_{k=0}^{K-1} \lambda_i^2 W_i^2(k)}{\sum_{k=0}^{K-1} \lambda_i^2 W_i^2(k) + \sum_{k=0}^{K-1} E^2(k)}.
\end{aligned}
\tag{4.34}
$$

According to Eq. (4.17), the alternative objective measure can be expressed as

$$
\begin{aligned}
&G^{I}(\mathbf{\Lambda}) \\
&= \left[\frac{\sum_{k=0}^{K-1} |\lambda_1 W_1(k) + \cdots + \lambda_L W_L(k)|^2 + \sum_{k=0}^{K-1} E^2(k)}{\sum_{k=0}^{K-1} |V'(k)|^2} \right] \\
&\quad \times \prod_{i=1}^{L} \left[1 + \frac{\sum_{k=0}^{K-1} E^2(k)}{\sum_{k=0}^{K-1} \lambda_i^2 W_i^2(k)} \right] \\
&= \left[\frac{\lambda_1^2 \sum_{k=0}^{K-1} W_1^2(k)}{\sum_{k=0}^{K-1} |V'(k)|^2} + \cdots + \frac{\lambda_L^2 \sum_{k=0}^{K-1} W_L^2(k)}{\sum_{k=0}^{K} |V'(k)|^2} \right. \\
&\qquad \left. + \frac{\sum_{k=0}^{K-1} E^2(k)}{\sum_{k=0}^{K-1} |V'(k)|^2} \right] \times \left[1 + \frac{\sum_{k=0}^{K-1} E^2(k)}{\lambda_1^2 \sum_{k=0}^{K-1} W_1^2(k)} \right] \\
&\quad \times \cdots \times \left[1 + \frac{\sum_{k=0}^{K-1} E^2(k)}{\lambda_L^2 \sum_{k=0}^{K-1} W_L^2(k)} \right].
\end{aligned}
\tag{4.35}
$$

Since the quality of the original image signal and the watermarks must be considered jointly during the watermark injection process, we define the constraints for this optimization problem as $SINR^I_{\text{image}} \geq \phi_1$ and $SIM_i \geq \varphi_1$, $\forall i$ where $\phi_1 \geq 0$ and $\varphi_1 \geq 0$. According the Eqs. (4.8) and (4.9), we can rewrite the constraints for this optimization problem as follows:

$$\begin{aligned} g^I_1(\mathbf{\Lambda}) &= \frac{\sum_{k=0}^{K-1} |V'(k)|^2}{\sum_{k=0}^{K-1} \left|\sum_{i=1}^{L} \lambda_i W_i(k)\right|^2 + \sum_{k=0}^{K-1} E^2(k)} \geq \phi_1, \\ g^I_{i+1}(\mathbf{\Lambda}) &= \frac{\lambda_i^2 \sum_{k=0}^{K-1} W_i^2(k)}{\lambda_i^2 \sum_{k=0}^{K-1} W_i^2(k) + \sum_{k=0}^{K-1} E^2(k)} \geq \varphi_1, \end{aligned} \tag{4.36}$$

$$i = 1, 2 \ldots, L. \tag{4.37}$$

In order to facilitate a constrained geometric program, we rewrite the constraints as

$$\begin{aligned} g^I_1(\mathbf{\Lambda}) &= \frac{1}{\phi_1} \left[\frac{\lambda_1^2 \sum_{k=0}^{K-1} W_1^2(k)}{\sum_{k=0}^{K-1} |V'(k)|^2} + \cdots + \frac{\lambda_L^2 \sum_{k=0}^{K-1} W_L^2(k)}{\sum_{k=0}^{K-1} |V'(k)|^2} \right. \\ &\quad \left. + \frac{\sum_{k=0}^{K-1} E^2(k)}{\sum_{k=0}^{K-1} |V'(k)|^2} \right] \leq 1, \end{aligned} \tag{4.38}$$

$$\begin{aligned} g^I_{i+1}(\mathbf{\Lambda}) &= \frac{1}{\varphi_1} + \frac{1}{\varphi_1} \frac{\sum_{k=0}^{K-1} E^2(k)}{\sum_{k=0}^{K-1} \lambda_i^2 W_i^2(k)} \leq 1, \\ &\quad i = 1, 2 \ldots, L. \end{aligned} \tag{4.39}$$

The objective constrained geometric program for *Type-I* watermarking can thus be expressed

as follows:

$$\text{CGP} \stackrel{\text{def}}{=} \quad \arg\min_{\mathbf{\Lambda}} \; G^I(\mathbf{\Lambda})$$
$$\text{subject to} \begin{cases} g_1^I(\mathbf{\Lambda}) \leq 1, \\ \quad \vdots \qquad \vdots \\ g_{L+1}^I(\mathbf{\Lambda}) \leq 1, \end{cases}$$
$$\text{where } \lambda_1 > 0, \cdots, \lambda_L > 0. \tag{4.40}$$

The CGP stated by Eq. (4.40) can be solved efficiently by our proposed algorithm in the appendix.

4.3.2 Scale-Factor Optimization for Type-II Watermarking

In this subsection, we will formulate the scale-factor optimization problem mathematically for *Type-II* watermarking as well. According to Eqs. (4.9), (4.23), and (4.25), the overall SINR can be expressed as

$$SINR_{\text{overall}}^{II} = \left[\frac{\sum_{k=0}^{K-1} |V'(k)|^2}{\sum_{k=0}^{K-1} \left| \sum_{i=1}^{L} \lambda_i W_i(k) V'(k) + E(k) \right|^2} \right] \times \prod_{i=1}^{L} \frac{\sum_{k=0}^{K} \lambda_i W_i(k) \mathcal{W}_i(k)}{\sum_{k=0}^{K} \mathcal{W}_i^2(k)}. \tag{4.41}$$

According to Eq. (4.24), we can rewrite Eq. (4.41) as

$$\begin{aligned} & SINR_{\text{overall}}^{II} \\ &= \left[\frac{\sum_{k=0}^{K-1} |V'(k)|^2}{\sum_{k=0}^{K-1} \left| \left[\lambda_1 W_1(k) + \cdots + \lambda_L W_L(k)\right] V'(k) + E(k) \right|^2} \right] \\ &\quad \times \prod_{i=1}^{L} \frac{\sum_{k=0}^{K-1} \lambda_i^2 W_i^2(k) + \sum_{k=0}^{K-1} \frac{\lambda_i W_i(k) E(k)}{V'(k)}}{\sum_{k=0}^{K-1} \lambda_i^2 W_i^2(k) + \sum_{k=0}^{K-1} \frac{2\lambda_i W_i(k) E(k)}{V'(k)} + \sum_{k=0}^{K-1} \left[\frac{E(k)}{V'(k)}\right]^2}. \end{aligned} \tag{4.42}$$

Since $W_i(k)$, $V'(k)$ are both statistically independent of $E(k)$, we have

$$\sum_{k=0}^{K-1} \frac{W_i(k)}{V'(k)} E(k) \approx 0. \tag{4.43}$$

Therefore,

$$\begin{aligned} & SINR_{\text{overall}}^{II} \\ &= \left[\frac{\sum_{k=0}^{K-1} |V'(k)|^2}{\sum_{k=0}^{K-1} \left| \left[\lambda_1 W_1(k) + \cdots + \lambda_L W_L(k)\right] V'(k) + E(k) \right|^2} \right] \\ &\quad \times \prod_{i=1}^{L} \frac{\sum_{k=0}^{K-1} \lambda_i^2 W_i^2(k)}{\sum_{k=0}^{K-1} \lambda_i^2 W_i^2(k) + \sum_{k=0}^{K-1} \left[\frac{E(k)}{V'(k)}\right]^2}. \end{aligned} \tag{4.44}$$

According to Eq. (4.29), the alternative objective measure can be expressed as

$$
\begin{aligned}
& G^{II}(\mathbf{\Lambda}) \\
&= \left[\frac{\sum_{k=0}^{K-1} \left| \left[\lambda_1 W_1(k) + \cdots + \lambda_L W_L(k)\right] V'(k) + E(k) \right|^2}{\sum_{k=0}^{K-1} |V'(k)|^2} \right] \\
&\quad \times \prod_{i=1}^{L} \left[1 + \frac{\sum_{k=0}^{K-1} \left[\frac{E(k)}{V'(k)} \right]^2}{\sum_{k=0}^{K-1} \lambda_i^2 W_i^2(k)} \right] \\
&= \left[\frac{\lambda_1^2 \sum_{k=0}^{K-1} [W_1(k)V'(k)]^2}{\sum_{k=0}^{K-1} |V'(k)|^2} + \cdots \right. \\
&\quad \left. + \frac{\lambda_L^2 \sum_{k=0}^{K-1} [W_L(k)V'(k)]^2}{\sum_{k=0}^{K-1} |V'(k)|^2} + \frac{\sum_{k=0}^{K-1} E^2(k)}{\sum_{k=0}^{K-1} |V'(k)|^2} \right] \\
&\quad \times \left[1 + \frac{\sum_{k=0}^{K-1} \left[\frac{E(k)}{V'(k)} \right]^2}{\lambda_1^2 \sum_{k=0}^{K-1} W_1^2(k)} \right] \times \cdots \\
&\quad \times \left[1 + \frac{\sum_{k=0}^{K-1} \left[\frac{E(k)}{V'(k)} \right]^2}{\lambda_L^2 \sum_{k=0}^{K-1} W_L^2(k)} \right]. \qquad (4.45)
\end{aligned}
$$

Similar constraints $SINR_{\text{image}}^{II} \geq \phi_2$ and $SIM_i \geq \varphi_2$, $\forall i$, where $\phi_2 \geq 0$, and $\varphi_2 \geq 0$, can also be employed here. The constraints for this optimization problem can be written as follows:

$$
g_1^{II}(\mathbf{\Lambda}) = \frac{\sum_{k=0}^{K-1} |V'(k)|^2}{\sum_{k=0}^{K-1} \left| \sum_{i=1}^{L} \lambda_i W_i(k) V'(k) + E(k) \right|^2} \geq \phi_2, \qquad (4.46)
$$

$$g_{i+1}^{II}(\mathbf{\Lambda}) = \frac{\lambda_i^2 \sum_{k=0}^{K} W_i^2(k)}{\lambda_i^2 \sum_{k=0}^{K} W_i^2(k) + \sum_{k=0}^{K} \left[\frac{E(k)}{V'(k)}\right]^2} \geq \varphi_2,$$

$$i = 1, 2 \ldots, L. \tag{4.47}$$

Rewrite the above constraints as

$$g_1^{II}(\mathbf{\Lambda}) = \frac{1}{\phi_2} \left[\frac{\lambda_1^2 \sum_{k=0}^{K-1} [W_1(k)V'(k)]^2}{\sum_{k=0}^{K-1} |V'(k)|^2} + \cdots + \frac{\lambda_L^2 \sum_{k=0}^{K-1} [W_L(k)V'(k)]^2}{\sum_{k=0}^{K-1} |V'(k)|^2} + \frac{\sum_{k=0}^{K-1} E^2(k)}{\sum_{k=0}^{K-1} |V'(k)|^2} \right] \leq 1, \tag{4.48}$$

$$g_{i+1}^{II}(\mathbf{\Lambda}) = \frac{1}{\varphi_2} + \frac{1}{\varphi_2} \frac{\sum_{k=0}^{K-1} \left[\frac{E(k)}{V'(k)}\right]^2}{\lambda_i^2 \sum_{k=0}^{K-1} W_i^2(k)} \leq 1,$$

$$i = 1, 2 \ldots, L. \tag{4.49}$$

Consequently, the objective constrained geometric program for this problem is expressed as follows:

$$\begin{aligned} \text{CGP} \stackrel{\text{def}}{=} \quad & \arg\min_{\mathbf{\Lambda}} G^{II}(\mathbf{\Lambda}) \\ & \text{subject to} \begin{cases} g_1^{II}(\mathbf{\Lambda}) \leq 1, \\ \quad \vdots \qquad \vdots \\ g_{L+1}^{II}(\mathbf{\Lambda}) \leq 1, \end{cases} \\ & \text{where } \lambda_1 > 0, \cdots, \lambda_L > 0. \end{aligned} \tag{4.50}$$

The CGP stated by (4.50) can also be solved by our proposed algorithm in the appendix.

4.4 Simulation

An example is provided here for illustration. The original image (256 pixel $\times$ 256 pixels) is shown in Figure 4.1 and three different watermarks (one Gaussian random sequence consisting of 9,600 samples and two signature images) are embedded in it by employing the two aforementioned watermarking techniques.

Figure 4.1: The original image.

The signal-to-noise ratio during signal transmission is set to be 60 dB. We arbitrarily set $\phi_1 = \phi_2 = 10$ and $\varphi_1 = \varphi_2 = 0.5$. According to our proposed algorithm in the appendix, we find the optimal scale-factors $\lambda_1^{\text{opt}} = 0.6$, $\lambda_2^{\text{opt}} = 0.005$, and $\lambda_3^{\text{opt}} = 0.002$ for the *Type-I*

Figure 4.2: The watermarked image using the *Type-I* watermarking technique stated in Section 4.2.1.

Figure 4.3: The watermarked image using the *Type-II* watermarking technique stated in Section 4.2.2.

watermarking scheme stated in Section 4.2.1 and the optimal scale-factors $\lambda_1^{\text{opt}} = 4 \times 10^{-3}$, $\lambda_2^{\text{opt}} = 5 \times 10^{-5}$, and $\lambda_3^{\text{opt}} = 2 \times 10^{-5}$ for the *Type-II* watermarking scheme stated in Section 4.2.2 to maximize $SINR^{I}_{\text{overall}}$ and $SINR^{II}_{\text{overall}}$, respectively.

Based on the optimal linear spatial-frequency-domain watermarking techniques introduced in Sections 4.2.1 and 4.2.2, we establish the watermarked image as depicted in Figures 4.2 and 4.3, respectively. After dewatermarking, we acquire the reconstructed subject image as depicted in Figures 4.4 and 4.5 accordingly.

The extracted watermark quality for the Gaussian random sequence can be evaluated by invoking the absolute value of the *cross-correlation coefficient* between the extracted watermark sequence and the original watermark sequence. This cross-correlation coefficient for the i^{th} watermark is given by

$$\rho_i \stackrel{\text{def}}{=} \frac{\frac{1}{K}\sum_{k=0}^{K-1} W_i(k)\,\mathcal{W}_i(k)}{\sqrt{\frac{1}{K}\sum_{k=0}^{K-1} W_i^2(k)}\,\sqrt{\frac{1}{K}\sum_{k=0}^{K-1} \mathcal{W}_i^2(k)}}. \tag{4.51}$$

Figure 4.4: The dewatermarked image using the *Type-I* watermarking technique stated in Section 4.2.1.

Figure 4.5: The dewatermarked image using the *Type-II* watermarking technique stated in Section 4.2.2.

The original and extracted watermark sequences $W_1(k)$ and $\mathcal{W}_1(k)$ (the first 200 samples only, $k = 0, 1, \ldots, 199$) are shown in Figures 4.6 and 4.7. Figures 4.8, 4.9, 4.10 and 4.11 depict the extracted watermarks $\mathcal{W}_2(k)$ and $\mathcal{W}_3(k)$ resulting from the *Type-I* and *Type-II* watermarking techniques.

According to these figures, the watermark injection does not cause much image quality degradation and they can be extracted out easily at a satisfactory quality level. Based on the definition in Eq. (4.51), we have $|\rho_1^I| = 0.91$, $|\rho_2^I| = 0.93$, $|\rho_3^I| = 0.93$ from the *Type-I* watermarking method and $|\rho_1^{II}| = 0.99$, $|\rho_2^{II}| = 0.99$, $|\rho_3^{II}| = 0.99$ from the *Type-II* watermarking method, respectively. Note that the additional superscripts "I" and "II" to ρ_i are used to denote the watermarking types. In addition, we investigate the relation and the tradeoff among the SINR of the subject image, the overall SINR, and the average SER for all watermarks. We conduct the simulations for both *Type-I* and *Type-II* watermarking techniques. For each type of watermarking technique, we compare two different choices of the scale-factors, namely (i) λ_i, $i = 1, 2, 3$ to be randomly picked, and (ii) λ_i, $i = 1, 2, 3$ to be optimized using

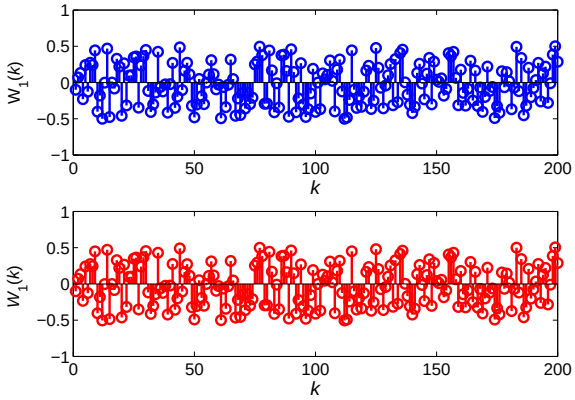

Figure 4.6: The original and extracted Gaussian random sequence watermarks (the first 200 samples only, $k = 0, 1, \ldots, 199$) using the *Type-I* watermarking technique stated in Section 4.2.1.

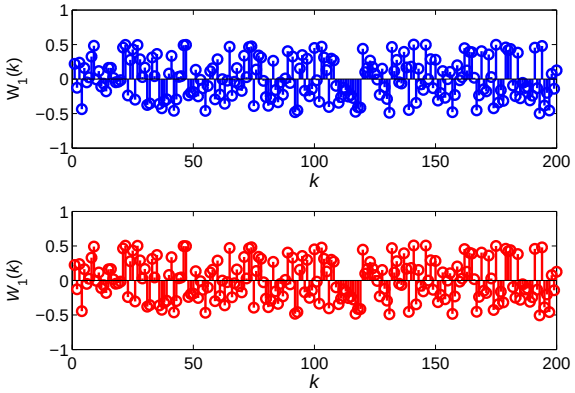

Figure 4.7: The original and extracted Gaussian random sequence watermarks (the first 200 samples only, $k = 0, 1, \ldots, 199$) using the *Type-II* watermarking technique stated in Section 4.2.2.

Figure 4.8: The extracted signature watermark "Barack Obama" using the *Type-I* watermarking technique stated in Section 4.2.1.

Figure 4.9: The extracted signature watermark "John McCain" using the *Type-I* watermarking technique stated in Section 4.2.1.

Figure 4.10: The extracted signature watermark "Barack Obama" using the *Type-I* watermarking technique stated in Section 4.2.2.

Figure 4.11: The extracted signature watermark "John McCain" using the *Type-I* watermarking technique stated in Section 4.2.2.

our proposed algorithm in the appendix. In Figure 4.12, we plot six signal quality measures for the *Type-I* watermarking method, namely the overall SINRs $SINR_{\text{overall,ran}}$(dB), $SINR_{\text{overall,opt}}$(dB), the SINRs of the subject image $SINR_{\text{image,ran}}$(dB), $SINR_{\text{image,opt}}$(dB), and the average SERs over all watermarks $SER_{\text{wm,ave,ran}}$(dB), $SER_{\text{wm,ave,opt}}$(dB) where the last subscript of each measure ("ran" or "opt") denotes the underlying scale-factor choice as (i) or (ii).

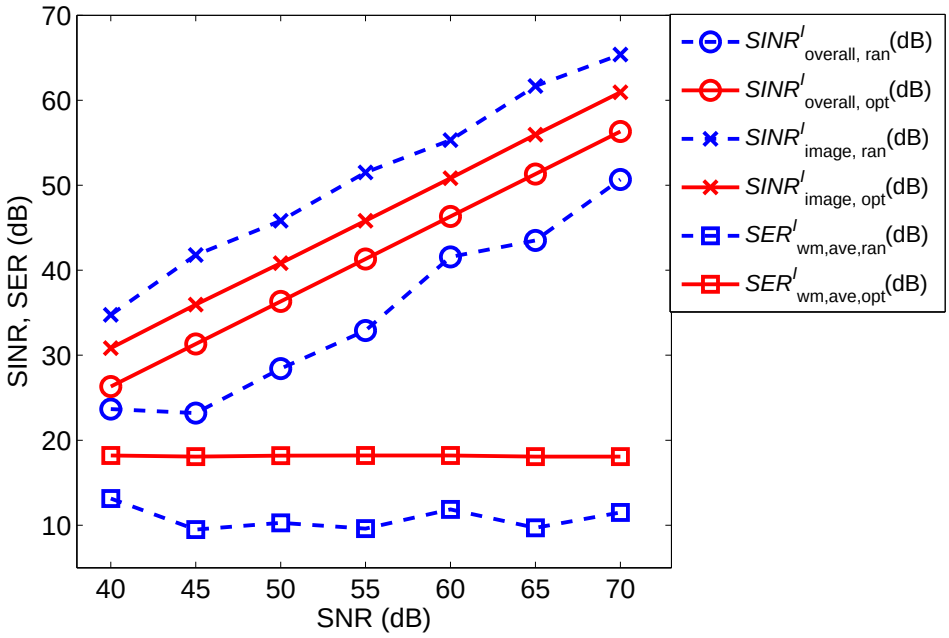

Figure 4.12: The signal quality measures versus signal-to-noise ratio resulting from the *Type-I* watermarking technique stated in Section 4.2.1.

Note that the additional superscripts "I" are attached to all these measures to denote the watermarking type. In a similar manner, the signal quality measures for the *Type-II* watermarking method instead are also delineated in Figure 4.13.

It can be found that our proposed optimal watermark injection scheme can help both *Type-I* and *Type-II* methods to seek the "best tradeoff" between the SINR of the subject image

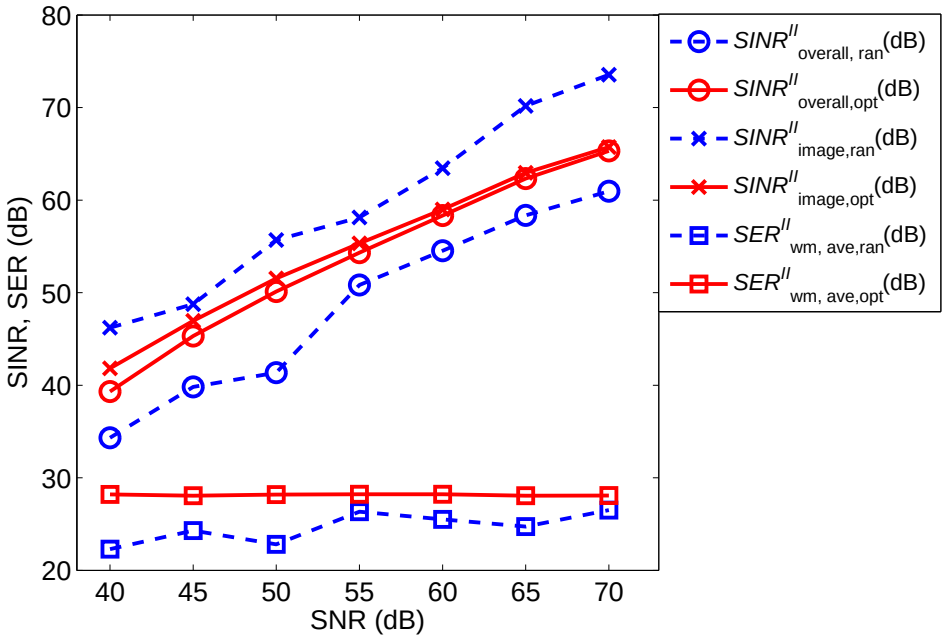

Figure 4.13: The signal quality measures versus signal-to-noise ratio resulting from the *Type-II* watermarking technique stated in Section 4.2.2.

and the average SER over all watermarks. This can be reflected by two phenomena in these figures. First, the overall SINRs resulting from our proposed optimal scheme are superior to those resulting from the randomly picked scale-factors. Second, the difference between the SINR of the subject image and the average SER over all watermarks is much less when the optimal scale-factors are used than when randomly picked scale-factors are used.

Finally in Figure 4.14, we depict the three *a posteriori* signal quality measures for the *Type-I* watermarking method, namely $SQ^I_{\text{apos,ran}_1}(\text{dB})$, $SQ^I_{\text{apos,ran}_2}(\text{dB})$, and $SQ^I_{\text{apos,opt}}(\text{dB})$ where the last subscript of each measure ("ran_1", "ran_2", or "opt") denotes the underlying scale-factor choice. Note that "ran_1" and "ran_2" denote two different sets of randomly picked scale-factors while "opt" denotes the optimal scale-factors resulting from our proposed optimization scheme. In a similar manner, the three *a posteriori* signal quality measures for the *Type-II* watermarking method instead are also illustrated in Figure 4.14. According to

Figure 4.14, it can be discovered that the *a posteriori* signal quality using our proposed scheme is always the best for both watermarking techniques. Besides, the *a posteriori* signal quality resulting from the *Type-II* watermarking technique is much better than that resulting from the *Type-I* watermarking technique.

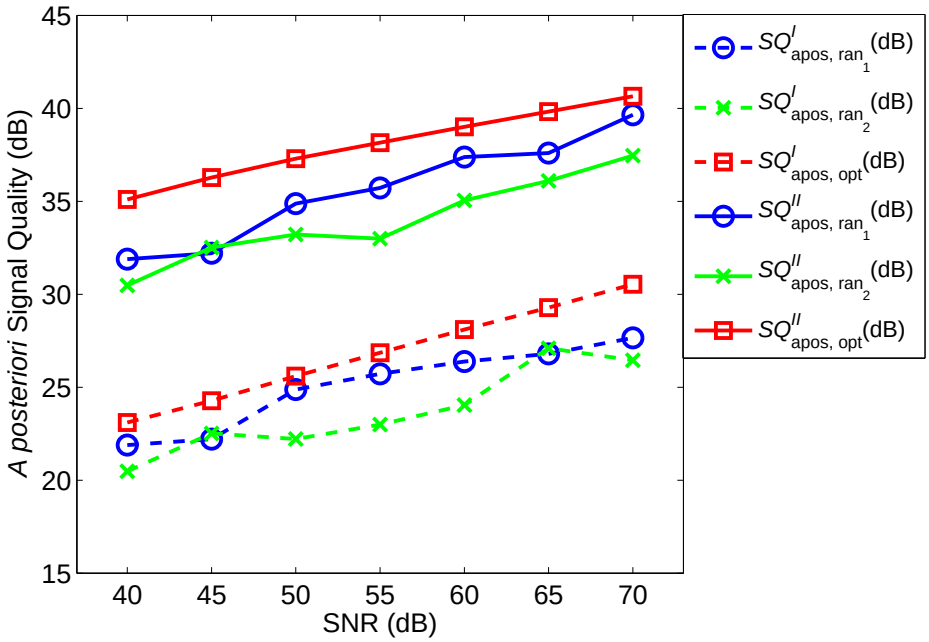

Figure 4.14: The *a posteriori* signal quality measures versus signal-to-noise ratio for both *Type-I* and *Type-II* watermarking methods.

4.5 Conclusion

The scale-factor optimization problem in linear watermarking has been studied rigorously in this chapter. We define the new tradeoff measures, namely overall signal-to-interference-plus-noise ratio and *a posteriori* signal quality, as the crucial objectives of the two prevalent linear watermarking schemes. Given the original image and the watermarks, one can optimize the overall system performance by selecting the appropriate scale-factors according to our proposed new method. We also transform this new scale-factor optimization problem into a computationally-efficient constrained geometric programming problem. Thus, we can benefit from the neat solution to this constrained geometric programming problem to facilitate a novel optimal linear spatial-frequency-domain watermarking system.

5. CONCLUSION

In this dissertation work, we focus on the linear identification research. We try to provide answers in theory and practice to the unsolved problems in this field. The outcomes of this dissertation research can be reflected by the rigorous theoretical analysis and the computationally-efficient algorithms.

Two prevalent applications of linear identification in wireless communications and signal processing, namely DTV transmitter identification and digital watermarking, have been tackled in this work. For the DTV transmitter identification, the sensitivity of transmitter identification to different topologies and Kasami sequences with different lengths has been investigated. A new measure to quantify the overall DTV system performance has been proposed. Based on this new measure, the optimization of buried-ratios or injection-levels has been carried out. Consequently, we have greatly simplified the injection-level optimization problem through sophisticated mathematical manipulations. The ultimate optimization algorithm we have achieved is very computationally-efficient and our proposed new TxID technique, foreseeably, would be very useful for the next generation DTV industry in practice. Moreover, digital watermarking techniques have also been investigated in this dissertation work. We formulate and investigate the scale-factor optimization problem for the spatial-frequency-domain multiple-watermarking systems. We define a new objective measure to govern the tradeoff between the dewatermarked subject signal quality and the retrieved

individual watermark qualities. Consequently, one can optimize the overall system performance by selecting the appropriate scale-factors. Thus, we can benefit from a neat solution and facilitate a new optimal linear spatial-frequency-domain watermarking system.

Furthermore, through rigorous mathematics, we show that the aforementioned optimization problems can be transformed into a well-known constrained geometric programming problem. According to the extended arithmetic-geometric mean inequality, the feasible solutions can be undertaken easily. Therefore, we can benefit from the existing computationally-efficient solutions to these transformed optimization problems and determine the appropriate buried-ratios (injection-levels) and scale-factors.

Our scientific findings and engineering solutions would pose great impacts on digital terrestrial broadcasting industry and digital imaging applications. This dissertation can be deemed as the first-ever attempt to seek the tradeoff objectives together with the efficient optimal solutions for the linear identification problems in wireless communications and signal processing. The future research, though predictably much more complicated, would be the potential extension of the investigation to nonlinear identification.

BIBLIOGRAPHY

[1] J. G. Proakis, *Digital Communications*. McGraw-Hill, 1989.

[2] R. E. Ziemer and R. L. Peterson, *Digital Communication and Spread Spectrum Systems*. Macmillan, 1985.

[3] X. Wang, Y. Wu, and B. Caron, "Transmitter identification using embedded pseudo random sequences," *IEEE Transactions on Broadcasting*, vol. 50, pp. 244–252, September 2004.

[4] S. I. Park, J.-Y. Lee, H. M. Kim, and W. Oh, "Transmitter identification signal analyzer for single frequency network," *IEEE Transactions on Broadcasting*, vol. 54, pp. 383–393, September 2008.

[5] R. B.Wolfgang, C. I. Podilchuk, and E. J. Delp, "Perceptual watermarks for digital images and video," *Proceedings of the IEEE*, vol. 87, pp. 1108–1126, July 1999.

[6] C. Fei, D. Kundur, and R. H. Kwong, "Analysis and design of secure watermark-based authentication systems," *IEEE Transactions on Information Forensics and Security*, vol. 1, pp. 43–55, March 2006.

[7] S. Huang and J. K. Wu, "Optical watermarking for printed document authentication," *IEEE Transactions on Information Forensics and Security*, vol. 2, pp. 164–173, June 2007.

[8] I. Mahafeno, Y. Louet, and J.-F. Helard, "Peak-to-average power ratio reduction using second order cone programming based tone reservation for terrestrial digital video broadcasting systems," *IET Communications*, vol. 3, pp. 1250 – 1261, July 2009.

[9] F. Lehmann, A. Kazem, and G. Salut, "Blind turbo-detection in the presence of phase noise," *IET Communications*, vol. 3, pp. 1343 – 1353, August 2009.

[10] W.-M. Chen, C.-J. Lai, H.-C. Wang, H.-C. Chao, and C.-H. Lo, "H.264 video watermarking with secret image sharing," accepted for publication in *IET Image Processing*.

[11] *ATSC Digital Television Standard*. Prentice Hall, 1995.

[12] ATSC, *ATSC Standard A/110:Synchronization Standard for Distributed Transmission*. December 2007.

[13] ATSC, *ATSC Standard A/82:Automatic Transmitter Power Control (ATPC) Data Return Link (DRL) Standard*. February 2008.

[14] T. Kasami, *Weight distribution formula for some class of cyclic codes.* Technology Report, University of Illinois, 1966.

[15] X. Feng, H.-C. Wu, and Y. Wu, "Geometric capacity studies for DTV transmitter identification using Kasami sequences," in *Proceedings of IEEE International Symposium on Broadband Multimedia Systems and Broadcasting (BMSB)*, March 2010.

[16] Y. Wu, X. Wang, R. Citta, B. Ledoux, S. Lafleche, and B. Caron, "An ATSC DTV receiver with improved robustness to multipath and distributed transmission environments," *IEEE Transactions on Broadcasting*, vol. 50, pp. 32–41, March 2004.

[17] W. W. Peterson and E. J. Weldon, *Error-correction Codes.* MIT press, 1972.

[18] D. V. Sarwate and M. B. Pursley, "Cross correlation properties of pseudorandom and related sequences," *Proceedings of the IEEE*, vol. 68, pp. 593–619, May 1980.

[19] J. G. Proakis, *Digital Communications.* McGraw-Hill, 1989.

[20] H. Y. Huang, C. H. Yang, and W. H. Hsu, "A video watermarking technique based on pseudo-3-d dct and quantization index modulation," *IEEE Transactions on Information Forensics and Security*, vol. 5, pp. 625–637, December 2010.

[21] X. Wang, J. Wu, and P. Niu, "A new digital image watermarking algorithm resilient to desynchronization attacks," *IEEE Transactions on Information Forensics and Security*, vol. 2, pp. 655–663, December 2007.

[22] W. N. Lie, G. S. Lin, and S. L. Cheng;, "Dual protection of jpeg images based on informed embedding and two-stage watermark extraction techniques," *IEEE Transactions on Information Forensics and Security*, vol. 3, pp. 330–341, September 2006.

[23] R. van Schyndel, A. Tirkel, and C. Osborne, "A digital watermark," in *Image Processing, 1994. Proceedings. ICIP-94., IEEE International Conference*, vol. 2, pp. 86–90, November 1994.

[24] A. Piva and T. B. A. D. Rosa, "Secure client-side st-dm watermark embedding," *IEEE Transactions on Information Forensics and Security*, vol. 5, pp. 13–26, March 2010.

[25] T. Y. Liu and W. H. Tsai, "Generic lossless visible watermarkinga new approach," *IEEE Transactions on Image Processing*, vol. 19, pp. 1224–1235, May 2010.

[26] X. Zhang and S. Wang, "Watermarking scheme capable of resisting sensitivity attack," *IEEE Signal Processing Letters*, vol. 14, pp. 125–128, February 2007.

[27] L. Ghouti, A. Bouridane, M. K. Ibrahim, and S. Boussakta, "Digital image watermarking using balanced multiwavelets," *IEEE Transactions on Signal Processing*, vol. 54, pp. 1519–1536, April 2006.

[28] T. Y. Kim, H. Choi, K. Lee, and T. Kim, "An asymmetric watermarking system with many embedding watermarks corresponding to one detection watermark," *IEEE Signal Processing Letters*, vol. 11, pp. 375–377, March 2004.

[29] V. Korzhik, G. Morales-Luna, D. Marakov, and I. Marakova, "Watermarking of binary messages in conditions of an additive binary noise attack," *IEEE Signal Processing Letters*, vol. 10, pp. 277–279, September 2003.

[30] S. C. Pei and J. J. Ding, "Reversible integer color transform," *IEEE Transactions on Image Processing*, vol. 16, pp. 1686–1691, June 2007.

[31] S. D. Larbi and M. Jaidane-Saidane, "Audio watermarking: a way to stationnarize audio signals," *IEEE Transactions on Signal Processing*, vol. 53, pp. 816–823, Feburary 2005.

[32] W. Chen, C.-H. Lo, H.-C. Chao, and C. C. Chang, "Gabor filter aided 3D ultrasonography diagnosis system with WLAN transmission consideration," *Journal of Universal Computer Science*, no. 10, pp. 1327 – 1342.

[33] M. K. Simon, J. K. Omura, R. A. Scholtz, and B. K. Levitt, *Spread Spectrum Communications Handbook*. McGraw-Hill, 2001.

[34] X. Zeng, J. Liu, and L. Hu, "Generalized Kasami sequences: The large set," *IEEE Transactions on Information Theory*, vol. 53, pp. 2587–2598, July 2007.

[35] T. Helleseth and P. V. Kumar, *Sequences with low correlation in Handbook of Coding Theory*. V. S. Pless and W. C. Huffman Eds. Amsterdam, 2001.

[36] X. Zeng, L. Hu, Q. Liu, and Y. Zhu, "Binary sequences with optimal correlations and large linear span," in *Proceedings of IEEE International Conference on Communications*, vol. 1, pp. 385–390, June 2006.

[37] A. Chow, *Performance of spreading Codes for direct sequence code division multiple access (DS-CDMA)*. Technical Report, Stanford University, 2003.

[38] J. D. H. White and R. E. Challis, "A Golay sequencer based ndt system for highly attenuating materials," in *Proceedings of IEE Colloquium on Noncontacting and Remote NDT*, pp. 7/1–7/7, November 1992.

[39] S. Z. Budisin, B. M. Popovic, and I. M. Indjin, "Designing radar signals using complementary sequences," in *Proceedings of the International Conference on Radar*, pp. 593–597, October 1987.

[40] M. Hazas and A. Ward, "A high performance privacy-oriented location system," in *Proceedings of the 1st IEEE International Conference on Pervasive Computing and Communications*, pp. 216–233, March 2003.

[41] T. Helleseth, C. Ding, and H. Niederreiter, "Correlation of m-sequences and related topics," in *in Proceedings of SETA 1998*, pp. 49–66, October 1999.

[42] H. M. Trachtenberg, *On the cross-correlation functions of maximal linear recurring sequences*. Ph.D. Dissertation, University of Southern California, 1970.

[43] R. Gold, "Optimal binary sequences for spread spectrum multiplexing," *IEEE Transactions on Information Theory*, vol. 13, pp. 619–621, October 1967.

[44] R. Gold, "Maximal recursive sequences with 3-valued recursive cross correlation functions," *IEEE Transactions on Information Theory*, vol. 14, pp. 154–156, January 1968.

[45] S. W. Golomb, *Shift Register Sequences*. Holden-Day, 1967.

[46] A. Goldsmith, *Wireless communications*. Cambridge University Press, 2005.

[47] L. R. Welch, "Lower bounds on the maximum cross correlation of signals," *IEEE Transactions on Information Theory*, vol. 20, pp. 397–399, May 1974.

[48] C.-Y. Chen, H.-C. Chao, S.-Y. Kuo, and K.-D. Chang, "Rule-based intrusion detection mechanism for IP multimedia subsystem," *Journal of Internet Technology*, vol. 9, pp. 329 – 336, December 2008.

[49] L. Zhou, B. Geller, X. Wang, A. Wei, B. Zheng, and H.-C. Chao, "Multi-user video streaming over multiple heterogeneous wireless networks: A distributed, cross-layer design paradigm," *Journal of Internet Technology*, vol. 10, pp. 1 – 12, January 2009.

[50] A. Mattsson, "Single frequency networks in DTV," *IEEE Transactions on Broadcasting*, vol. 51, pp. 413–422, December 2005.

[51] O. Bendov, "Areas of cochannel interference and multi-path created by 8-VSB modulated distributed transmitters in flat terrain," *IEEE Transactions on Broadcasting*, vol. 52, pp. 31–37, March 2006.

[52] ATSC, *ATSC Standard A/111:Design Of Synchronized Multiple Transmitter Networks*. September 2009.

[53] B. Liu, Y. Wu, B. Rong, G. Gagnon, C. Nadeau, M. El-Tanany, L. Gui, and W. Zhang, "Transmitter identification of ATSC DTV under mobile environment," in *Proceedings of IEEE International Symposium on Broadband Multimedia Systems and Broadcasting (BMSB)*, pp. 1–6, March 2010.

[54] A. Takahashi, R. Nishimura, and Y. Suzuki, "Multiple watermarks for stereo audio signals using phase-modulation techniques," *IEEE Transactions on Signal Processing*, vol. 53, pp. 806–815, February 2005.

[55] P. H. W. Wong, O. C. Au, and Y. M. Yeung, "Novel blind multiple watermarking technique for images," *IEEE Transactions on Circuits and Systems for Video Technology*, vol. 13, pp. 813–830, August 2003.

[56] X. Wang and H. Zhao, "A novel synchronization invariant audio watermarking scheme based on DWT and DCT," *IEEE Transactions on Signal Processing*, vol. 54, pp. 4835–4840, December 2006.

[57] J. S. Seo and C. D. Yoo, "Image watermarking based on invariant regions of scale-space representation," *IEEE Transactions on Signal Processing*, vol. 54, pp. 1537–1549, April 2006.

[58] I. J. Cox, J. Kilian, F. T. Leighton, and T. Shamoon, "Secure spread spectrum watermarking for multimedia," *IEEE Transactions on Image Processing*, vol. 6, pp. 1673–1687, December 1997.

[59] A. L. Peressini, F. E. Sullivan, and J. J. Uhl, Jr., *The Mathematics of Nonlinear Programming*. Springer, 1991.

APPENDIX A: EXTENDED ARITHMETIC-GEOMETRIC MEAN INEQUALITY AND CONSTRAINT GEOMETRIC PROGRAMMING

The adopted extended arithmetic-geometric mean inequality is presented here. Refer to [59] for mathematical details. Suppose that $x_1, ..., x_n$ are all positive numbers. If $\delta_1, ..., \delta_n$ are the numbers that are either all positive or all zero and if $\eta = \delta_1 + \cdots + \delta_n$, then

$$\left(\sum_{i=1}^{n} x_i\right)^{\eta} \geq \eta^{\eta} \left[\prod_{i=1}^{n} \left(\frac{x_i}{\delta_i}\right)^{\delta_i}\right] \tag{5.1}$$

under the conventions $0^0 = 1$ and $(x_i/0)^0 = 1$. The equality in (5.1) holds if and only if $\delta_1 = \delta_2 = ... = \delta_n = 0$ or

$$x_i = \frac{\delta_i}{\eta} \left(\sum_{j=1}^{n} x_j\right), \tag{5.2}$$

for $i = 1, \ldots, n$. The extended arithmetic-geometric mean inequality can be used to solve the constrained geometric program. For a positive integer m, define a posynomial as

$$g(\mathbf{\Lambda}) \stackrel{\text{def}}{=} \sum_{i=1}^{n} c_i \prod_{j=1}^{m} \lambda_j^{\alpha_{ij}} \tag{5.3}$$

over all possible $\mathbf{\Lambda} \stackrel{\text{def}}{=} (\lambda_1, \ldots, \lambda_m)$ where $\lambda_j > 0$ for $j = 1, \ldots, m$, $c_i > 0$ for $i = 1, \ldots, n$, and $\alpha_{ij} \in \mathbf{R}$ for all i, j. $\mathbf{R}$ denotes the set of all real numbers.

Suppose that $g_0(\mathbf{\Lambda})$,$g_1(\mathbf{\Lambda})$,...,$g_k(\mathbf{\Lambda})$ are $(k+1)$ posynomials consisting of m positive real

variables $\lambda_1, \ldots, \lambda_m$ and $\mathbf{\Lambda} = (\lambda_1, \ldots, \lambda_m)$. Then the program

$$\begin{aligned} \text{CGP} \stackrel{\text{def}}{=} \quad & \min_{\mathbf{\Lambda}} \quad g_0(\mathbf{\Lambda}) \\ & \text{subject to } g_1(\mathbf{\Lambda}) \leq 1, g_2(\mathbf{\Lambda}) \leq 1, \ldots, g_k(\mathbf{\Lambda}) \leq 1, \\ & \text{where } \lambda_1 > 0, \lambda_2 > 0, \ldots, \lambda_m > 0 \end{aligned} \tag{5.4}$$

is called a constrained geometric program. For notional convenience, we denote the posynomial $u_i(\mathbf{\Lambda})$ by

$$u_i(\mathbf{\Lambda}) \stackrel{\text{def}}{=} c_i \lambda_1^{\alpha_{i1}} \lambda_2^{\alpha_{i2}} \cdots \lambda_m^{\alpha_{im}}. \tag{5.5}$$

Therefore, we can rewrite the CGP given by (5.4) as

$$\begin{aligned} \text{CGP} \stackrel{\text{def}}{=} \min_{\mathbf{\Lambda}} \quad & g_0(\mathbf{\Lambda}) = u_1(\mathbf{\Lambda}) + \cdots + u_{n_0}(\mathbf{\Lambda}) \\ \text{subject to } & \begin{cases} g_1(\mathbf{\Lambda}) = u_{n_0+1}(\mathbf{\Lambda}) + \cdots + u_{n_1}(\mathbf{\Lambda}) \leq 1, \\ \quad \vdots \qquad \vdots \qquad \vdots \qquad \vdots \\ g_k(\mathbf{\Lambda}) = u_{n_{k-1}+1}(\mathbf{\Lambda}) + \cdots + u_{n_k}(\mathbf{\Lambda}) \leq 1, \end{cases} \\ & \text{where } \lambda_1 > 0, \lambda_2 > 0, \ldots, \lambda_m > 0, \text{ and } n_k = v. \end{aligned} \tag{5.6}$$

Note that v is a positive integer corresponding to the number of "$u_j(\mathbf{\Lambda})$" terms such that $1 \leq j \leq v$. We may denote the optimal solution $\mathbf{\Lambda}^{\text{opt}} \stackrel{\text{def}}{=} (\lambda_1^{\text{opt}}, \ldots, \lambda_m^{\text{opt}})$ which minimizes $g_0(\mathbf{\Lambda})$. Then we can apply the extended arithmetic-geometric mean inequality given by (5.1) for $g_0(\mathbf{\Lambda})$ and choose $\eta = 1$. It yields

$$g_0(\mathbf{\Lambda}) \geq \left[\frac{u_1(\mathbf{\Lambda})}{\delta_1}\right]^{\delta_1} \left[\frac{u_2(\mathbf{\Lambda})}{\delta_2}\right]^{\delta_2} \cdots \left[\frac{u_{n_0}(\mathbf{\Lambda})}{\delta_{n_0}}\right]^{\delta_{n_0}}, \tag{5.7}$$

where

$$\delta_1 + \delta_2 + \cdots + \delta_{n_0} = 1. \tag{5.8}$$

For any $\eta > 0$, we re-employ (5.1) for $g_1(\mathbf{\Lambda})$ where $[g_1(\mathbf{\Lambda})]^\eta \leq 1$. It yields

$$\begin{aligned} g_0(\mathbf{\Lambda}) &\geq g_0(\mathbf{\Lambda})[g_1(\mathbf{\Lambda})]^\eta \\ &\geq g_0(\mathbf{\Lambda})\eta^\eta \left[\frac{u_{n_0+1}(\mathbf{\Lambda})}{\delta_{n_0+1}}\right]^{\delta_{n_0+1}} \cdots \left[\frac{u_{n_1}(\mathbf{\Lambda})}{\delta_{n_1}}\right]^{\delta_{n_1}} \end{aligned} \tag{5.9}$$

After applying the extended arithmetic-geometric mean inequality for $g_2(\mathbf{\Lambda})$, ..., $g_k(\mathbf{\Lambda})$ in the same manner as (5.9), we can achieve the ultimate inequality as

$$g_0(\mathbf{\Lambda}) \geq \mathcal{C}(\delta_1, \ldots, \delta_v)\ \lambda_1^{\alpha_{11}\delta_1 + \cdots + \alpha_{v1}\delta_v} \cdots \lambda_m^{\alpha_{1m}\delta_1 + \cdots + \alpha_{vm}\delta_v}, \tag{5.10}$$

where $\mathcal{C}(\delta_1, \ldots, \delta_v)$ is a function independent of $\lambda_1, \ldots, \lambda_m$. According to [59], when λ_1, λ_2, ..., λ_m are evaluated at the optimality ($g_0(\mathbf{\Lambda})$ is minimized), we need to enforce the following identity

$$\lambda_1^{\alpha_{11}\delta_1 + \cdots + \alpha_{v1}\delta_v} = \cdots = \lambda_m^{\alpha_{1m}\delta_1 + \cdots + \alpha_{vm}\delta_v} = 1 \tag{5.11}$$

such that

$$\begin{cases} \alpha_{11}\delta_1 + \cdots + \alpha_{v1}\delta_v = 0, \\ \alpha_{12}\delta_1 + \cdots + \alpha_{v2}\delta_v = 0, \\ \quad \vdots \qquad\quad \vdots \qquad\quad \vdots \\ \alpha_{1m}\delta_1 + \cdots + \alpha_{vm}\delta_v = 0. \end{cases} \tag{5.12}$$

Thus, we can consider the following *dual constrained geometric program* (DCGP), which is

equivalent to CGP given by (5.6):

$$\text{DCGP} \stackrel{\text{def}}{=} \max_{\delta_1,\delta_2,\ldots,\delta_v} \mathcal{C}(\delta_1,\ldots,\delta_v) = \left[\prod_{j=1}^{v}\left(\frac{c_j}{\delta_j}\right)^{\delta_j}\right]$$
$$\times \prod_{i=1}^{k}(\delta_{n_{i-1}+1}+\cdots+\delta_{n_i})^{\delta_{n_{i-1}+1}+\ldots+\delta_{n_i}}$$
$$\text{subject to} \begin{cases} \delta_1+\delta_2+\cdots+\delta_{n_0}=1, \\ \alpha_{11}\delta_1+\cdots+\alpha_{v1}\delta_v=0, \\ \alpha_{12}\delta_1+\cdots+\alpha_{v2}\delta_v=0, \\ \quad\vdots \qquad\quad \vdots \qquad\quad \vdots \\ \alpha_{1m}\delta_1+\cdots+\alpha_{vm}\delta_v=0. \end{cases} \tag{5.13}$$

The function $\mathcal{C}(\delta_1,\ldots,\delta_v)$ in (5.13) is the *dual objective function* to the original objective function $g_0(\mathbf{\Lambda})$ given by (5.6) and the constraints in DCGP are the dual constraints in CGP. We may denote a vector $\mathbf{\Delta} \stackrel{\text{def}}{=} (\delta_1,\ldots,\delta_v)$. By simply solving the constraints in (5.13), we can obtain a vector $\mathbf{\Delta}^{\text{opt}} = (\delta_1^{\text{opt}},\ldots,\delta_v^{\text{opt}})$ which maximizes the dual objective function $\mathcal{C}(\delta_1,\ldots,\delta_v)$=$\mathcal{C}(\mathbf{\Delta})$ in the DCGP. From the *Primal-Dual inequality* (see [59]), if $\mathbf{\Lambda}^{\text{opt}}$ is feasible for the CGP given by (5.6) and $\mathbf{\Delta}^{\text{opt}}$ is also feasible for the DCGP given by (5.13), then

$$g_0(\mathbf{\Lambda}) \geq g_0(\mathbf{\Lambda}^{\text{opt}}) = \mathcal{C}(\mathbf{\Delta}^{\text{opt}}) \geq \mathcal{C}(\mathbf{\Delta}). \tag{5.14}$$

Therefore, we may invoke $g_0(\mathbf{\Lambda}^{\text{opt}}) = \mathcal{C}(\mathbf{\Delta}^{\text{opt}})$ to reach the optimality for both CGP and DCGP.

APPENDIX B: OPTIMIZATION METHOD

According to [59], the entire optimization procedure can be simplified as follows:

Initialization:)

The numerical parameters in Eq. (5.4) are given.

Step 1:)

Invoke the following simultaneous equations to find the optimal solutions $\mathbf{\Delta}^{\rm opt} = (\delta_1^{\rm opt}, \ldots, \delta_v^{\rm opt})$ such that

$$\begin{aligned}
&\delta_1^{\rm opt} + \delta_2^{\rm opt} + \cdots + \delta_{n_0}^{\rm opt} = 1, \\
&\alpha_{11}\delta_1^{\rm opt} + \cdots + \alpha_{v1}\delta_v^{\rm opt} = 0, \\
&\alpha_{12}\delta_1^{\rm opt} + \cdots + \alpha_{v2}\delta_v^{\rm opt} = 0, \\
&\quad\vdots \qquad\quad \vdots \qquad\quad \vdots \\
&\alpha_{1m}\delta_1^{\rm opt} + \cdots + \alpha_{vm}\delta_v^{\rm opt} = 0.
\end{aligned} \tag{5.15}$$

Step 2:)

Invoke the following equations to find the optimal solutions $\mathbf{\Lambda}^{\rm opt} = (\lambda_1^{\rm opt}, \ldots, \lambda_m^{\rm opt})$:

$$\begin{aligned}
&\tfrac{\eta\ u_i(\mathbf{\Lambda}^{\rm opt})}{\delta_i^{\rm opt}} = \mathcal{C}(\mathbf{\Delta}^{\rm opt}),\ \ i = 1, \ldots, n_0, \\
&\tfrac{u_i(\mathbf{\Lambda}^{\rm opt})}{\delta_i^{\rm opt}} = \varepsilon_1,\ \ i = n_0 + 1, \ldots, n_1, \\
&\quad\vdots \qquad\quad \vdots \qquad\quad \vdots \\
&\tfrac{u_i(\mathbf{\Lambda}^{\rm opt})}{\delta_i^{\rm opt}} = \varepsilon_k,\ \ i = n_{k-1} + 1, \ldots, n_k = v,
\end{aligned} \tag{5.16}$$

where ε_1, ..., ε_k are the unknown numbers to be determined as well. □

Note that there are $(m + k)$ unknowns to be determined by $k + 1$ simultaneous equations in (5.16). Hence there might not exist any feasible solution or might exist multiple solutions for $\mathbf{\Lambda}^{\text{opt}}$. However, from our experience in adopting this optimization procedure, the unique optimal solution $\mathbf{\Lambda}^{\text{opt}}$ is achieved very often, especially for a few unknowns.

APPENDIX C: LETTER OF PERMISSION

Comments/Response to Case ID: 0013032F

ReplyTo: Pubs-Permissions@ieee.org

From: Jacqueline Hansson Date: 10/28/2011

Subject:Re: Request for Permission Send To: Xiaoyu Feng ¡xfeng4@tigers.lsu.edu¿

Dear Xiaoyu Feng

Thank you for your inquiry about re-use rights for IEEE copyrighted material.

IEEE is pleased to announce our partnership with Copyright Clearance Centers RightsLink service. RightsLink offers a fast and easy way to obtain permission to reuse and republish material from IEEE. You may obtain permission to reuse the IEEE copyrighted material requested by following the instructions below:.

1. Either click on this link or cut and paste it into your internet browser. It goes directly to A New Approach for Optimal Multiple Watermarks Injection, the first paper from which you requested IEEE copyrighted material:

http://ieeexplore.ieee.org/search/

2. Next, click on the orange Request Permissions link which can be found under the IEEE paper title. 3. A RightsLink account can then be created, reuse preferences can be selected. and permission can be obtained for the IEEE content requested.

Once you have created your RightsLinkaccount, you can go to RightsLink for all your future requests following the instructions below.

1. Go to http://ieeexplore.ieee.org/Xplore/guesthome.jsp 2. Type the title of the IEEE copyrighted paper into the IEEE Xplore Search Bar and click on the word "Search" . 3. Click on the underlined IEEE copyrighted paper's title that's in orange and blue print. 4. The title will appear again in orange print under the orange Browse tab. 5. Next, click on the orange Request Permissions link, which can be found under the IEEE paper title. 6. Continue the process to obtain permission for any material desired from each additional IEEE copyrighted paper.

Please call or write if you have any questions.

Sincerely,

Jacqueline Hansson, Coordinator

IEEE Intellectual Property Rights Office 445 Hoes Lane Piscataway, NJ 08855-1331 USA +1 732 562 3966 (phone) +1 732 562 1746(fax)

IEEE Fostering technological innovation and excellence for the benefit of humanity.

Dear Sir or Madam,

This is Xiaoyu Feng from Louisiana State University. I sincerely would like to ask for your permission to reprint the following articles accepted and published by IEEE journals and conferences:

Paper 1 Author(s) : Xiaoyu Feng; Hongting Zhang; Hsiao-Chun Wu; Yiyan Wu;

Paper Title: A New Approach for Optimal Multiple Watermarks Injection

IEEE publication title: IEEE Signal Processing Letters

Paper 2 Author(s) : Xiaoyu Feng; Hsiao-Chun Wu; Yiyan Wu;

Paper Title: Geometric capacity studies for DTV transmitter identification using Kasami sequences

IEEE publication title:IEEE International Symposium on Broadband Multimedia Systems and Broadcasting (BMSB), 2010

Paper 2 Author(s) : Xiaoyu Feng; Hsiao-Chun Wu; Shih Yu Chang;

Paper Title: On the Injection-Level Optimization for Digital Television Transmitter Identification Systems Using Kasami Sequences

IEEE publication title: IEEE International Conference on Communications (ICC), 2011

As one of the authors of these papers, I want to reprint the entire articles as Chapter 3 and Chapter 4 in my dissertation with the tile Advanced Linear Identification Techniques For Signal Processing And Digital Video Broadcasting. The requested permission extends to any future revisions and editions of my dissertation, and the dissertation will be put in the electronic thesis and dissertation library of Louisiana State University. These rights will in no way restrict republication of the materials in any other form by IEEE or by others authorized by IEEE. Your permission of this request will also confirm that IEEE owns the copyright of the above-described materials.

If these arrangements meet with your approval, I will greatly appreciate that you could response this email no later than Wednesday November 2nd, 2011. Thank you so much for your cooperation.

Sincerely, Xiaoyu Feng

Thesis / Dissertaion Reuse

We are happy to grant this permission. Our only requirement is that the requester provides a full credit notice to the original source (author, paper, publication), followed by the IEEE copyright notice.

Comments We would like to hear from you. E-mail us at customercare@copyright.com

VITA

Xiaoyu Feng received the Bachelor of Engineering in Automation Science degree from Beijing University of Aeronautics and Astronautics, Beijing, China, in 2007. He got a Master of Electrical Engineering degree from Louisiana State University in 2009. He is currently pursuing the Doctor of Philosophy degree in the Department of Electrical and Computer Engineering, Louisiana State University, Baton Rouge. His research interests are in the areas of optimization theory in communications and signal processing.